UNIVERSIDADE FEDERAL DO RIO GRANDE DO SUL
INSTITUTO DE FÍSICA
PROGRAMA DE PÓS GRADUAÇÃO EM FÍSICA

Gabriel Lauffer Ramos

Evolutionary Sequences for H and He Atmosphere Massive White Dwarf Stars

Porto Alegre, Brasil
July 10, 2018

Gabriel Lauffer Ramos

Evolutionary Sequences for H and He Atmosphere Massive White Dwarf Stars

Dissertação submetida ao Programa de Pós-Graduação em Física do instituto de Física da UFRGS, como quesito parcial para obtenção do título de Mestre em Física, com ênfase em Astronomia.

Supervisor: Alejandra D. Romero

Porto Alegre, Brasil
July 10, 2018

CIP - Catalogação na Publicação

Lauffer Ramos, Gabriel
Evolutionary Sequences for H and He Atmosphere Massive White Dwarfs Stars / Gabriel Lauffer Ramos. -- 2018.
90 f.
Orientadora: Alejandra D. Romero.

Coorientador: Kepler S. O..

Dissertação (Mestrado) -- Universidade Federal do Rio Grande do Sul, Instituto de Física, Programa de Pós-Graduação em Física, Porto Alegre, BR-RS, 2018.

1. Evolução Estelar. 2. Anãs Brancas. 3. Metodos Númericos. I. D. Romero, Alejandra, orient. II. S. O., Kepler, coorient. III. Título.

Elaborada pelo Sistema de Geração Automática de Ficha Catalográfica da UFRGS com os dados fornecidos pelo(a) autor(a).

Gabriel Lauffer Ramos

Evolutionary Sequences for H and He Atmosphere Massive White Dwarf Stars

Dissertação submetida ao Programa de Pós-Graduação em Física do instituto de Física da UFRGS, como quesito parcial para obtenção do título de Mestre em Física, com ênfase em Astronomia.

Trabalho aprovado. Porto Alegre, Brasil, *6* de *julho* de *2018*:

Alejandra D. Romero
Orientadora

Charles J. Bonatto
Convidado 1

Alan A. Brito
Convidado 2

Walter J. Maciel
Convidado 3

Porto Alegre, Brasil
July 10, 2018

À memória de Jacson Lauffer, o meu primeiro exemplo de cientista.

Acknowledgements

Agradeço ao Instituto de Física e a todos os professores que me ensinaram e auxiliaram ao longo do mestrado. Em especial, agradeço a Profa. Dra. Alejandra Daniela Romero e ao Prof. Dr. Kepler de Souza Oliveira Filho, pela paciência, ensinamentos, orientação e por todas as oportunidades de crescimento profissional que me deram. Também, agradeço à CAPES pelo financiamento da bolsa que, mesmo com todos os cortes de orçamento na ciência e tecnologia, continuam investindo em pesquisa. Agradeço aos meus colegas do grupo de pesquisa pelas disussões nas reunião que ajudaram no desenvolvimento do trabalho. Aos meus colegas de sala, agradeço por sempre estarem dispostos a ligarem o meu computador.

Quero agradecer todo o apoio e carinho da minha familia, em especial de meus pais, Eliane e Sandro, por todo o incentivo e apoio nas escolhas da vida. Também agradeço ao meu irmão Guilherme e ao meu tio Emerson por todas as caronas até a estação de trem. Agradeço em especial a minha noiva, Chaiana, por me aturar desde o início da graduação e por todo o carinho, amizade, compreensão, paciência e amor que demonstra durante estes quase 7 anos juntos. Tu é o principal mecanismo de pulsação do meu coração!

Abstract

White dwarf stars are the most common final stage of stellar evolution, corresponding to 99% of all stars in the Galaxy. White dwarf models can be used to obtain the age of stellar populations, to build an initial to final mass relation to understand the connection between the properties of white dwarfs and their progenitors, determine the upper mass limit that separates white dwarfs progenitors from Type II supernovae, enhance the comprehension of the physical properties of high density matter and derive ages and masses for observed white dwarfs from the cooling tracks. The literature is populated with low mass and intermediate mass white dwarf models, however the massive white dwarfs are often forgotten and the evolutionary sequences are incomplete. In this dissertation, we compute full evolutionary sequences for massive white dwarfs, exploring the evolution of hydrogen-rich and hydrogen-deficient white dwarfs stars with masses between 1.012 and 1.307 $M_\odot$, and initial metallicity of $Z = 0.02$. These sequences are the result of main sequence stars with masses between 8.8 and 11.8 $M_\odot$. The simulations were performed with the *Modules for Experiments in Stellar Astrophysics* - MESA code, starting at the zero-age main sequence, through thermally pulsing and mass-loss phases, ending as the white dwarfs at the cooling sequence. Our simulations are full evolutionary, in which we consider the entire evolutionary history of the progenitors. We present reliable nuclear chemical profiles for the whole mass range considered, covering the different expected central compositions, i.e. C/O, O/Ne and Ne/O/Mg, and their dependence with the stellar mass. In addition, we present detailed chemical profiles of hybrid C/O-O/Ne core white dwarfs, found in the mass range between 1.024 and 1.150 $M_\odot$. We present the initial-to-final mass relation, mass-radius relation, and cooling times with improved crystallization limits, considering the effects of atmosphere and core composition.

Keywords: star evolution; white dwarf; numerical methods.

Resumo

As estrelas anãs brancas são o estágio final mais comum da evolução estelar, correspondendo a 99% de todas as estrelas da galáxia. Os modelos de anãs brancas podem ser usados para obter a idade das populações estelares, para construir uma relação inicial e final de massa e entender a conexão entre as propriedades das anãs brancas e seus progenitores, determinar o limite de massa superior que separa as progenitoras de anãs brancas das supernovas Tipo II, melhorar a compreensão das propriedades físicas da matéria de alta densidade e derivar idades e massas para as anãs brancas observadas a partir das sequencias evolutivas na curva de esfriamento. A literatura é repleta de modelos de anãs brancas de baixa massa e massa intermediária, no entanto, as anãs brancas massivas são frequentemente esquecidas e as sequências evolutivas são incompletas. Nesta dissertação, nós computamos sequências evolutivas completas para anãs brancas massivas, explorando a evolução de estrelas anãs brancas ricas em hidrogênio e deficientes de hidrogênio com massas entre 1.012 e 1.307 $M_{\odot}$, e metalicidade inicial de $Z = 0.02$. Essas sequências são o resultado de estrelas da sequência principal com massas entre 8.8 e 11.8 $M_{\odot}$. As simulações foram realizadas com o código *Modules for Experiments in Stellar Astrophysics* - MESA, iniciando na sequência principal de idade zero, passando pelas fases de pulsação térmica e perda de massa, terminando como uma anã branca na curva de resfriamento. Nossas simulações são totalmente evolutivas, nas quais consideramos toda a história evolutiva dos progenitores. Apresentamos perfis químicos para toda a faixa de massas consideradas, abrangendo as diferentes composições centrais esperadas, ou seja, C/O, O/Ne e Ne/O/Mg, e sua dependência com a massa estelar. Além disso, apresentamos perfis químicos detalhados das anãs brancas do núcleo híbrido C/O-O/Ne, encontrados na faixa de massa entre 1.024 e 1.150 $M_{\odot}$. Apresentamos a relação massa inicial-final, relação massa-raio e tempos de resfriamento com melhores limites de cristalização, considerando os efeitos da atmosfera e composição do núcleo.

Palavras-chave: evolução estelar. anã branca. métodos numéricos.

List of Figures

Figure 1 – A Scheme of the evolutionary paths a single star may follow, depending on its mass. 24

Figure 2 – Histogram for the number density distribution of white dwarfs versus mass on the SDSS data release 12. Red lines show the -1σ and $+1\sigma$ uncertainties. The long dashed blue histogram is the one from Rebassa-Mansergas et al. (2015). Adapted from Kepler et al. (2016). 27

Figure 3 – A scheme of the evolutionary paths a white dwarf may follow. The left column informs the effective temperature. The second column presents the evolution of the most common type of white dwarf (DA spectral type). The DO type may follow different paths, either from a merger event or from a hot and helium, carbon, and oxygen rich PG 1159 star. The PG 1159 stars are also believed to be the progenitors of hot DQ stars. Accretion of metal from interstellar medium or from circumstellar matter by cool helium rich white dwarf may lead to a DZ white dwarf. Adapted from Althaus et al. (2010b). 29

Figure 4 – A scheme of how MESA computes its cell and face (boundary) variables. Adapted from Paxton et al. (2011). 37

Figure 5 – Evolutionary tracks for three sequences in the HR diagram, with initial masses 8.9 (solid line), 10 (dashed line) and 11 $M_\odot$ (dotted line) and final masses 1.019, 1.11 and 1.22 $M_\odot$, respectively. Each sequence has a different core composition in the cooling curve stage, being C/O, O/Ne and Ne/O/Mg, respectively. 42

Figure 6 – Example of chemical profile in terms of the outer mass fraction at $T_{eff} \approx 80\,000$ K on the cooling sequence for H atmosphere (top) and He atmosphere (bottom) white dwarf with 1.019 $M_\odot$. Hydrogen had to be added on all sequences due to losses on mass loss phase. The quantities added on each evolution are shown in table 2. This figure show that only the atmosphere of the star was changed. The nuclei composition are identical to both H and He atmosphere sequences. 44

Figure 7 – Mass location of the first ignition of carbon and mass location of closest to center flame extinction as function of white dwarf masses which experienced a carbon flame. Vertical dotted lines delimits the mass range for core composition defined in figure 8 47

Figure 8 – Central abundances versus final mass of the white dwarfs stars before crystallization starts ($T_{eff} \approx 40\,000$ K). The black circles represent ^{12}C, triangles are ^{16}O, squares are ^{20}Ne and empty circles are ^{24}Mg. We can identify three regions, one for C/O core for masses below or equal to 1.088 $M_\odot$ where neon is lower than carbon, another region between 1.088 and 1.147 $M_\odot$ in which neon is greater than carbon and lower than oxygen but magnesium is lower than carbon defining an O/Ne core, and a third region for masses greater than 1.147 $M_\odot$ with an O/Ne/Mg core due to neon being greater than oxygen and magnesium greater than carbon. 48

Figure 9 – Initial to Final Mass Relation comparison between this work and Siess (2010) and Doherty et al. (2015) for models with $Z = 0.02$. The Doherty et al. (2015) data was truncated to show only their massive models. Initial and final masses are on $M_\odot$ units. 49

Figure 10 – Chemical profile in terms of outer mass fraction for selected elements for three different stages of the cooling sequence: $T_{eff} \approx 80\,000$ K on top, $T_{eff} \approx 40\,000$ K on middle and $T_{eff} \approx 10\,000$ K on bottom panels. The chemical profiles are for a H atmosphere white dwarf with $M_{WD} = 1.11\ M_\odot$. The shaded region represents the crystallized zone of the star. 51

Figure 11 – Chemical profile in terms of outer mass fraction for selected elements and for three different H atmosphere white dwarf with $T_{eff} \approx 10\,000$ K. From top to bottom we depict the chemical profile for a $M_{WD} = 1.019, 1.11, 1.22$ $M_\odot$. The shaded region represents the crystallized zone of the star. 52

Figure 12 – Comparison of cooling times for selected H and He atmosphere sequences. There are presented 3 sets of H and He atmosphere. A C/O core set with mass 1.019 $M_\odot$ as solid line. An O/Ne set with mass 1.11 as dashed line and a Ne/O/Mg set with mass 1.22 $M_\odot$ as dotted line. Gray lines represent H atmosphere and black lines are He atmosphere white dwarfs. The final chemical profile for the H atmosphere are shown in figure 11. 53

Figure 13 – $\log g$ - T_{eff} relation for H atmosphere white dwarfs. T_{eff} from $\approx 250\,000$ K to $\approx 10\,000$ K. Empty circles are observed white dwarfs from the SDSS catalog. 54

List of Tables

Table 1 – Mass at ZAMS, white dwarf mass, age when hydrogen is depleted at center (t_H), age when helium is totally consumed at the center (t_{He}), progenitor ages (t_i), effective temperature on crystallization (T_{eff_c}) and age at crystallization (t_{cryst}, accounted from the beginning of the cooling sequence) and cooling time (t_{cool} = age at $T_{eff} = 1 \times 10^4$ K minus t_i) for H and He atmosphere white dwarfs. Ages (t_H, t_{He}, t_i) in units of Myr and crystallization and cooling times on units of Gyr. 43

Table 2 – Values of initial mass at ZAMS (M_{ZAMS}), white dwarfs masses (M_{WD}) and hydrogen content for H-rich sequences and helium contents for both H and He atmosphere sequences. Hydrogen abundances were extrapolated from Romero et al. (2012), Romero et al. (2013). The Helium abundances were extrapolated for sequences with $M_{WD} \geq 1.132$. 45

List of abbreviations and acronyms

AGB	Asymptotic Giant Branch
BaSTI	a Bag of Stellar Tracks and Isochrones
CS	Cooling Sequence
DSEP	Dartmouth Stellar Evolution Program
EOS	Equation of State
HB	Horizontal Branch
HELM	Timmes e Swesty (2000) table of equation of state
HR	Hertzprung-Russel diagram
IFMR	Initial-to-Final mass relation
MESA	Modules for Experiments in Stellar Astrophysics
MLT	Mixing Lenght Theory
MS	Main Sequence
OPAL	Rogers e Nayfonov (2002) table of equation of state
PC	Potekhin e Chabrier (2010) table of equation of state
RGB	Red Giant Branch
SCVH	Saumon, Chabrier e van Horn (1995) table of equation of state
SN	Supernova
SDSS	Sloan Digital Sky Survey
ZAMS	Zero Age Main Sequence

List of symbols

a_k	Lagrangian acceleration at cell face k
DA	Type of white dwarf with H-atmosphere
DB	White dwarf with He-atmosphere and effective temperature of $11\,000 - 30\,000$ K
DC	White dwarf with He-atmosphere, traces of carbon and effective temperature below $\sim 11\,000$ K
$D_{\mathrm{conv},0}$	MLT derived diffusion coefficient
DO	White dwarf with He-atmosphere and effective temperature of $45\,000 - 200\,000$ K
DQ	White dwarf with He-atmosphere, traces of metals and effective temperature below $\sim 11\,000$ K
f	Adjustable parameter for overshooting
HeI	Neutral helium
HeII	Singly ionized helium
K	Unit Kelvin
L_k	Luminosity interior to cell face k
m_k	Mass interior to cell face k
$M_\odot$	Solar Mass
M_{ZAMS}	Mass at ZAMS
P_k	Pressure at cell k
r_k	Radius interior to cell face k
$R_\odot$	Solar Radius
t	Time
T_{eff}	Effective Temperature
T_k	Temperature at cell k

v_k	velocity interior to cell face k
Z	Metallicity
$X_{i,k}$	Mass fraction of element i at cell k
α_{MLT}	Efficiency parameter of MLT formulation
$\alpha_{P,0}$	Local pressure scale height
Γ	Coulomb Coubling parameter
ε_{grav}	Rate of change of gravitational energy
ε_{nuc}	Nuclear energy
η	Mass loss efficiency parameter
κ	Opacity
ρ_k	Densitity at cell k
σ_k	Lagrangian diffusion coeficient at cell k
F_k	Mass flow rate at cell k

Contents

1 INTRODUCTION . . . 23
1.1 Stellar Evolution . . . 23
1.2 White Dwarf Stars . . . 25
1.3 The Evolution of Stellar Models . . . 29
1.4 Objective . . . 34

2 NUMERICAL METHODS . . . 35
2.1 Evolutionary Code . . . 35
2.2 Input Physics . . . 36
2.2.1 Evolution prior to the white dwarf stage . . . 37
2.2.2 Evolution on the Cooling Sequence . . . 38

3 NEW FULL EVOLUTIONARY SEQUENCES FOR H AND HE ATMOSPHERE MASSIVE WHITE DWARFS . . . 41
3.1 Evolutionary Sequences . . . 41
3.2 Carbon Flame and Core Composition . . . 45
3.3 Initial to Final Mass relation . . . 47
3.4 Chemical Abundance in the Cooling Sequence . . . 49
3.5 Cooling Times . . . 50
3.6 Mass Radius Relation . . . 53
3.7 Conclusion . . . 54

4 CONCLUSION . . . 57

BIBLIOGRAPHY . . . 59

APPENDIX A – SUBMITTED PAPER . . . 71

1 Introduction

1.1 Stellar Evolution

Stars are born from massive gas clouds which collapse due to self gravity. In the contraction, gravitational potential energy is released and partly transformed into thermal energy, heating the matter which compose the protostar. If in virial equilibrium, half of the potential energy is released as radiation. Eventually the central region reaches enough density and temperature to start burning hydrogen into helium at the core. The released energy from nuclear reaction balances the gravitational contraction and the star enters the *Zero Age Main Sequence* (ZAMS). If the protostar mass is lower than 0.08 $M_\odot$, it will never reach the threshold temperature ($T \sim 6 \times 10^6$ K) to start the hydrogen burning. In this case, the matter becomes degenerate and its pressure balances the gravitational contraction, which prevents further heating and forming a brown dwarf.

The stage where the star first ignites hydrogen is known as ZAMS and the entire process of core H-burning is known as *Main Sequence* (MS), the longest stage in stellar evolution, prior to the last compact state. In the MS, the star is in hydrostatic equilibrium due to the balance between thermonuclear energy and gravitational contraction. For larger initial masses, the release of energy from nuclear reactions is larger, resulting in larger luminosities and shorter lifetime in the MS. For example, a 20 $M_\odot$ initial mass star has a MS lifetime of $\sim 6 \times 10^6$ years while a 1 $M_\odot$ star has a life time of $\sim 10^{10}$ years. When hydrogen is extinguished at the core, the stars are left with a helium core surrounded by a layer of hydrogen burning. At this stage the MS is over.

After the end of the MS the star core contracts and the envelope expands. This expansion reduces the effective temperature and the star enters the *Red Giant Branch* (RGB). In this stage the star increases its luminosity at almost constant temperatures. The mass of the inert helium core increases as the star burns hydrogen at the surrounding layers. This increase in core mass leads to more contraction and larger temperatures. When the core temperature reaches $\sim 10^8$ K the star starts to burn helium into carbon and oxygen. This stage is known as *Horizontal Branch* (HB).

The subsequent evolutionary stages after the HB depend on the metallicity and stellar mass at the beginning of the MS. Hence, for solar metallicity, the stars can be divided in three groups: low mass stars, with initial masses between 0.08 $M_\odot$ and ~ 12 $M_\odot$; intermediate mass stars with masses in a range of ~ 12 to 25 $M_\odot$; and massive stars with masses greater than ~ 25 $M_\odot$. A schematic view of the three possibles paths of stellar evolution is shown in figure 1.

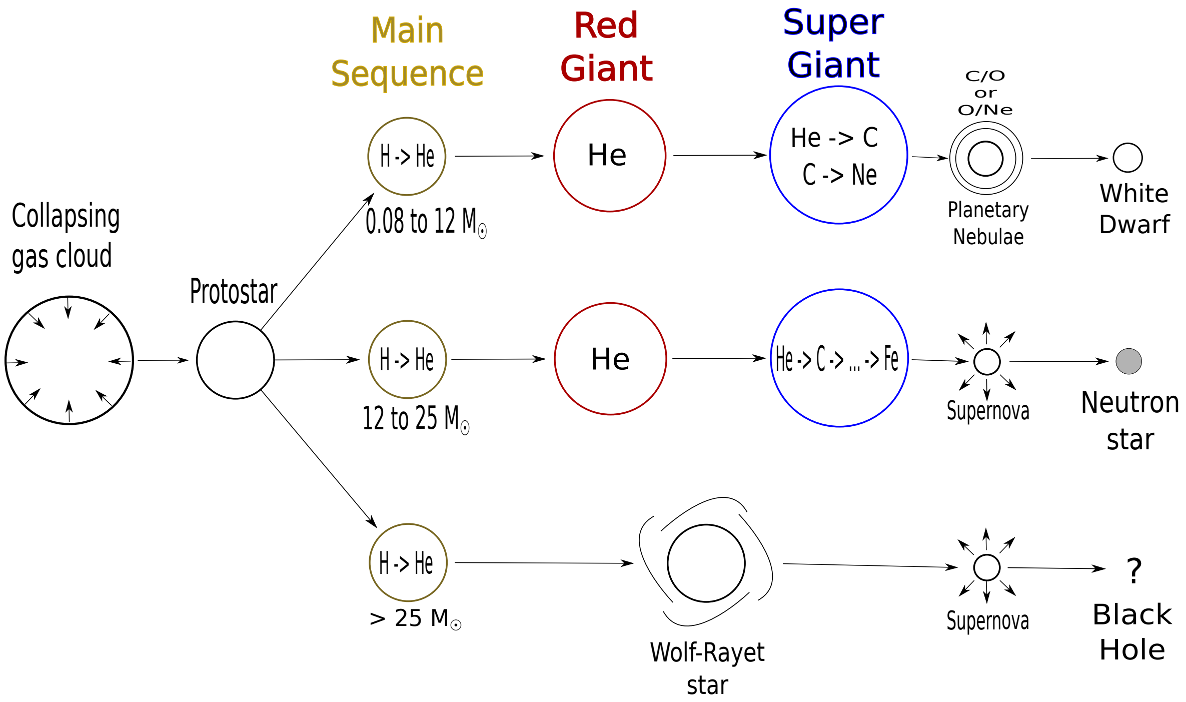
Main Sequence
Red Giant
Super Giant
Collapsing gas cloud
Protostar
H -> He
0.08 to 12 M☉
He
He -> C
C -> Ne
C/O or O/Ne
Planetary Nebulae
White Dwarf
H -> He
12 to 25 M☉
He
He -> C -> ... -> Fe
Supernova
Neutron star
H -> He
> 25 M☉
Wolf-Rayet star
Supernova
?
Black Hole

Figure 1 – A Scheme of the evolutionary paths a single star may follow, depending on its mass.

After core He burning, the low mass stars develop a degenerate core of carbon and oxygen surrounded by a layer of helium burning. On top of the helium layer the star still has a hydrogen burning layer. As there are no nuclear reactions in the core, the core contracts and the regions between the burning layer expand. Thus, the envelope expands and the star enters the *Asymptotic Giant Branch* phase (AGB), reaching higher luminosities. In our models, stars with initial masses $M_{ZAMS} < 9\ M_\odot$ the core never reaches temperature high enough to burn carbon ending as a carbon/oxygen core. This happens because the carbon/oxygen core density become high enough to form a degenerate gas, and the neutrinos produced in the core are radiated away without interacting with matter, reducing the temperature in the core. Stars with initial masses of $M_{ZAMS} = 9 \sim 12\ M_\odot$ burn carbon resulting in a core composed of oxygen/neon or oxygen/neon/magnesium for the more massive cases. At the end of the AGB, the He-burning layer become unstable and the star undergoes a series of thermal pulses. As the evolution proceeds through the AGB, the core mass increases due to the He-burning on the surrounding layer. Also, the mass loss due to thermal pulses and radiation pressure expels almost the entire envelope together with most part of the hydrogen. This leaves a star with a degenerate core and a small envelope with radius comparable to the Earth size. The ejected material around the remaining star shines for 10 to 100 thousand years as a *Planetary Nebula* due to the absorption of the ultraviolet radiation emitted from the central object, before dissipating into the interstellar medium. The final result is a *White Dwarf* star.

For the intermediate mass stars ($\sim 12 - 25\ M_{\odot}$) case, after the stars burns all helium in the core, the core does not become degenerate. This allows a series of nuclear reaction, from carbon burning to iron burning, without changing the outer layers. These series of reactions last for hundreds of years. As a result, the star creates a layered structure, with layers of increasingly heavy elements towards the center of the stars. When the star reaches the iron burning, it stops producing energy from nuclear sources in the core because iron fusion is an endothermic reaction. Thus, the only source of energy is the gravitational contraction, which increases the core temperature and causes the dissociation of the atomic nuclei into protons and neutrons. With increasing density, the protons capture electrons forming neutrons and emitting neutrinos, finally forming a degenerate gas. This gas becomes incompressible and stops the gravitational collapse of the outer layers. As a result, a shock wave is generated, and together with neutrino emission, transfers momentum to the envelope, expelling the outer layer in a *Supernova* (SN) explosion that last for a couple of minutes. The remaining core transforms into a *neutron stars*, with masses of $1.4\ M_{\odot}$ to $\sim 2.2\ M_{\odot}$. The upper limit depends on the equation of state of nuclear matter, still uncertain, on rotation and magnetic field.

Last, stars with initial masses greater than $\sim 25\ M_{\odot}$ became luminous *Wolf-Rayet* stars. As the massive star evolves, the processed material in the core gradually reaches the surface due convection. When a sufficient amount accumulates on the surface, it absorbs almost the entire emitted radiation producing strong winds, with mass loss rates of order $10^{-6} - 10^{-5}\ M_{\odot}/\text{year}$. These winds hide the stars. It is believed that the process occurring in the interior of massive stars are similar to the intermediate mass stars, with the layered structure and iron core leading to a Supernova event. In this case, the mass of the remaining core exceeds the upper mass limit for neutron stars, hence the gravitational contraction is higher than the pressure from the degenerate neutron gas. The contraction of the core leads to a *Black Hole* or total disruption of the star.

The star formation rate is not the same for the entire mass range. According to the *Initial Mass Function*, for each $10\ M_{\odot}$ star that is born, there are ≈ 300 stars with $1\ M_{\odot}$ (Salpeter, 1955). Hence, the white dwarf stars are the most common final stage of stellar evolution.

1.2 White Dwarf Stars

White dwarf stars are the most common final stage of stellar evolution. They are the end product of MS stars with masses up to $5 - 12$ M$_{\odot}$ (García-Berro; Isern; Hernanz, 1997; Poelarends et al., 2008; Siess, 2010; Langer, 2012; Woosley; Heger, 2015; Doherty et al., 2015), depending on metallicity. Considering the upper limit for solar metallicity,

$M = 12\ M_\odot$, the percentage of white dwarf stars in the Galaxy can be calculated by the Salpeter Initial Mass Function (Salpeter, 1955):

$$\int_{0.1}^{12} 0.06M^{-2.35} = \frac{0.06}{1.35}\left(0.1^{-1.35} - 12^{-1.35}\right) = 0.9934 \tag{1.1}$$

hence, the white dwarf stars correspond to 99% of all stars in the Galaxy. Most start their lives as hot cores remnants of a planetary nebulae. Then, as there are no nuclear reactions, the star start to cool. The pressure from the degenerate core balances the gravitational force leading to a final evolution with almost constant radius. The degenerate core is the primary responsible for the curious inversed *Mass-Radius relation* of white dwarfs: Higher masses have lower radii. Also, the core degeneracy in the relativistic regime is responsible for the upper mass limit of white dwarf stars, known as the *Chandrasekhar limit*, with value of $\sim 1.4\ M_\odot$ (Chandrasekhar, 1931). With relativistic corrections and neutron dripping corrections, the upper limit decreases to $1.36\ M_\odot$, but magnetic field and rotation increase it significantly.

The degenerate electrons in the core are excellent heat conductors, making the white dwarf core almost isothermic. In the effective temperature range of $T_{eff} \approx 16\,000 - 8\,000\ K$, where most of the white dwarf stars are found, the core temperature varies from $\sim 2\times10^7\ K$ to $5 \times 10^6\ K$. This temperature gradient creates convective zones on the surface, which regulates the heat transfer from the core to surface, affecting the rate of cooling, increasing the rate when compared to a pure radioactive heat transport. As the white dwarf cools, the gas changes from a gaseous state to liquid and then to solid state. This phase transition to solid is known as *crystallization*, and it releases latent heat during the phase transition, affecting the rate of cooling.

In the recent years, the number of spectroscopically confirmed white dwarf stars has increase to more than $\approx 30\,000$ with surveys like the *Sloan Digital Sky Survey* (SDSS) (Ahn et al., 2014). From the data of the SDSS the mass distribution for white dwarf stars could be calculated. The mass distribution is centered at 0.649 $\mathrm{M}_\odot$ (Kleinman et al., 2013) but presents another peak at 0.811 $\mathrm{M}_\odot$ (Kepler et al., 2015). In some early analysis was discovered that around 20% of all white dwarfs are more massive than 0.8 $\mathrm{M}_\odot$ (Liebert; Bergeron; Holberg, 2005; Kepler et al., 2007) and about 9% have mass $\sim 1.12\ \mathrm{M}_\odot$ (Kepler et al., 2007). Some recent works present a high mass tail on the mass distribution with an excess for masses around $M_{WD} \approx 1.0\ \mathrm{M}_\odot$ (Falcon et al., 2010; Tremblay et al., 2013; Rebassa-Mansergas et al., 2015; Kepler et al., 2016). Figure 2 show a density distribution versus mass for white dwarfs on the SDSS data release 12 (Kepler et al., 2016). In this figure both the central peak around $\sim 0.6\ M_\odot$ and the high mass tail are evident.

White dwarfs with stellar mass in the range $0.4 - 1.05\ M_\odot$ are believed to harbor a carbon-oxygen (C/O) core after central hydrogen and helium burning on earlier stages of evolution. On the other hand, the progenitors of white dwarfs with masses larger than

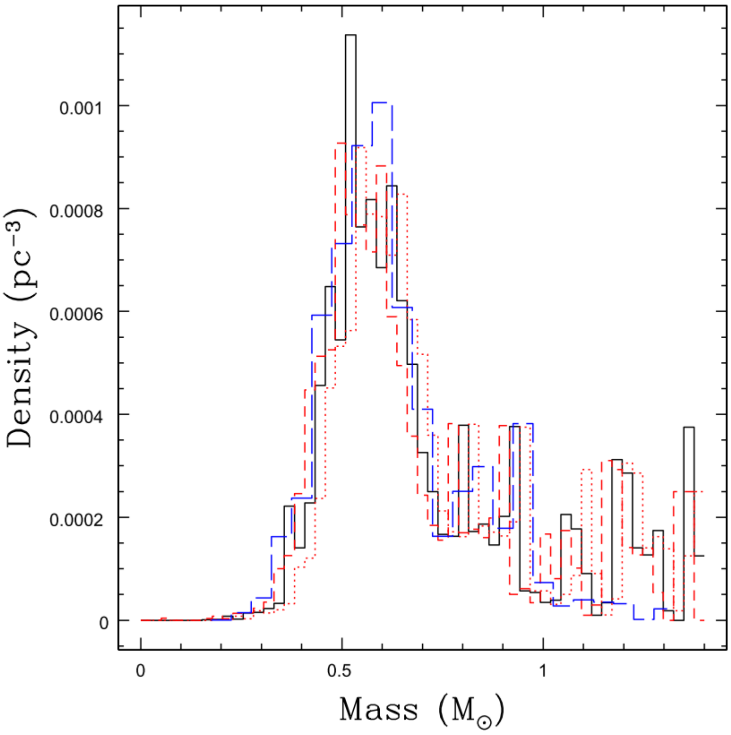

Figure 2 – Histogram for the number density distribution of white dwarfs versus mass on the SDSS data release 12. Red lines show the -1σ and $+1\sigma$ uncertainties. The long dashed blue histogram is the one from Rebassa-Mansergas et al. (2015). Adapted from Kepler et al. (2016).

$\approx 1.05\ M_\odot$ (García-Berro; Isern; Hernanz, 1997; Siess, 2007) should reach temperature high enough to achieve stable carbon burning forming an oxygen-neon (O/Ne) or neon-oxygen-magnesium (Ne/O/Mg) core, depending on if carbon burning ignites off-center or at the center of the star. When carbon burning starts off-center, ignition is followed by an inward propagation of the burning front (hereafter carbon flame). This carbon flame may or may not reach the center. If the flame does not reach the center a hybrid C/O+O/Ne white dwarf will form (Denissenkov et al., 2013; Farmer; Fields; Timmes, 2015), whilst a flame which reaches the center will form a Ne/O/Mg white dwarf. The determination of the mass range for each type of core composition is fundamental to improve our understanding of the populations of massive white dwarf stars.

The white dwarf stars can be divided into two main classes: DA and non-DA types, based on the main component of their atmosphere. The DA spectral class shows a hydrogen rich atmosphere and represent $\simeq 84\%$ of all white dwarfs (e.g. Kepler et al. (2007)) while non-DA's have hydrogen deficient and helium rich atmospheres. The helium-rich white dwarfs are believed to be progeny of PG 1159 stars (McGraw et al., 1979) formed by a Born-Again episode (Schoenberner, 1979; Iben JR. et al., 1983) in which a helium flash occurs during the cooling sequence (i.e. very late thermal pulse) forcing the star to evolve back to the AGB. As a result, this very late thermal pulse burns out all hydrogen left in the atmosphere of the star. The non-DA white dwarfs can be classified by the dominant element in the atmosphere and effective temperature: DO class with strong lines of singly ionized helium (HeII) and effective temperatures of $T_{eff} \approx 45,000 - 200,000$ K, DB class with strong lines of neutral helium (HeI) and $T_{eff} \approx 11,000 - 30,000$ K, and for effective temperatures bellow $T_{eff} \approx 11,000$ K there are DC with no lines, and DQ and DZ types with traces of carbon and metals in their spectra. Along the evolution of a DO type white dwarf, the HeII recombines to form HeI and become a DB white dwarf. The transition from a DO to DB white dwarf ($32\ 000\ K\ < T_{eff} < 45\ 000\ K$) is known as *DB Gap* (Liebert et al., 1986; Liebert; Fontaine; Wesemael, 1987), a region where few objects are observed with a hydrogen deficient atmosphere (Kleinman et al., 2013). Also, the hot DQ type, or white dwarfs with carbon rich atmosphere and $T_{eff} \approx 20\ 000\ K$ are believed to be a cold descendant of PG 1159 stars formed by mixing between the outer He convection zone with the underlying convective carbon intershell at cold temperatures (Dufour et al., 2007; Dufour et al., 2008; Althaus et al., 2009). A scheme of the possible evolutionary paths that a white dwarf may follow is shown in figure 3.

The massive white dwarfs are believed to be formed by mergers of two intermediate mass white dwarfs in binaries systems (Guerrero; García-Berro; Isern, 2004; Lorén-Aguilar; Isern; García-Berro, 2009) or by the evolution of a single, isolated star with initial masses $M_{ZAMS} = 9 \sim 12\ M_{\odot}$ which undergoes a series of carbon flashes (Ritossa; García-Berro; Iben JR., 1999).

The cooling of massive white dwarfs are somewhat different from their low mass counterparts. In particular, massive white dwarfs crystallize at higher luminosities, because of their higher densities, hence releasing latent heat earlier than low mass white dwarfs. Also, the core composition impacts the rate of cooling because the difference in heat capacity of the main elements in the core. A lower heat capacity, as for an O/Ne core, makes a white dwarf cool faster when compared to a C/O core with greater heat capacity (García-Berro; Isern; Hernanz, 1997). The massive white dwarfs are relevant for the understanding of the lower limit of core collapse SN, but also on SN type Ia, when a companion transfer mass to a massive white dwarf which reaches the Chandrasekhar limit.

The study of white dwarf stars has several applications. The age of stellar populations can be obtained by comparisons of theoretical computations with the distribution in the Color-Magnitude Diagram (Hansen et al., 2007; Campos et al., 2016) or from the white dwarf luminosity function (Winget et al., 1987; Bedin et al., 2010; García-Berro et al., 2014). The connection between the properties of progenitor stars and white dwarfs is printed in the Initial-to-Final mass relation (IFMR) which leads to constraints on the upper mass limit that separates white dwarfs progenitors of Type II supernovae (Siess, 2007; Catalán et al., 2008). Also, binaries systems with white dwarfs are believed to produce Type Ia supernovae as result of accretion that exceeds the upper mass limit (e.g. Wang,

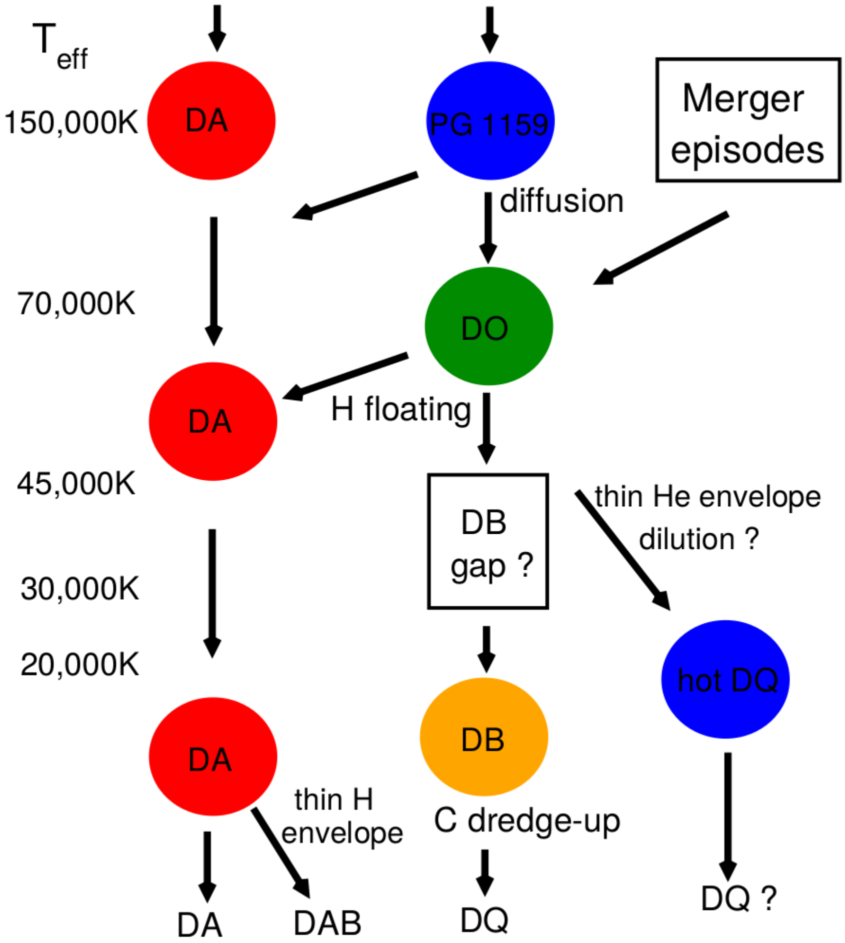
T_eff
150,000K
70,000K
45,000K
30,000K
20,000K
DA
PG 1159
Merger episodes
diffusion
DO
H floating
DA
DB gap ?
thin He envelope dilution ?
hot DQ
DA
DB
thin H envelope
C dredge-up
DA
DAB
DQ
DQ ?

Figure 3 – A scheme of the evolutionary paths a white dwarf may follow. The left column informs the effective temperature. The second column presents the evolution of the most common type of white dwarf (DA spectral type). The DO type may follow different paths, either from a merger event or from a hot and helium, carbon, and oxygen rich PG 1159 star. The PG 1159 stars are also believed to be the progenitors of hot DQ stars. Accretion of metal from interstellar medium or from circumstellar matter by cool helium rich white dwarf may lead to a DZ white dwarf. Adapted from Althaus et al. (2010b).

Podsiadlowski e Han (2017)). Finally, a comparison between models and observations of white dwarfs can enhance the comprehension of the physical properties of high density matter (e.g. Prada Moroni e Straniero (2002), Isern et al. (2010)).

1.3 The Evolution of Stellar Models

In order to understand the main purpose of this dissertation it is necessary to revise the current state of white dwarf modeling, and for this a brief overview of the history of stellar evolution models is required.

The first stellar models to emerge were the work on gaseous spheres bound by their own gravity of Helmholtz, in 1854, and Kelvin, in 1861. Their work used a simplification that the pressure was a function only of the density. This type of models are called *Polytropes*. These models addressed correctly the problem of equilibrium among pressure force and gravity, and energy transport, which at the time was believed to be done only by convection. Later, Lane (1870) developed a theoretical solution for his study of gas spheres and polytropic models. Lane discovered that a self-gravitating gas sphere grows hotter as it loses energy and shrinks. The gravitational energy released is partly radiated and partly is used to increase the star's temperature. This behavior came to be known as *Lane's Law*.

In 1883, A. Ritter who also discovered the heating of contracting bodies, proposed a theory of stellar evolution in which a star begins its life as a diffuse mass which contracts and heats, and after a brief period of fixed temperature it enters a cooling period (Ritter, 1898). During the first decade of the 20th century the stellar models were the polytropes of Lane, Ritter and Emden (1907), which performed detailed work on polytropes. All of those models considered that energy was transported by convection.

The first stellar models to incorporate radiative transport were constructed by Eddington (1916). He based his models on the earlier work of Sampson (1895) and Schwarzschild (1906) who were the first to suppose that radiation was an important mechanism of energy transport in stars. The inclusion of radiative equilibrium complicated the models because it added opacity and a dependency on composition of the star's molecular weight. This was problematic due to the interior composition of stars being unknown at the time. Eddington and others continued to further develop and investigate the stellar evolution theory and in 1924 Eddington derived the *Mass-Luminosity Law* from his theory (Eddington, 1924).

Despite the improvements, the stellar models still lacked an energy source. In 1938, Gamow published a series of model stars assuming that the energy was produced by nuclear reaction, without knowing the details of the mechanism (Gamow, 1938a; Gamow, 1938b). However, Gamow's models did not evolve off the MS. Therefore, he could not explain red giant stars which were known at the time. Also, his models did not obey the Mass-Luminosity law derived by Eddington. It was the work of Öpik (1938) on red giants which correctly anticipated some features of nuclear burning and stellar structure. Öpik proposed a scheme of nuclear reactions which initially hydrogen was burnt into helium and later helium burnt into carbon. He also pointed out that the core gradually increased molecular weight and the energy production should shift from the core to a shell, however the properties of his energy process remained unknown. It was only with the work of von Weizsäcker (1938) and Bethe (1939) who independently gave a detailed description of how hydrogen could be converted into helium in the interior of stars. Their work solved the energy supply problem and lead to understanding of MS stars, but red giants remained an unsolved problem.

In 1941, Henrich e Chandrasekhar (1941) discussed an upper limit to the core mass of a star with an isothermal core. As hydrogen is converted into helium, the core contracts and the envelope expands, allowing an explanation for giant stars. The next development in the search for red giant models was the work done by the Brazilian physicist Mario Schoenberg and the Indian physicist S. Chandrasekhar (Schönberg; Chandrasekhar, 1942). They asserted that nuclear reactions made the helium core, increasing its molecular weight to greater values than the envelope. They also explored the idea of a maximum mass for isothermal core, and noted that in massive stars the core might grow to values greater than this limit, leading to a core collapse and explosion. The first models accepted as red giants were the work of Oke e Schwarzschild (1952) and Hoyle e Schwarzschild (1955), which created evolutionary sequences that moved from the MS to the RGB. They considered that the gradual increase in core mass due to conversion of hydrogen into helium at the core boundary lead a contraction of the core, which rises the core temperature causing an increase in the star's radius. However, their models did not increase significantly the star's luminosity.

It is important to note that all models discussed until now were generated one at the time by hand-operated office desk calculators. These models allowed only a snap-shot view of a star's history. The first stellar models constructed using a digital computer were performed in 1955 by L. Henyey and colaborators (Henyey; Lelevier; Levée, 1955). The speed and power of the computers allowed entire sequences of models to be computed. In 1959, Henyey et al. (1959) improved the method to compute evolutionary sequences by introducing a finite-difference scheme to solve the structure equations. This allowed to construct entire evolutionary sequences rapidly. This improvement became known as *Henyey style code* and is the base of all modern evolutionary codes used nowadays.

Meanwhile, in 1957, Margaret Burbidge, Geoffrey Burbidge, Willian A. Fowler and Fred Hoyle published a work entitled "Synthesis of the Elements in Stars" (Burbidge et al., 1957). This is a landmark paper on the origin of the chemical elements. The paper became known as the *B^2FH paper*, named after the initial of the authors.

Despite the improvements in model computations, understanding the helium ignition in the core and its consequences were still a problem. Also, in those early days of computers, the time it took to calculate the evolution of the helium ignition was longer than the actual process in the star. The burst of energy caused by the ignition of helium was studied in the early 1960s and became known as *Helium Flash* (Härm; Schwarzschild, 1961), although the explosive ignition of nuclear burning in degenerate gases was discovered by L. Mestel in 1952 in his work on white dwarfs (Mestel, 1952).

The first attempt to calculate stellar models on the HB was done by Obi (1957). He built models with helium burning in the core and hydrogen burning in a surrounding shell. The resulting stars fell along the horizontal branch. Over the next 10 years, Hayashi and collaborators studied stellar models of these advanced stages (Hayashi; Hōshi; Sugimoto, 1962).

Work proceeded with a series of detailed works done by Iben, showing how different initial masses evolve from the MS through helium burning (Iben JR., 1965a; Iben JR., 1965b; Iben JR., 1966a; Iben JR., 1966c; Iben JR., 1966b; Iben JR., 1967; Iben, 1967). Also, Faulkner e Iben Jr. (1966) constructed stellar models assuming either mixing or non-mixing and showed that unmixed models reproduced HB stars reasonably well. Thus, stellar models ranging from the MS to the HB and even evolving toward the white dwarf region were already present.

From the 1970s and onward, new groups and codes focusing on specific evolutionary stages or evolutionary libraries started to appear. On the early 1970s were developed the Eggleton's stellar evolutionary code for low mass stars evolution (Eggleton, 1971) and the `WDEC` code for white dwarfs cooling and pulsations (Lamb; van Horn, 1975; Bischoff-Kim; Montgomery, 2018). The `WDEC` code was one of the first evolutionary codes focused only on white dwarf evolution. It constructed stellar models of white dwarfs on top of the cooling sequence and evolved along the cooling curve, computing their pulsations. However, the code does not evolve the chemical profile, which impacts the cooling time. The `KEPLER` evolutionary code was developed on the late 1970s to study the complete evolution of massive and supermassive stars, all major classes of supernovae, hydrostatic and explosive nucleosynthesis, and x- and gamma-ray bursts on neutron stars and white dwarf (Weaver; Zimmerman; Woosley, 1978).

In the 1990s grids of stellar models were produced. The Geneva group released a series of stellar evolutionary models for low and supermassive stars, in a range of metallicities $Z = 0.001 - 0.1$. Their grids of models are known as the *Geneva Grid of Stellar Evolution Models* (Schaller et al., 1992; Schaerer et al., 1993; Meynet et al., 1994; Charbonnel et al., 1996; Mowlavi et al., 1998). The *Yale Rotating Stellar Evolution Code* (Guenther et al., 1992) developed for solar models served as base to the *Dartmouth Stellar Evolution Program* - `DSEP` (Chaboyer et al., 2001) used for isochrones grids and tracks for open cluster, metal-rich and metal-poor stars, low mass stars and stellar population models (Dotter et al., 2008). More recently, The *a Bag of Stellar Tracks and Isochrones* - `BaSTI` project published tracks and isochrones for scaled solar models, white dwarf cooling sequences and extremely metal-poor and super-metal-rich models for population synthesis studies (Pietrinferni et al., 2004; Hidalgo et al., 2018). Also, the *Nugrid* project (Pignatari et al., 2016; Ritter et al., 2017) and the *MIST* project (Dotter, 2016; Choi et al., 2016) built a set of stellar evolution sequences, providing tracks and isochrones for a range of masses and metallicities. Unfortunately, the *BaSTI* and the *Nugrid* projects only evolve until the first thermal pulses on the AGB phase, thus not producing full evolutionary white dwarf models. The *MIST* project evolve full evolutionary models for low mass white dwarfs ($M_{WD} \lesssim 1\ M_{\odot}$), but the massive ones ($M_{WD} \gtrsim 1\ M_{\odot}$) are only evolved until the

AGB.

The next evolutionary code developed for white dwarf models was the `LPCODE` (Althaus et al., 2003; Althaus et al., 2005), developed in the early 2000s. It evolves full evolutionary models, from ZAMS to the cooling sequence. Later, a code for linear, adiabatic and non-radial stellar pulsation was added to `LPCODE` (Córsico; Althaus, 2006). It has been extensively used to produce low mass white dwarf models and to compute their pulsations. Some recent work were published by Althaus et al. (2009), Althaus et al. (2010a), Romero et al. (2012), Althaus, Miller Bertolami e Córsico (2013), Romero et al. (2013), Salaris, Althaus e García-Berro (2013), Romero, Campos e Kepler (2015). However, the `LPCODE` has a nuclear network from ^{1}H to ^{22}Ne and nuclear reactions considering H and He burning, thus it does not compute the nuclear reactions to produce elements heavier than neon, either allowing the computations of massive white dwarfs models with core composed O/Ne/Mg.

The massive white dwarfs models started to be studied in more details in the work of Garcia-Berro e Iben (1994) where they calculate the formation of an O/Ne/Mg core for a 10 $M_\odot$ star evolved until the AGB phase. Usually, the massive white dwarfs are studied in the context of core collapse SN progenitors and carbon burning, hence many sequences are evolved until the AGB (Ritossa; Garcia-Berro; Iben JR., 1996; Iben JR.; Ritossa; García-Berro, 1997; García-Berro; Ritossa; Iben JR., 1997; Siess, 2006; Siess, 2010; Denissenkov et al., 2013; Woosley; Heger, 2015; Farmer; Fields; Timmes, 2015; Doherty et al., 2015). When a cooling sequence for a massive white dwarf was computed by García-Berro, Isern e Hernanz (1997), their models started with fixed composition at the top of the cooling sequence evolving until low luminosities. The most recent cooling tracks for massive white dwarfs are the tracks from Althaus et al. (2007) where they used the same artificial method as García-Berro, Ritossa e Iben Jr. (1997). Also, the recent works on massive white dwarfs from Siess (2010), Doherty et al. (2015) and Woosley e Heger (2015) present evolutionary sequences until the AGB, without computing the cooling tracks. The passage from AGB to the white dwarf stage is still a problem in stellar evolutionary models that needs further investigation.

One of the most recent codes is the *Modules for Experiments in Stellar Astrophysics* - `MESA` code (Paxton et al., 2011; Paxton et al., 2013; Paxton et al., 2015; Paxton et al., 2018), a suite of open source libraries for a wide range of applications in computational stellar astrophysics. In the context of white dwarfs, it has been used to compute extremely low-mass white dwarfs (Istrate et al., 2016; Istrate; Fontaine; Heuser, 2017; Sun; Arras, 2017), hybrid C/O/Ne white dwarfs(Jones et al., 2013; Denissenkov et al., 2013; Chen et al., 2014; Farmer; Fields; Timmes, 2015; Brooks et al., 2017b), accreting white dwarf binaries (Brooks et al., 2016; Wang; Podsiadlowski; Han, 2017; Schwab; Bildsten; Quataert, 2017; Brooks et al., 2017a), and white dwarf isochrones (Dotter, 2016; Choi et al., 2016;

Pignatari et al., 2016; Ritter et al., 2017). For a complete overview of the history of stellar evolution theory and models until the 1970s the reader is refereed to Arny (1990).

1.4 Objective

In order to derive properties for white dwarf stars, two main ingredients are necessary: observations and theoretical models. Stellar models of full evolutionary sequences have a range of applications. From grids of stellar models a table of isochrones may be built. In the field of stellar astrophysics, stellar models can be used as a reference either in the study of individual binaries or in the study of the stellar populations of individual clusters. The nucleosynthesis resulting from stellar evolution and the yields of the matter expelled by the pre-white dwarf stages, either in winds or in planetary nebulae, are basic ingredients for studying the chemical evolution of galaxies.

In the literature, several evolutionary models for low and intermediate mass white dwarf stars can be found. On the other hand, there is a lack of full evolutionary models for massive white dwarfs. The sequences for massive white dwarfs in the literature only compute the evolution until the AGB, never achieving the white dwarf stage. Also, the entire chemical profile for the model stars are rarely published, only parts of it, decreasing the confidence in these models. Even more, the cooling tracks found in literature for high mass white dwarf does not consider the full evolutionary history of the progenitors.

In the mass range of the massive white dwarfs is expected to cover central compositions of C/O and O/Ne/Mg. Also, depending on if the star experiences an inward propagation of carbon burning that does not reach the center, a hybrid core composition of C/O-O/Ne may form. The mass range for those core compositions are dependent on the evolutionary code and input physics applied. Again, the works found in literature about carbon burning and the evolution of super asymptotic giant branch stars, only evolve the sequences until the AGB, never producing white dwarfs properly, and never presenting the entire chemical profile for the hybrids white dwarfs. Furthermore, the discovery of massive and ultramassive pulsating white dwarfs (Hermes et al., 2013; Castanheira et al., 2013; Curd et al., 2017) has raised the necessity for evolutionary sequences with reliable chemical structure to study and understand the properties of those massive pulsators.

With that in mind, this dissertation is intended to fill the gap due to the lack of full evolutionary sequences for massive white dwarfs, computed from the zero age main sequence to the white dwarf cooling sequence, considering the full evolutionary history of the progenitors to build reliable chemical profiles, cooling sequences, initial to final mass relation and mass-radius relationship. Also, an emphasis is given to the chemical profile along the cooling sequence, together with the mass range for the different core compositions, including the hybrid type of white dwarfs.

2 Numerical Methods

In this chapter it is presented a description of the numerical code used to compute the evolutionary sequences in this dissertation. First, the evolutionary code MESA will be described followed by a discussion of the input physics applied to the code.

2.1 Evolutionary Code

The numerical simulations presented at this dissertation were performed using the *Modules for Experiments in Stellar Astrophysics* - MESA code (Paxton et al., 2011; Paxton et al., 2013; Paxton et al., 2015; Paxton et al., 2018), a suite of open source, robust, efficient, thread-safe libraries for a wide range of applications in computational stellar astrophysics. It is a one-dimensional stellar evolution module which combines many of the numerical and physics modules for simulations of a wide range of stellar evolution scenarios, ranging from very low mass to massive stars, including advanced evolutionary phases. The code solves the fully coupled structure and composition equations simultaneously, using adaptive mesh refinement and time-step controls. It provides equation of state, opacity, nuclear reaction rates, element diffusion data, and atmosphere boundary conditions. Each module is constructed as a separate `Fortran 95` library with its own explicitly defined public interface to facilitate independent development.

The MESA evolutionary code has been extensively used to perform calculations of extremely low-mass white dwarfs (Istrate et al., 2016; Istrate; Fontaine; Heuser, 2017; Sun; Arras, 2017), hybrid C/O/Ne white dwarfs and Type Ia SN progenitors (Jones et al., 2013; Denissenkov et al., 2013; Chen et al., 2014; Farmer; Fields; Timmes, 2015; Brooks et al., 2017b), accreting white dwarf binaries with C/O core (Brooks et al., 2016; Wang; Podsiadlowski; Han, 2017) and O/Ne core (Schwab; Bildsten; Quataert, 2017; Brooks et al., 2017a), white dwarf isochrones (Dotter, 2016) and set of sequences covering the white dwarf mass range (Choi et al., 2016; Pignatari et al., 2016; Ritter et al., 2017).

The MESA code is a Henyey style code (Henyey et al., 1959) with automatic mesh refinement, analytic Jacobians, and coupled solution of the structure and composition equations. The code builds one-dimensional, spherically symmetric models by dividing the structure into cells. For a cell k, the cell mass-averaged variables are density ρ_k, temperature T_k, and mass fraction vector $X_{i,k}$. The boundary variables are mass interior to the face (boundary) m_k, radius r_k, luminosity L_k, and velocity v_k. In addition to these basic variables, composite variables are calculated for every cell and face, such as nuclear energy ε_{nuc}, opacity κ, Lagrangian diffusion coefficient σ_k, and mass flow rate F_k. All variables are evaluated at time $t + \delta t$. Figure 4 shows a scheme of cell and face variables.

The code solves the mass conservation equation, hydrostatic equilibrium, energy transport and energy conservation in the following form:

$$\ln r_k = \frac{1}{3} \ln \left[r_{k+1}^3 + \frac{3}{4\pi} \frac{\mathrm{d}m_k}{\rho_k} \right] \tag{2.1}$$

$$P_{k-1} - P_k = \overline{\mathrm{d}m_k} \left[-\frac{Gm_k}{4\pi r_k^4} - \frac{a_k}{4\pi r_k^2} \right] \tag{2.2}$$

$$T_{k-1} - T_k = \overline{\mathrm{d}m_k} \left[\nabla_{T,k} \left(\frac{\mathrm{d}P}{\mathrm{d}m} \right)_{\mathrm{hydrostatic}} \frac{\overline{T_k}}{\overline{P_k}} \right] \tag{2.3}$$

$$L_k - L_{k+1} = \mathrm{d}m_k \left(\varepsilon_{nuc} - \varepsilon_{v,\mathrm{thermal}} + \varepsilon_{\mathrm{grav}} \right) \tag{2.4}$$

where P_k is pressure at cell k, $\overline{\mathrm{d}m_k} = 0.5(\mathrm{d}m_{k-1} + \mathrm{d}m_k$, a_k is the Lagrangian acceleration at face k, $\nabla_{T,k} = \mathrm{d}\ln T / \mathrm{d}\ln P$ at face k, $\overline{T_k}$ and $\overline{P_k}$ are the mass averaged values of temperature and pressure between cell k and $k-1$, $\varepsilon_{v,\mathrm{thermal}}$ is the specific thermal neutrino-loss rate and $\varepsilon_{\mathrm{grav}}$ is the specific rate of change of gravitational energy. This formulation was chosen to enhance numerical stability.

The chemical composition is calculated considering both the nuclear reaction ($\mathrm{d}X_{\mathrm{burn}}$) and the mixing ($\mathrm{d}X_{\mathrm{mix}}$) caused by convection. The equation for mass fraction $X_{i,k}$ for species i in cell k is given by:

$$X_{i,k}(t + \delta t) - X_{i,k}(t) = \mathrm{d}X_{\mathrm{burn}} + \mathrm{d}X_{\mathrm{mix}} \tag{2.5}$$

$$= \frac{\mathrm{d}X_{i,k}}{\mathrm{d}t} \delta t + (F_{i,k+1} - F_{i,k}) \frac{\delta t}{\mathrm{d}m_k} \tag{2.6}$$

where $\mathrm{d}X_{i,k}/\mathrm{d}t$ is the rate of change from nuclear reactions and $F_{i,k}$ is the mass of species i flowing across face k:

$$F_{i,k} = (X_{i,k} - X_{i,k-1}) \frac{\sigma_k}{\overline{\mathrm{d}m_k}} \tag{2.7}$$

The code does not require the structure equations to be solved separately from the composition equations. It simultaneously solves the full set of coupled equations for all cells from the surface to the center by using a Newton-Raphson solver.

In this dissertation it was used the MESA version `r8845` which has improvements in the computations of opacities, week reaction rate and binaries mass accretion (Paxton et al., 2018). The code was used in all phases of evolution for the sequences presented in this dissertation, both for the white dwarf stage and for the previous stages of evolution for the progenitor stars.

2.2 Input Physics

In this section we describe the physical aspects and numerical choices made for the computations of all evolutionary sequences in this dissertation, both for the white dwarf

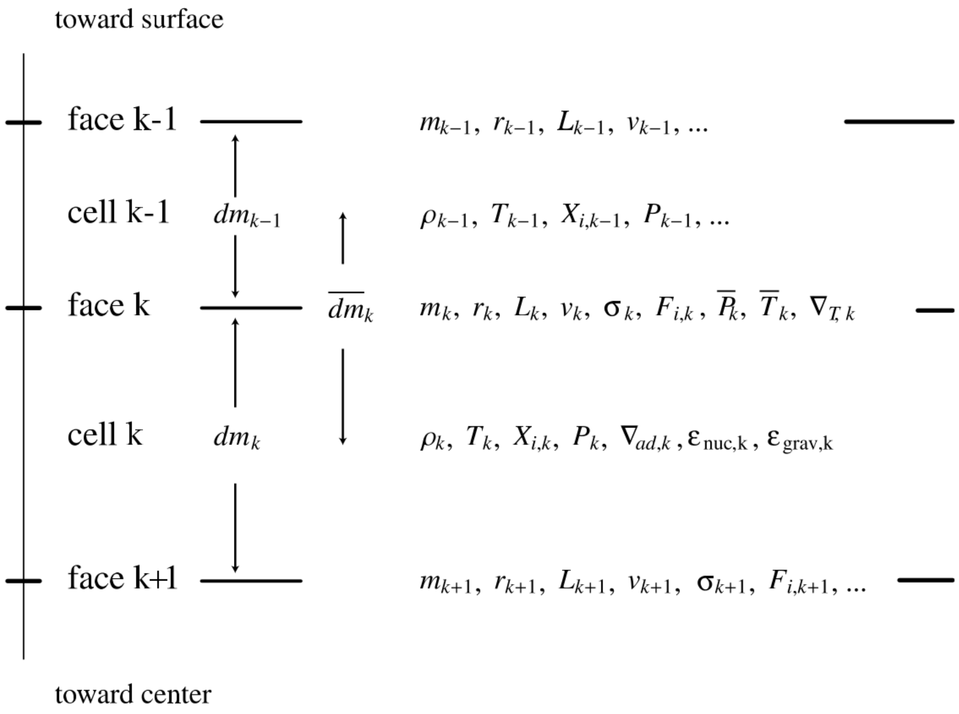
toward surface
face k-1
cell k-1
face k
cell k
face k+1
toward center
dm_{k-1}
$\overline{dm}_k$
dm_k
m_{k-1}, r_{k-1}, L_{k-1}, v_{k-1}, ...
ρ_{k-1}, T_{k-1}, $X_{i,k-1}$, P_{k-1}, ...
m_k, r_k, L_k, v_k, σ_k, $F_{i,k}$, $\overline{P}_k$, $\overline{T}_k$, $\nabla_{T,k}$
ρ_k, T_k, $X_{i,k}$, P_k, $\nabla_{ad,k}$, $\varepsilon_{\rm nuc,k}$, $\varepsilon_{\rm grav,k}$
m_{k+1}, r_{k+1}, L_{k+1}, v_{k+1}, σ_{k+1}, $F_{i,k+1}$, ...

Figure 4 – A scheme of how MESA computes its cell and face (boundary) variables. Adapted from Paxton et al. (2011).

stage and for the previous stages of evolution for the progenitor stars.

2.2.1 Evolution prior to the white dwarf stage

On the evolutionary phases prior to the cooling sequence we considered the nuclear network `co_burn_plus.net` which has 16 elements from hydrogen to silicon, ^{1}H, ^{3,4}He, ^{12,13}C, $^{13-15}$N, $^{16-18}$O, ^{19}F, ^{20,22}Ne, ^{24}Mg, and ^{28}Si. This network has 67 nuclear reactions, including pp-chain, CNO cycle, triple-alpha and some auxiliary reactions. We used JINA reaclib (Cyburt et al., 2010) with electron screening factors for thermonuclear reactions from Graboske et al. (1973) and DeWitt, Graboske e Cooper (1973) for weak and intermediate screening, and Alastuey e Jancovici (1978) for the strong screening regime. Plasma parameters are those from Itoh et al. (1979). The energy-loss rates including the derivatives from thermal neutrinos are from Itoh et al. (1996). The equation of state (EOS) is based on the OPAL EOS tables (Rogers; Nayfonov, 2002) including the SCVH tables (Saumon; Chabrier; van Horn, 1995) for lower temperatures and densities and the HELM (Timmes; Swesty, 2000) and PC (Potekhin; Chabrier, 2010) EOS for higher temperatures and densities.

Convection was considered using the Ledoux criterion, which takes into account the composition gradient, along with the Cox implementation of MLT (Cox; Giuli, 1968) with a mixing length free parameter $\alpha_{MLT} = 2$. The diffusion and gravitational settling in MESA are calculated by solving the equations from Burgers (1969) with coefficients of

Thoul, Bahcall e Loeb (1994). In the overshoot region MESA treats convective mixing as a time-dependent diffusion process, with a diffusion coefficient given by,

$$D_{OV} = D_{\mathrm{conv},0} \exp -\frac{2z}{f\lambda_{P,0}} \tag{2.8}$$

where $D_{\mathrm{conv},0}$ is the MLT derived diffusion coefficient at the convective boundary, z is the distance from the convective boundary, $\lambda_{P,0}$ is the local pressure scale height and f is the adjustable parameter (Herwig, 2000), which can have different values at the upper and lower convective boundaries for H-burning, He-burning, metal-burning (i.e all burning regions that are not H or He-burning) and non-burning convection zones. Due to convergence issues, overshooting was only considered for the lower boundary of metal-burning convective region with parameters set to `overshoot_f_below_burn_z_shell` = 0.1 and `overshoot_f0_below_burn_z_shell` = 0.01. The mixing in regions unstable to Schwarzschild but stable to Ledoux is treated by semiconvection (Langer; Fricke; Sugimoto, 1983) using the dimensionless efficiency parameter $\alpha_{sc} = 0.01$. Thermohaline mixing (Ulrich, 1972; Kippenhahn; Ruschenplatt; Thomas, 1980) is also considered with efficiency parameter set to $\alpha_{th} = 2$. For details in the implementation of semiconvection and thermohaline mixing the reader is referred to section 4 of Paxton et al. (2013).

Mass loss was considered during the giant phases, i.e. RGB and AGB. We used the mass loss formula from Reimers (1975) with $\eta = 0.1$ during RGB, followed by the Bloecker (1995) scheme with $\eta = 10$ on the AGB. The opacity tables are those from OPAL type 2 (Iglesias; Rogers, 1996) for enhanced C/O variations in composition.

2.2.2 Evolution on the Cooling Sequence

White dwarf stars are expected to undergo crystallization as a result of strong Coulomb interactions in their dense interiors (van Horn, 1968). The transition occurs when the energy of the Coulomb interaction between neighboring ions is much larger than their thermal energy. The ratio between these two contributions can be expressed as a coupling parameter $\Gamma = \bar{Z}^2 e^2 / a_i k_B T$ where $\bar{Z}$ is the average ion charge, a_i is the mean ion spacing, e is the electron charge, k_B is the Boltzmann constant and T is temperature. Crystallization for pure oxygen plasma begins when $\Gamma \approx 175$ (Van Horn, 1969). The onset of crystallization also depends on the adopted phase diagram. Near the crystallization limit ($\Gamma \sim 175$) MESA uses the Potekhin e Chabrier (2010) equation of state (PC EOS) which accounts for the thermodynamics of crystals. By default, MESA changes from HELM EOS to PC EOS when the Coulomb coupling parameter $\Gamma > 80$ and considers a mixture of solid and liquid for $\Gamma_i = 150$ and a full crystal when $\Gamma_{full} = 175$. Those values were obtained by Potekhin e Chabrier (2010). Results from the asteroseismological analysis performed by Romero et al. (2013) indicates that the azeotropic type phase diagram from Horowitz, Schneider e Berry (2010) (see also Schneider et al. (2012), Hughto et al. (2012))

better represents the crystallization on white dwarfs cores. Hence, it was modified the values for the coupling constant Γ to $\Gamma_i = 215$ and $\Gamma_{full} = 220$ in our computations. This modification had to be done on the file `pc_eos.f` located inside MESA `eos` module. Until MESA version r8845 used in this work there was not an option to control those parameters.

The diffusion and gravitational setting routine `diffusion_use_cgs_solver`, which is better suited for electron degeneracy as reported by Sun e Arras (2017), was not used because of numerical instabilities in the calculations of the chemical profile and convergence problems. Instead, the default diffusion equation from Burgers (1969) was considered. Convection was shut off either due to convergence problems.

3 New Full Evolutionary Sequences for H and He atmosphere massive White Dwarfs

In the work Lauffer, Romero e Kepler (2018) submitted to MNRAS, we explore the evolution of hydrogen-rich (H-atmosphere) and hydrogen-deficient (He-atmosphere) white dwarf stars with masses between 1.012 and 1.307 $M_{\odot}$, and initial metallicity of $Z = 0.02$. The main aspects and results will be described in this chapter, but for an entire discussion the paper is attached at the Appendix A.

3.1 Evolutionary Sequences

We calculated 16 full evolutionary sequences with initial metallicity $Z = 0.02$ and initial mass at the ZAMS between 8.80 and 11.80 $M_{\odot}$. As a result, we obtained white dwarf models with stellar masses ranging from 1.012 to 1.307 $M_{\odot}$. Within this mass range there are two possible outcomes for core compositions, C/O and O/Ne/Mg (García-Berro; Isern; Hernanz, 1997; Siess, 2007). These computations complement at high stellar masses the works of Romero et al. (2012), Romero et al. (2013) who computed C/O core white dwarf sequences with stellar masses below $M_{WD} = 1.050$ M$_{\odot}$. Is important to note that our H and He atmosphere sequences have evolved equally on the stage prior to the cooling sequence, therefore there is no distinction on the evolution previous to the white dwarf stage.

Figure 5 presents a Hertzprung-Russel (HR) diagram for three sequences with initial mass 8.9, 10 and 11 M$_{\odot}$ and final masses of 1.019, 1.11 and 1.22 M$_{\odot}$ in the cooling curve, respectively. Each sequence in this figure has a different core composition as a white dwarf star. The solid, dashed, and dotted lines represent a C/O core white dwarf with $M_{WD} = 1.019$ M$_{\odot}$, an O/Ne core white dwarf with $M_{WD} = 1.11$ M$_{\odot}$ and a Ne/O/Mg white dwarf with $M_{WD} = 1.22$ M$_{\odot}$, respectively. The initial and final masses for all sequences are shown as columns 1 and 2 in table 1. The age when hydrogen was depleted at core (t_H), age when helium is consumed at the center (t_{He}) and progenitor age (age before the cooling sequence, t_i), are listed in Table 1 as columns 3, 4, and 5. From those columns can be seen that all ages decrease as initial masses increase, agreeing with stellar theory.

During the AGB it was used the mass loss scheme of Bloecker (1995) with an efficiency parameter for mass loss of $\eta = 10$, which led to the complete removal of the hydrogen envelope. A different mass loss scheme achieved the same results, removing the hydrogen on the outer layer. Also, a lower value of the mass loss parameter did not allowed further computations, leading to numerical inconsistencies. The method of increasing the

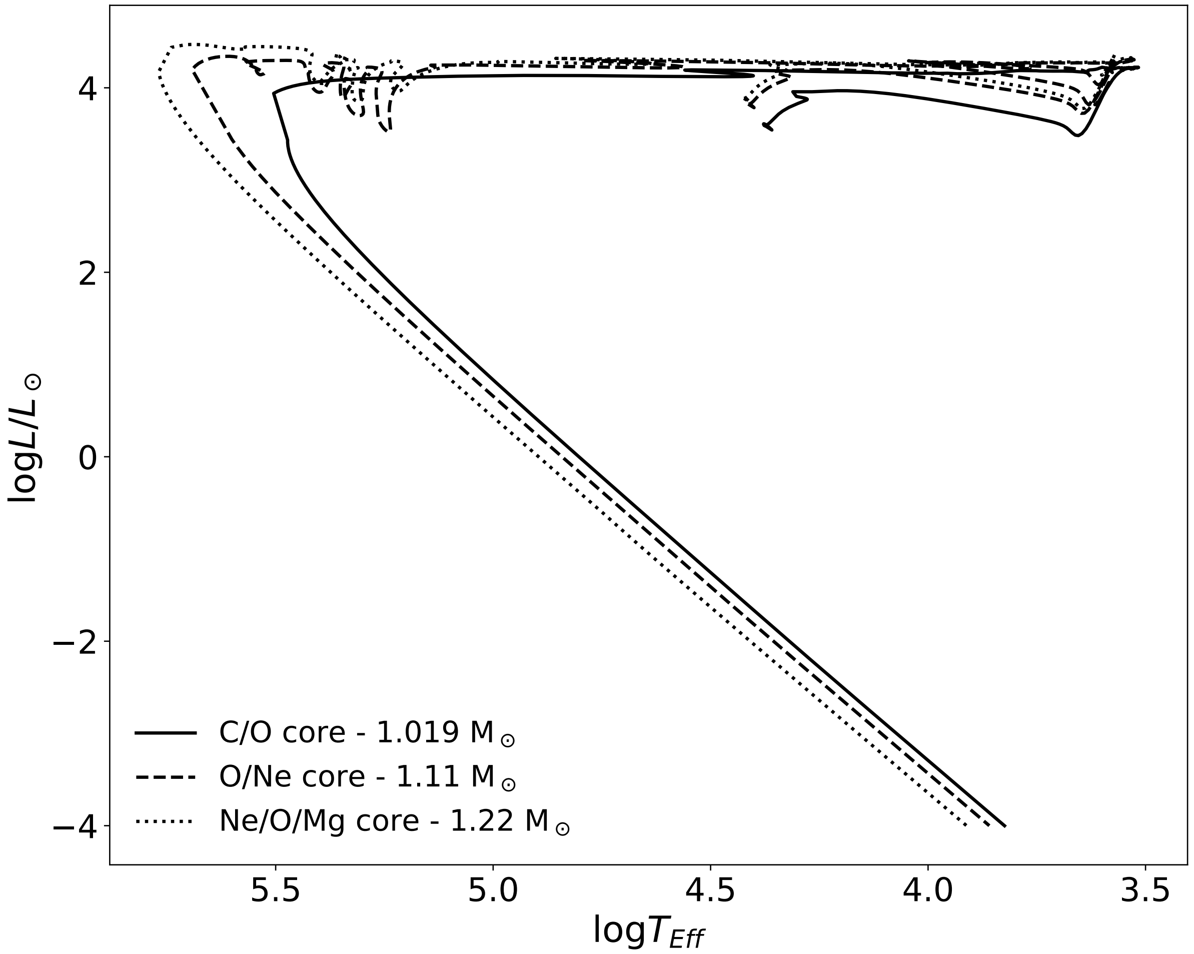

Figure 5 – Evolutionary tracks for three sequences in the HR diagram, with initial masses 8.9 (solid line), 10 (dashed line) and 11 $M_\odot$ (dotted line) and final masses 1.019, 1.11 and 1.22 $M_\odot$, respectively. Each sequence has a different core composition in the cooling curve stage, being C/O, O/Ne and Ne/O/Mg, respectively.

efficiency parameter was discussed by García-Berro, Isern e Hernanz (1997). The authors discussed that models with rapid radiative wind during AGB phase are expected to lose all their hydrogen layer on atmosphere and most of their helium layer, leading to PG 1159 stars. However, real massive white dwarfs are known with H and He envelopes. Thus, to produce hydrogen atmosphere white dwarfs sequences, hydrogen was artificially added at the surface of the models. The procedure was performed at high effective temperature, near the beginning of the cooling sequences, so the transitory effects caused by the artificial procedure are rapidly washed out. The amount of hydrogen added to each sequence was computed by a linear extrapolation to higher stellar masses the results of Romero et al. (2012), Romero et al. (2013).

The sequences with final masses $M_{WD} \geq 1.024\ M_\odot$ experience carbon shell-burning (carbon flame) followed by helium shell-burning in the post-AGB stage. These late shell-burning events are represented as loops at high luminosity and high effective temperature

Table 1 – Mass at ZAMS, white dwarf mass, age when hydrogen is depleted at center (t_H), age when helium is totally consumed at the center (t_{He}), progenitor ages (t_i), effective temperature on crystallization (T_{eff_c}) and age at crystallization (t_{cryst}, accounted from the beginning of the cooling sequence) and cooling time (t_{cool} = age at $T_{eff} = 1 \times 10^4$ K minus t_i) for H and He atmosphere white dwarfs. Ages (t_H, t_{He}, t_i) in units of Myr and crystallization and cooling times on units of Gyr.

					H-atmosphere			He-atmosphere		
M_{ZAMS} [M$_\odot$]	M_{WD} [M$_\odot$]	t_H [Myr]	t_{He} [Myr]	t_i [Myr]	T_{eff_c} [K]	t_{cryst} [Gyr]	t_{cool} [Gyr]	T_{eff_c} [K]	t_{cryst} [Gyr]	t_{cool} [Gyr]
8.80	1.012	24.99	27.87	28.53	13 152	0.870	3.65	13 738	0.839	2.99
8.90	1.019	24.50	27.30	27.94	13 396	0.847	3.69	13 837	0.839	2.99
9.00	1.024	23.88	26.61	27.26	13 584	0.924	4.09	13 634	0.933	3.48
9.20	1.036	22.99	25.73	26.24	14 281	0.810	3.75	14 714	0.756	3.36
9.50	1.064	21.63	24.17	24.63	14 643	0.754	3.13	14 098	0.924	2.85
9.80	1.088	20.49	22.82	23.24	16 585	0.636	3.39	15 858	0.742	2.90
10.00	1.11	19.75	22.03	22.45	19 356	0.415	3.04	17 945	0.538	2.62
10.10	1.125	19.42	21.64	22.03	20 941	0.338	2.65	19 552	0.405	2.34
10.20	1.131	19.06	21.23	21.62	21 963	0.310	2.72	19 815	0.387	2.48
10.30	1.132	18.75	20.87	21.26	22 276	0.296	2.71	20 383	0.376	2.57
10.45	1.147	18.35	20.37	20.74	23 673	0.253	2.52	23 006	0.285	2.21
10.50	1.151	18.19	20.17	20.54	24 001	0.250	2.51	23 339	0.278	2.21
10.80	1.216	17.38	19.31	19.55	29 651	0.183	2.28	29 982	0.181	1.91
11.00	1.22	16.83	18.63	18.88	30 177	0.177	2.25	30 244	0.179	1.90
11.40	1.267	15.86	17.51	17.73	36 584	0.133	1.93	36 808	0.132	1.71
11.80	1.307	15.02	16.55	16.75	44 953	0.098	1.54	45 137	0.099	1.31

on the HR diagram of Figure 5 (upper left region). For sequences with $M_{WD} \geq 1.132 M_\odot$, the late helium shell-burning burns all the helium content in the outer layers, thus helium had to be added on top of those models at the beginning of the cooling sequence using the same procedure as to add hydrogen. The amount of helium to be added was extrapolated from our sequences which had not burnt all helium. The amount of hydrogen and helium for each sequence is presented in columns 3 and 4 of Table 2. Also, an example of two chemical profiles in terms of outer mass fraction at $T_{eff} \approx 80\,000$ K on the cooling curve is shown in Figure 6 for a sequence with stellar mass $M_{WD} = 1.019 M_\odot$. The bottom panel shows the chemical profile for the helium atmosphere case and the top panel presents the chemical profile for the hydrogen atmosphere sequence, after $M_H = 1 \times 10^{-5.7} M_{WD}$ of hydrogen was artificially added to the model. The only difference between the two chemical profiles is the chemical abundance of the outer layers. The core regions remain the same.

The evolutionary sequences were stopped at the point of maximum effective temperature to add helium in sequences with $M_{WD} \geq 1.132\ M_\odot$ and hydrogen to all sequences. From this point, the evolutions were resumed in two separated ways: sequences with only helium in their atmosphere were evolved through the cooling sequence ending as

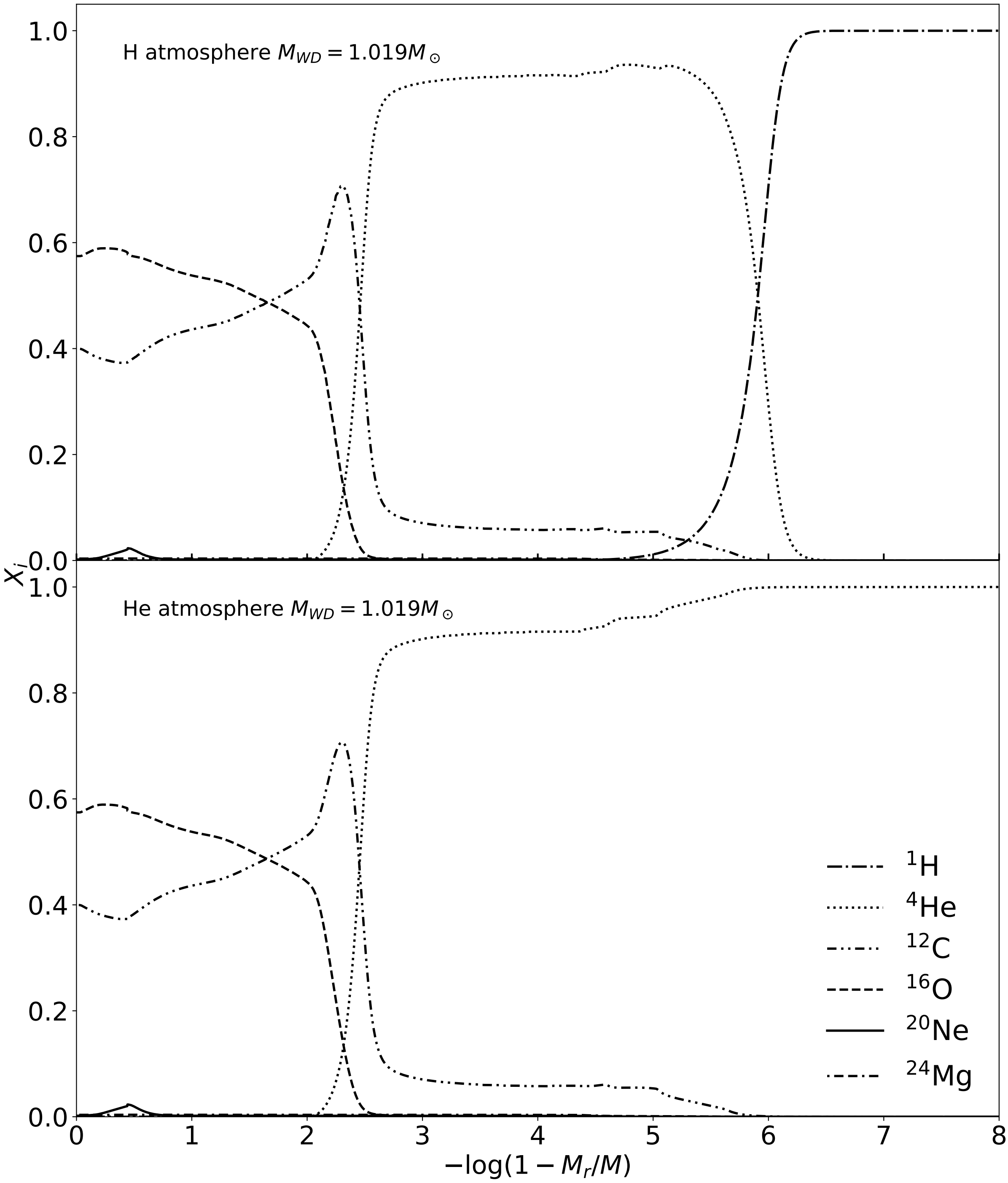

Figure 6 – Example of chemical profile in terms of the outer mass fraction at $T_{eff} \approx 80\,000$ K on the cooling sequence for H atmosphere (top) and He atmosphere (bottom) white dwarf with 1.019 $M_\odot$. Hydrogen had to be added on all sequences due to losses on mass loss phase. The quantities added on each evolution are shown in table 2. This figure show that only the atmosphere of the star was changed. The nuclei composition are identical to both H and He atmosphere sequences.

Table 2 – Values of initial mass at ZAMS (M_{ZAMS}), white dwarfs masses (M_{WD}) and hydrogen content for H-rich sequences and helium contents for both H and He atmosphere sequences. Hydrogen abundances were extrapolated from Romero et al. (2012), Romero et al. (2013). The Helium abundances were extrapolated for sequences with $M_{WD} \geq 1.132$.

M_{ZAMS} [$M_\odot$]	M_{WD} [$M_\odot$]	$-\log M_H/M_{WD}$	$-\log M_{He}/M_{WD}$
8.80	1.012	5.722	2.451
8.90	1.019	5.732	2.466
9.00	1.024	5.740	3.477
9.20	1.036	5.785	3.349
9.50	1.064	6.076	2.958
9.80	1.088	6.365	4.006
10.00	1.110	6.446	3.517
10.10	1.125	6.484	2.447
10.20	1.131	6.498	2.489
10.30	1.132	6.500	2.495
10.45	1.147	6.536	2.597
10.50	1.151	6.547	2.628
10.80	1.216	6.711	3.089
11.00	1.220	6.720	3.116
11.40	1.267	6.838	3.449
11.80	1.307	6.939	3.735

He-atmosphere white dwarfs, and sequences with both hydrogen and helium in their atmosphere were evolved, ending as H-atmosphere white dwarfs. In both cases the evolutions ended at solar luminosity $\log L/L_\odot \approx -4$.

The MESA code considers, as a standard input value, that a mixture of solid and liquid phases occurs for a coupling parameter $\Gamma_i = 150$ while a full crystal structure occurs when $\Gamma_{full} = 175$. However, Romero et al. (2013) calculated white dwarf sequences considering two types of phase diagrams and concluded that the azeotropic type from Horowitz, Schneider e Berry (2010) better represents the crystallization on the nuclei of white dwarfs. Hence, the values of the Γ parameters were modified to $\Gamma_i = 215$ for a liquid/solid coexisting phases and $\Gamma_{full} = 220$ for a full crystal phase, more consistent with the results obtained using the Horowitz, Schneider e Berry (2010) phase diagram.

3.2 Carbon Flame and Core Composition

The evolutionary sequences with $M_{WD} \geq 1.024\ M_\odot$ experienced a carbon shell burning followed by a helium shell burning, represented as loop on upper left region of the HR diagram on figure 5. The carbon burning ignited off center and propagates inwards to the center of the star (carbon flame). Before the extinction of the carbon flame, helium ignites on a shell near the surface and for sequences with $M_{WD} \geq 1.132\ M_\odot$ the subsequent helium burning consumes all the helium content in the star. All sequences which experienced a carbon flame presented subsequent flames which started further away from the center and were quenched before the starting point of the previous flame. The location in mass where the first carbon ignition occurs (full line) and the location of closest to center extinction of the carbon flame (dashed line) are shown in fFgure 7 as function of the white dwarf mass which experienced a carbon flame. The dotted vertical lines separate the mass range for core composition, as will be discussed in the following paragraph. The position of the first carbon ignition get closest to the center of the model for increasing white dwarf mass. The explanation for this is as the core mass increases, the central degeneracy is lower, allowing the inner maximum temperature to be near the center causing a carbon ignition closer to the center on more massive sequences. The same trend for carbon flames are reported in the works of Siess (2006), Siess (2007), Denissenkov et al. (2013), Farmer, Fields e Timmes (2015). Also, Denissenkov et al. (2013) discuss that a carbon flame which does not reach the center of the stars will form a hybrid C/O-O/Ne white dwarf, while a flame which propagates to the center will produce an O/Ne/Mg white dwarf. However, Denissenkov et al. (2013) does not present a complete chemical profile for their models.

The impact of the carbon flame on the core composition can be seen on figure 8, which presents the central regions in logarithmic scale for selected elements as fraction of the white dwarf mass. The abundances were taken at $T_{eff} \approx 40\,000$ K, a effective temperature low enough to give time for diffusion to act on the central composition. The C/O core is dominant for $M_{WD} \leq 1.088\ M_\odot$ due to carbon being more abundant than neon. Between $1.088 < M_{WD} \leq 1.147\ M_\odot$ we have an O/Ne core as neon increases its composition but is still lower than oxygen, whilst for masses $M_{WD} > 1.147\ M_\odot$ neon is the most abundant element on the central region, followed by oxygen and then by magnesium, so we define the core composition as Ne/O/Mg core. Note that sequences with $M_{WD} > 1.15\ M_\odot$ experienced a carbon flame which reaches to the center of the stars as shown on figure 7. Also, the sequence with $M_{WD} = 1.024\ M_\odot$ is the sequences with the lowest stellar mass to experience carbon burning, but it did not reach the center producing a hybrid C/O-O/Ne white dwarf. This explains the step in the central ^{20}Ne abundance observed in figure 8 for that stellar mass.

Within the stellar mass range studied in this dissertation, there are three main core composition expected from the literature: C/O and O/Ne (García-Berro; Ritossa; Iben JR., 1997; Doherty et al., 2015) or Ne/O/Mg, changing with increasing stellar mass. The mass range for those core composition is dependent on the evolutionary code and input physics applied. Doherty et al. (2015) computed sequences for super-AGB stars and found that, for initial metallicity $Z = 0.02$, sequences with core mass $M_c < 1.075\ M_\odot$ become a C/O core white dwarf, sequences with core mass $1.075 \leq M_c < 1.154\ M_\odot$ presented a C/O/Ne core and for core masses $M_c \geq 1.154\ M_\odot$ the sequences are O/Ne white dwarfs. Woosley e

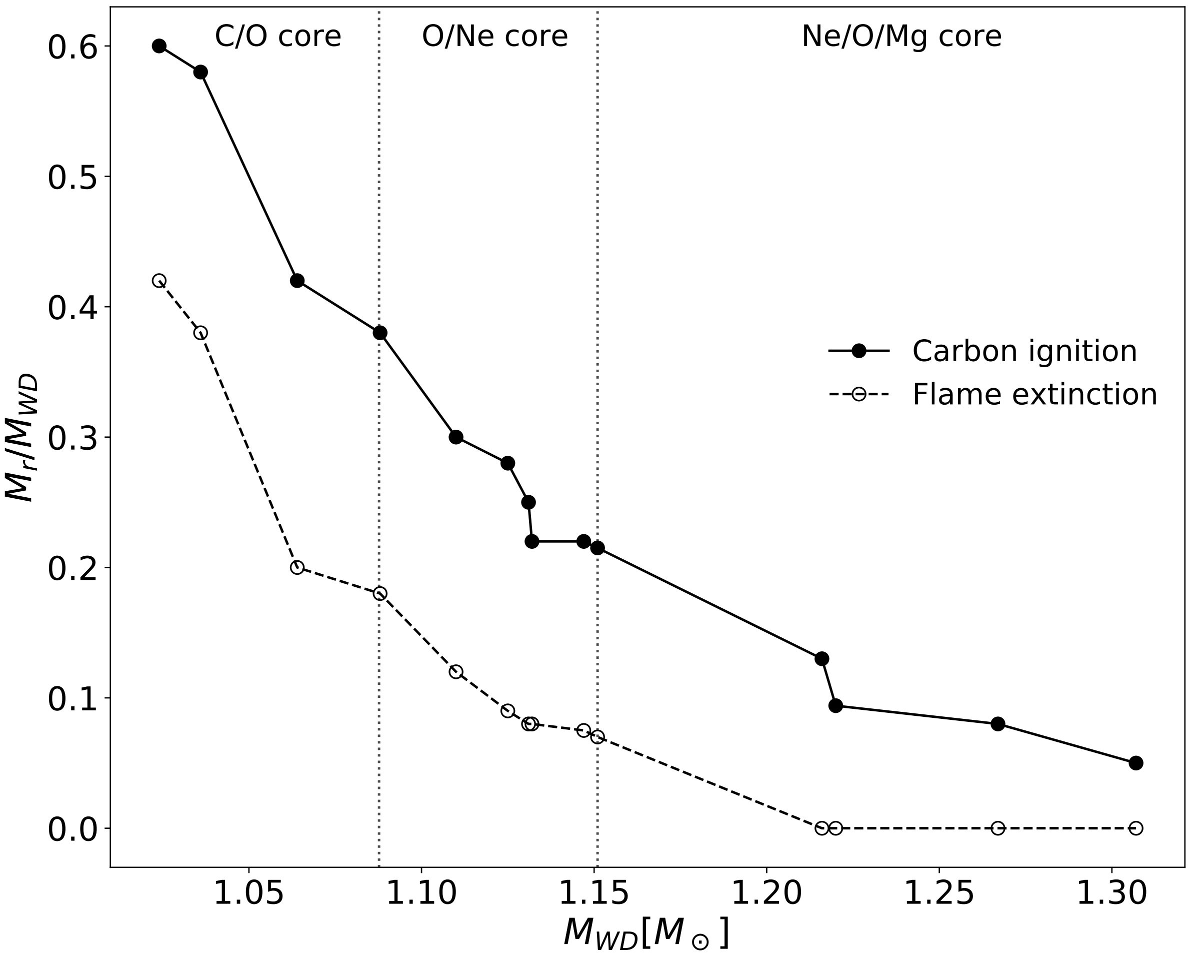

Figure 7 – Mass location of the first ignition of carbon and mass location of closest to center flame extinction as function of white dwarf masses which experienced a carbon flame. Vertical dotted lines delimits the mass range for core composition defined in figure 8 .

Heger (2015) also calculated sequences on the limit of SN progenitors and obtained models with O/Ne core for a range of core mass $1.088 \leq M_c \leq 1.345\ M_\odot$. It is important to note that Doherty et al. (2015) and Woosley e Heger (2015) did not compute the cooling curve, leading to non-full evolutionary model, opposite to the present work. They also used different evolutionary codes with different nuclear reaction and input physics

3.3 Initial to Final Mass relation

Figure 9 presents the Initial to Final Mass Relation obtained from our computations compared to the results of Siess (2010) and Doherty et al. (2015), within the stellar mass range considered in this work. We consider models with initial metallicity $Z = 0.02$. Because of the different evolutionary code and input physics, with emphasis on the mass loss scheme, the final mass obtained in this work is systematically lower than previous

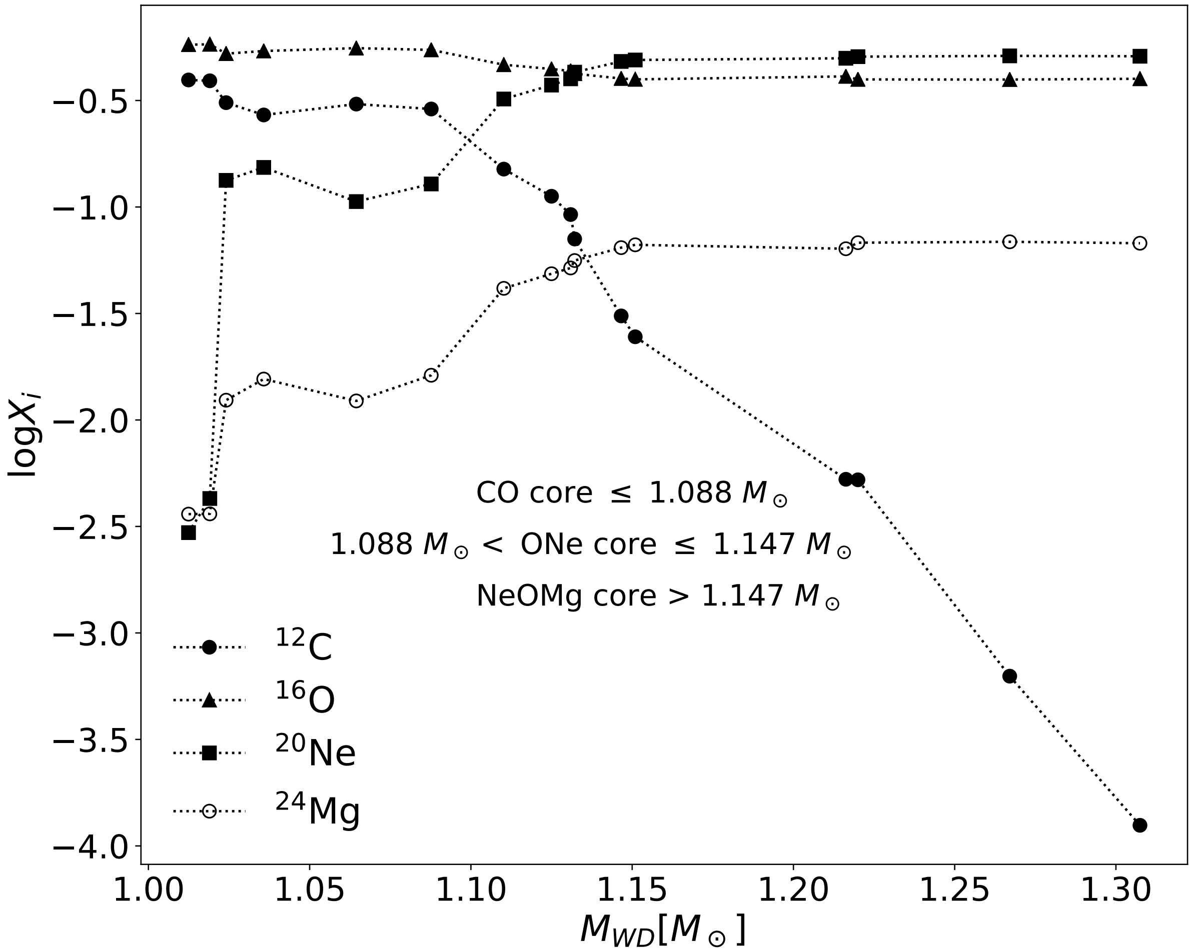

Figure 8 – Central abundances versus final mass of the white dwarfs stars before crystallization starts ($T_{eff} \approx 40\,000$ K). The black circles represent ^{12}C, triangles are ^{16}O, squares are ^{20}Ne and empty circles are ^{24}Mg. We can identify three regions, one for C/O core for masses below or equal to 1.088 $M_\odot$ where neon is lower than carbon, another region between 1.088 and 1.147 $M_\odot$ in which neon is greater than carbon and lower than oxygen but magnesium is lower than carbon defining an O/Ne core, and a third region for masses greater than 1.147 $M_\odot$ with an O/Ne/Mg core due to neon being greater than oxygen and magnesium greater than carbon.

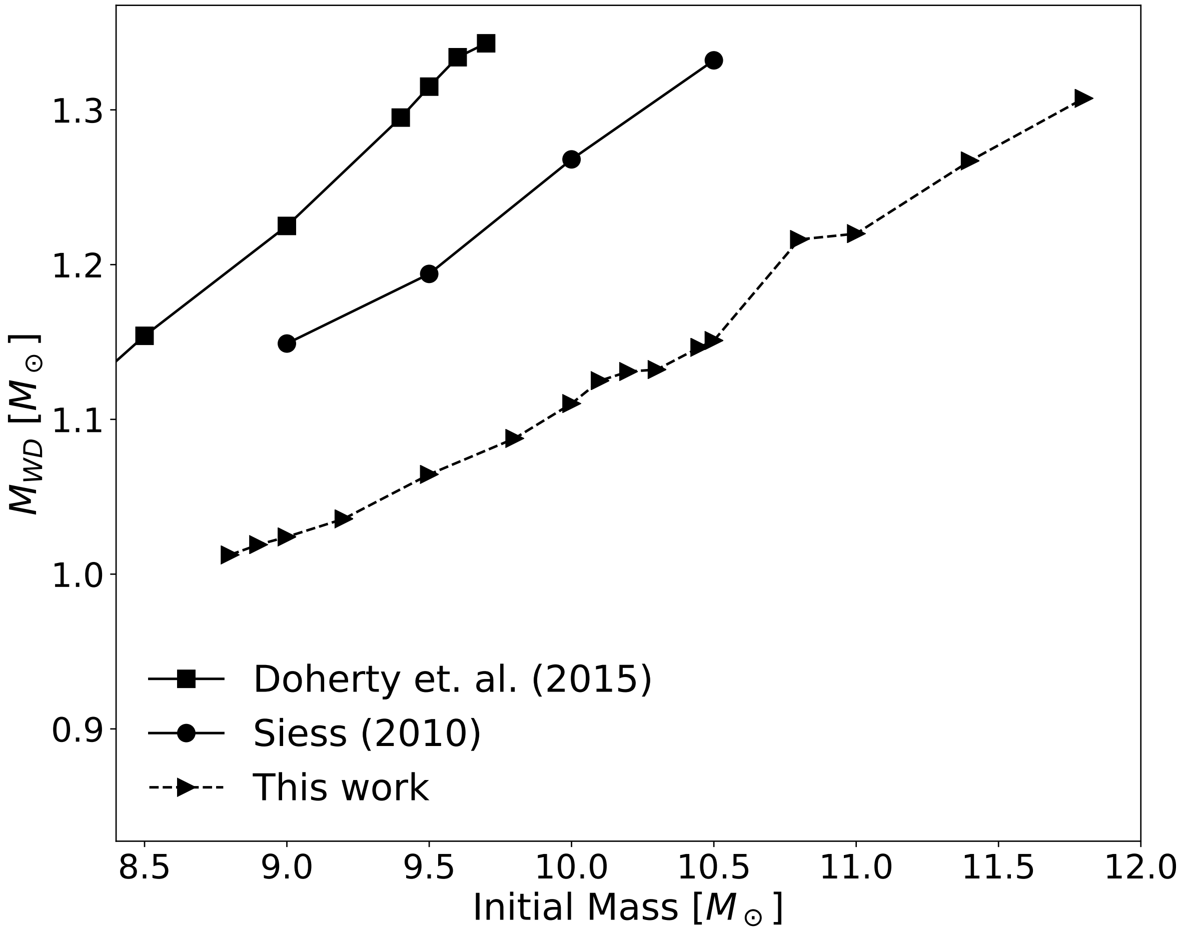

Figure 9 – Initial to Final Mass Relation comparison between this work and Siess (2010) and Doherty et al. (2015) for models with $Z = 0.02$. The Doherty et al. (2015) data was truncated to show only their massive models. Initial and final masses are on $M_\odot$ units.

results. However, both Siess (2010) and Doherty et al. (2015) evolved their sequences until TP-AGB phase, considering the mass of the He-free core as the final mass in the white dwarf stage. In this work, the evolutionary sequences were evolved to post-AGB phase, leading to a lower final mass in the cooling sequences. Thus, from our computations, the upper limit of progenitor mass to produce a white dwarf star is $M_{ZAMS} = 11.8\ M_\odot$ for $Z = 0.02$, 21.6% greater than the value found by Doherty et al. (2015) and 12.4% greater compared to Siess (2010) for the same initial metallicity.

3.4 Chemical Abundance in the Cooling Sequence

In Figure 10 is shown three chemical profiles for models along the cooling sequence for an O/Ne core H–atmosphere white dwarf with stellar mass $M_{WD} = 1.11\ M_\odot$. The abundance profiles are in terms of outer mass fraction and correspond to three effective temperatures, $T_{eff} \approx 80\,000, 40\,000$ and $10\,000$ K, on top, middle and bottom panels, respectively. The effects of diffusion and gravitational settling on the entire chemical profile as the star cools are evident from this figure, as the core composition changes to a flat profile on the bottom panel due to rehomogenization. The shaded region on the bottom panel depicts the crystallized zone, which is defined as the regions where $\Gamma \geq 220$. Note that, for the sequence with white dwarf mass 1.11 $M_{\odot}$ the carbon flame experienced in the pre-white dwarf stage, did not reach the center of the model, giving rise to a hybrid C/O-O/Ne core white dwarfs (Denissenkov et al., 2013; Doherty et al., 2015; Farmer; Fields; Timmes, 2015). This is the first time a chemical profile for the entire stars is presented for a hybrid C/O-O/Ne white dwarf.

Figure 11 shows the chemical profiles in terms of outer mass fraction for three hydrogen atmosphere white dwarfs models with $T_{eff} \approx 10\,000$ K, with stellar mass $M_{WD} = 1.019\ M_{\odot}$ (C/O core - top panel), $M_{WD} = 1.11\ M_{\odot}$ (O/Ne core - middle panel) and $M_{WD} = 1.22 M_{\odot}$ (Ne/O/Mg core - bottom panel). The shaded region represents the crystallized region of the model. From this figure, we note that the crystallization front is closer to the surface of the model for higher stellar mass.

3.5 Cooling Times

The cooling time is defined as the time spent by a star in the cooling sequence (t_{cool}). We define the beginning of the cooling sequences as the point of maximum effective temperature in the post-AGB stage, before the star enters the cooling sequence. The progenitor age (t_i) is defined as the time from the ZAMS to the beginning of the cooling sequence. Then the total age of a white dwarf star can be computed as $t_{total} = t_i + t_{cool}$. Table 1 summarizes the characteristic time-scales for all the sequences computed in this work. The progenitor age t_i is listed in column 5. The effective temperature and the age in the cooling curve at the onset of crystallization are listed in columns 6 and 7 for the hydrogen and in columns 9 and 10 for helium atmosphere sequences. Finally, the cooling times corresponding to an effective temperature of 10 000 K are listed in columns 8 and 12 for sequences with hydrogen and helium atmospheres, respectively.

Figure 12 shows a comparison of cooling times between H and He atmosphere sequences with the same stellar mass, 1.019 (solid line), 1.11 (dashed line) and 1.22 $M_{\odot}$ (dotted line), whose chemical profiles are presented in Figure 11. Gray lines represent hydrogen atmosphere and black lines correspond to helium atmosphere sequences. The release of internal energy due to crystallization occurs at higher luminosities for He atmosphere sequences, delaying the cooling for luminosities $\log L/L_{\odot} \gtrsim -2.8$. On the other hand, He-atmosphere sequences cools considerably faster for luminosities $\log L/L_{\odot} \lesssim -2.8$ because helium is more transparent than hydrogen, which leads to differences in cooling age of ~ 1 Gyr for luminosities of $\log L/L_{\odot} \sim -4$.

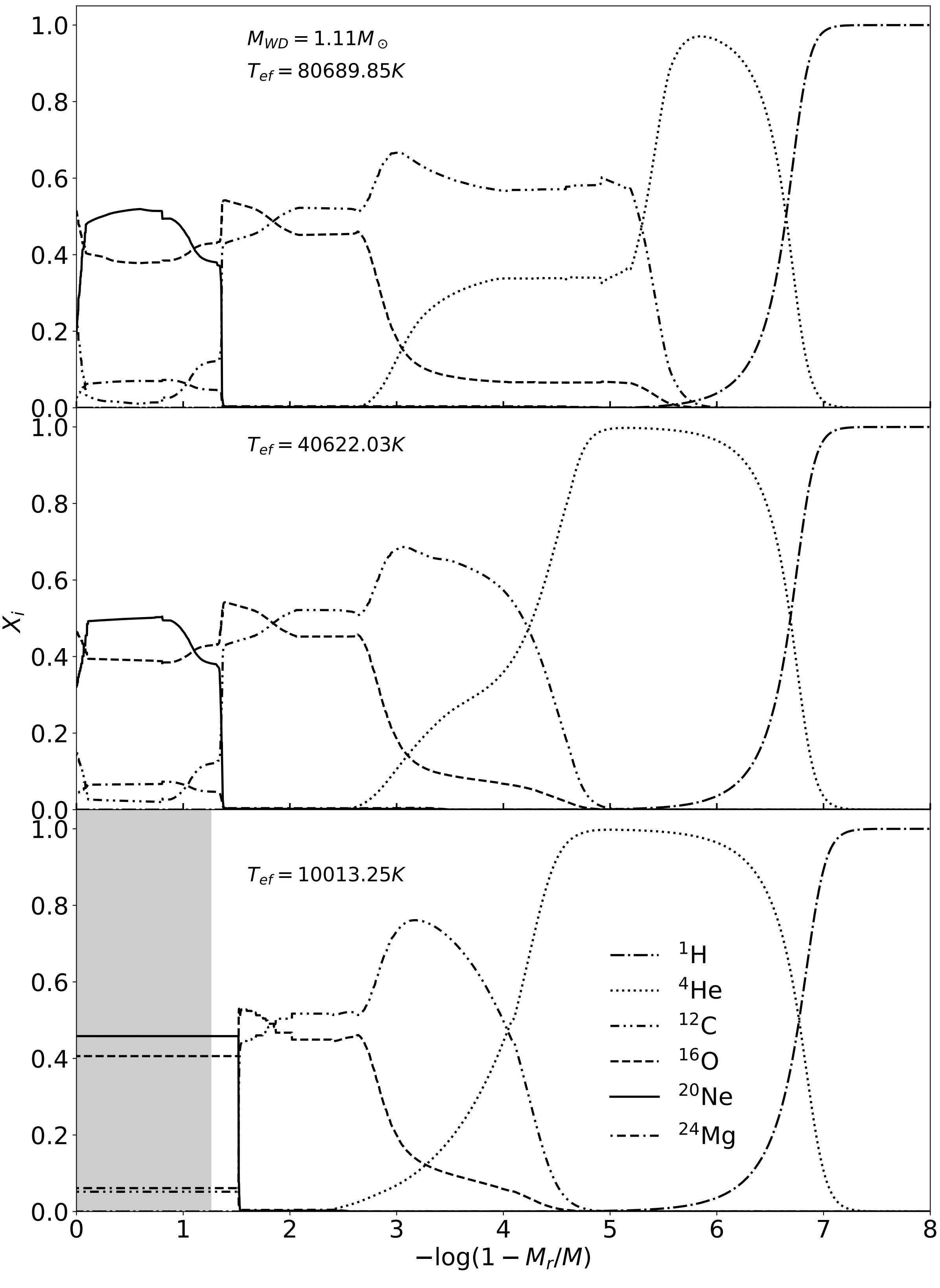

Figure 10 – Chemical profile in terms of outer mass fraction for selected elements for three different stages of the cooling sequence: $T_{eff} \approx 80\,000$ K on top, $T_{eff} \approx 40\,000$ K on middle and $T_{eff} \approx 10\,000$ K on bottom panels. The chemical profiles are for a H atmosphere white dwarf with $M_{WD} = 1.11\ M_\odot$. The shaded region represents the crystallized zone of the star.

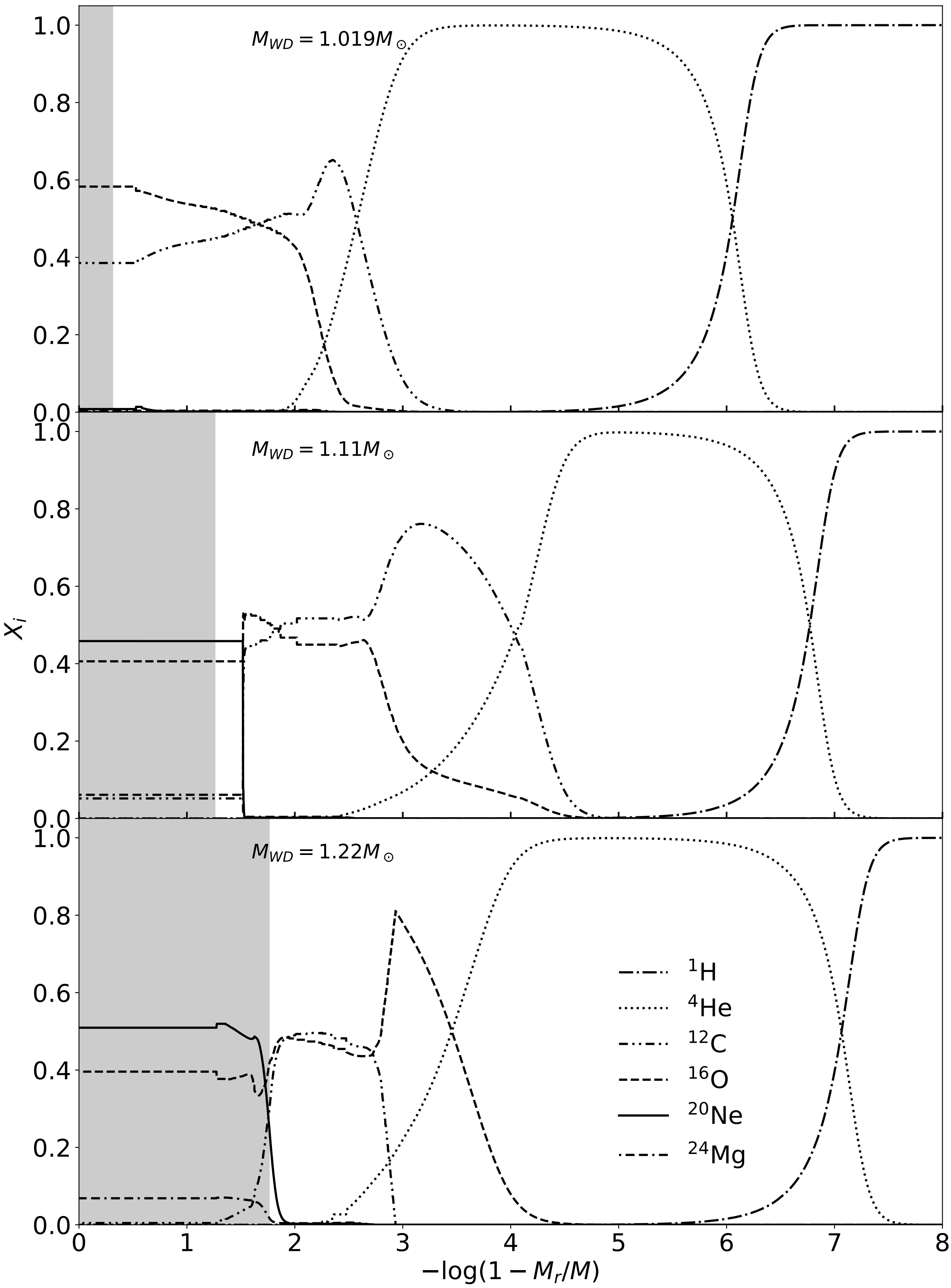

Figure 11 – Chemical profile in terms of outer mass fraction for selected elements and for three different H atmosphere white dwarf with $T_{eff} \approx 10\,000$ K. From top to bottom we depict the chemical profile for a $M_{WD} = 1.019, 1.11, 1.22$ $M_\odot$. The shaded region represents the crystallized zone of the star.

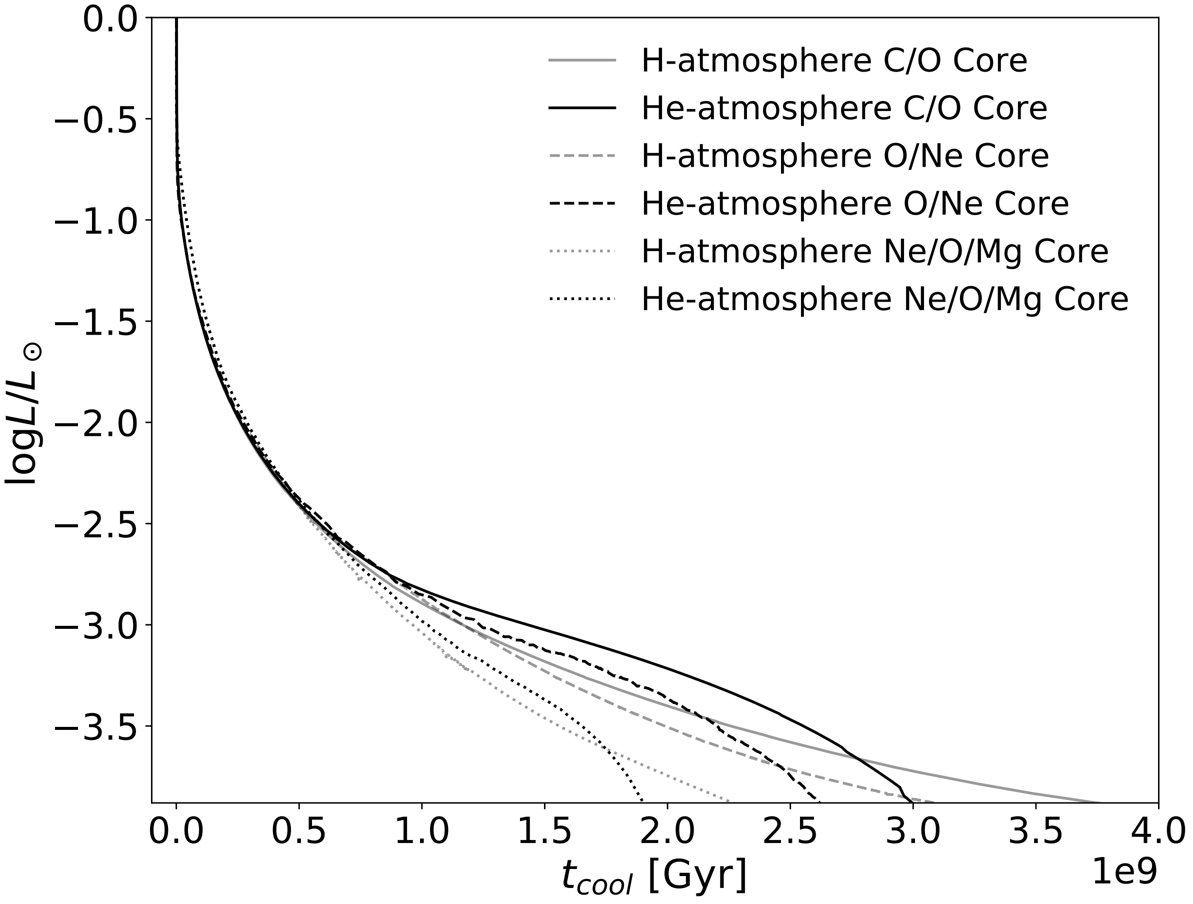

Figure 12 – Comparison of cooling times for selected H and He atmosphere sequences. There are presented 3 sets of H and He atmosphere. A C/O core set with mass 1.019 $M_\odot$ as solid line. An O/Ne set with mass 1.11 as dashed line and a Ne/O/Mg set with mass 1.22 $M_\odot$ as dotted line. Gray lines represent H atmosphere and black lines are He atmosphere white dwarfs. The final chemical profile for the H atmosphere are shown in figure 11.

3.6 Mass Radius Relation

From our computations we found that a H-atmosphere sequences have a higher rate of contraction compared to the He-atmosphere sequences, however the final radii are greater for the H-atmosphere sequences. We found that a small amount of hydrogen of the order of $M_H \approx 1 \times 10^{-6} M_{WD}$ can change the radius by 8.6×10^{-4} $R_\odot$ for the $M_{WD} = 1.064$ $M_\odot$ sequence.

In Figure 13 is shown the surface gravity $\log g$ as a function of effective temperature T_{eff} for H atmosphere sequences. The effective temperature is on logarithmic scale and range values from ≈ 250 000 K to ≈ 10 000 K. The solid lines correspond to C/O cores sequences while dashed and dotted lines correspond to O/Ne and Ne/O/Mg core sequences, respectively. Stellar mass decreases from top to bottom. Also, are plotted a selection of 400 white dwarfs with masses $M_{WD} > 1$ $M_\odot$ from the SDSS DR12 catalog (Kepler et al., 2016).

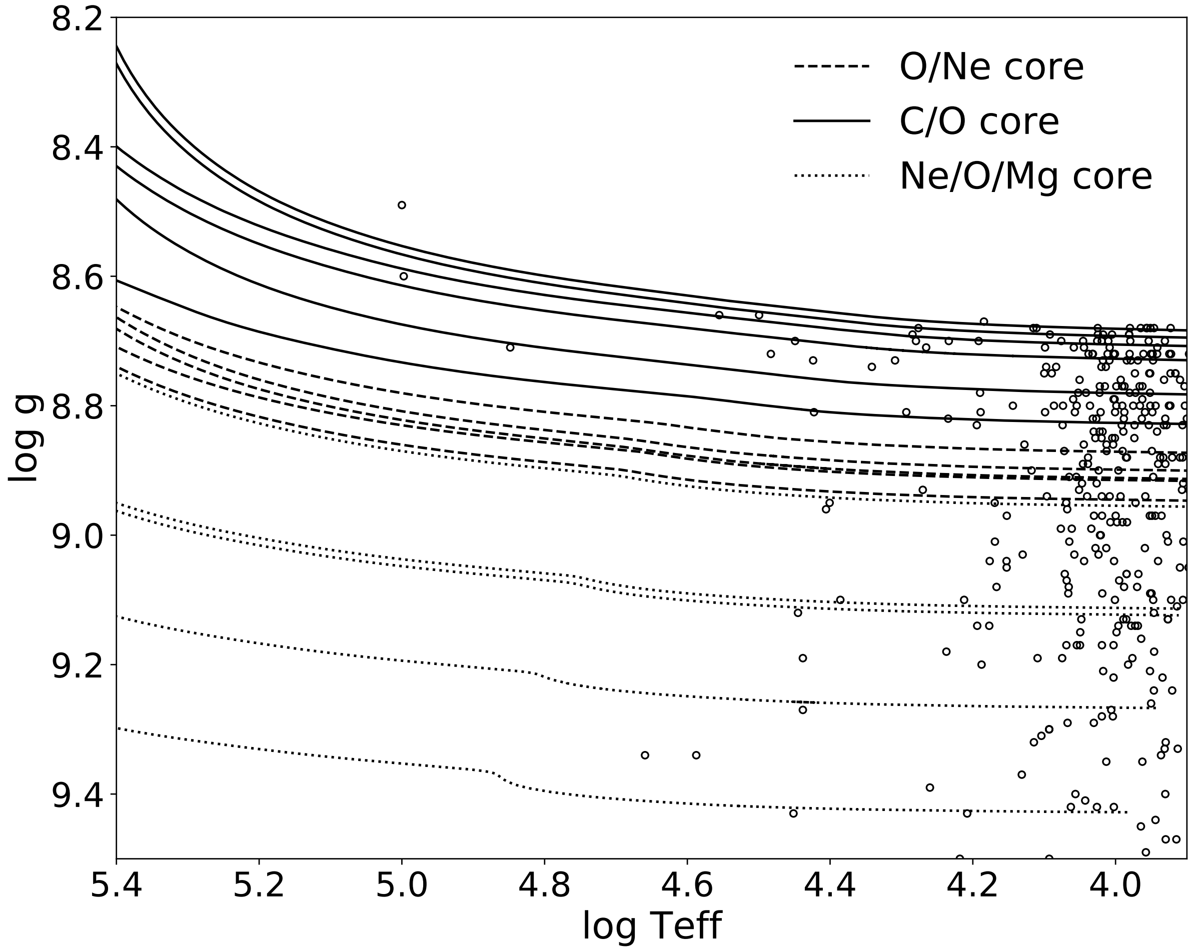

Figure 13 – $\log g$ - T_{eff} relation for H atmosphere white dwarfs. T_{eff} from $\approx 250\,000$ K to $\approx 10\,000$ K. Empty circles are observed white dwarfs from the SDSS catalog.

Surface gravities and effective temperatures are corrected to 3D convection (Tremblay et al., 2013) and have mean values of $\langle \log g \rangle = 8.987 \pm 0.21$ and $\langle T_{eff} \rangle = 11\,591 \pm 501$. There is a good agreement between observations and our sequences with masses $M_{WD} \leq 1.151$ $M_{\odot}$.

For comparison purposes, we compute the stellar mass of a sample of 252 stars from the SDSS DR12 catalog of Kepler et al. (2016) using the cooling sequence computed in this work and those obtained using the LPCODE evolutionary code (Althaus et al., 2005; Romero et al., 2013). We found practically no difference between the two determinations, only for masses around 1.05 $M_{\odot}$ due to the transition from C/O to O/Ne core composition occurs at 1.05 $M_{\odot}$ for LPCODE while in our simulations occurs at 1.088 $M_{\odot}$.

3.7 Conclusion

Unlike models that only evolve to the AGB, our white dwarf sequences considers the entire evolutionary history of the corresponding progenitors, leading to realistic chemical profiles which are also consistent with stellar mass. The final mass range of our sequences covers the entire range of C/O, O/Ne and Ne/O/Mg core composition and also accounts for hybrids C/O-O/Ne white dwarfs. The core mass range from our simulations are: C/O cores for $M_{WD} \leq 1.088$ M$_\odot$, O/Ne cores for $1.088 < M_{WD} \leq 1.147$ M$_\odot$ and Ne/O/Mg cores for $M_{WD} > 1.147$ M$_\odot$. Our Hybrid models presents an O/Ne core surrounded by a triple-layer of oxygen-carbon-helium, differing from the work of Denissenkov et al. (2013) where they reported a C/O core surrounded by an O/Ne zone for hybrid C/O/Ne Super AGB stars. Is important to note that the models from Denissenkov et al. (2013) evolved only until the AGB while the sequences in this dissertation evolved to the white dwarf stage at low luminosities on the cooling curve. The carbon flame experienced by our hybrid models started in regions with density $\rho \sim 1.5 \times 10^6$ g/cm^3, agreeing with the results from Farmer, Fields e Timmes (2015) which calculated models for super-AGB with MESA. Reliable chemical composition of core and the chemical transition regions presented on figure 8 are of relevance for asteroseimological studies of pulsating white dwarf stars. The set of tracks presented here is the first in the literature to cover those core composition for massive white dwarfs, considering the evolutionary history of the progenitors, and presenting the entire chemical profiles for the sequences.

The amount of hydrogen and helium in the star atmosphere affects both the age and mass determinations of DA and non-DA white dwarfs. Even low quantities of hydrogen, as the ones expected for massive white dwarfs, can impact the radii and cooling times. In particular, our H-atmosphere sequences shows cooling times $\sim 0.23 - 0.66$ Gyr larger at $T_{eff} \approx 10\,000$ K, depending on stellar mass, when compared to He atmosphere sequence with the same mass. Also, our choice of the Coulomb Coupling parameter for crystallization $\Gamma_{full} = 220$, based on the latest asteroseismology results, instead of the default $\Gamma = 175$, can increase the cooling times by ≈ 0.26 Gyr and decrease the effective temperature at the onset of crystallization by $\approx 2000K$. Finally, the core composition also impacts the cooling times of white dwarfs stars, as reported by García-Berro, Isern e Hernanz (1997), but unlike models that uses fixed composition for a mass range, our sequences considers the entire history of the progenitors which leads to reliable chemical compositions and hence reliable cooling times.

The derived masses for a selection of 252 massive stars from the SDSS DR12 catalog (Kepler et al., 2016) using our simulations are in fine agreement with masses computed using the evolutionary tracks of LPCODE Althaus et al. (2005), Romero et al. (2012), Romero et al. (2013). Also, there are a significant amount of observed white dwarf stars which agrees with our evolutionary tracks for masses $M_{WD} \leq 1.151$ M$_\odot$, as shown on Figure 13, allowing further investigations of those observed objects.

4 Conclusion

In this dissertation, full evolutionary sequences for massive H and He atmosphere white dwarf stars were calculated using the evolutionary code MESA version `r8845`. The simulations started at the zero-age main sequence and evolved through stable core hydrogen and helium burning, thermally pulsing and mass-loss phases, ending as white dwarfs at the cooling sequence, evolving until luminosities of $\log L/L_\odot \approx -4$. Evolutionary sequences of white dwarfs which consider the entire evolutionary history of the progenitors are essential to obtain reliable chemical composition, cooling times, initial to final mass relation and mass-radius relation. These informations are mandatory to derive ages and masses for observed massive white dwarfs, to compute asteroseismological models for pulsations, to determine upper mass limit that separates white dwarfs from type II SN, understand the properties of the Galactic population of white dwarfs and determine age and distances of globular clusters. Hence, improving the sequences also improves the information derived from it.

The simulations were performed with the MESA evolutionary code for solar metalicity $Z = 0.02$. The sequences started from the zero-age main sequence with masses from 8.8 to 11.8 $M_\odot$ resulting in white dwarfs with stellar masses in a range of $M_{WD} = 1.012 - 1.307$ $\mathrm{M}_\odot$. The sequences considered diffusion, convection, mass loss, overshooting and a modified crystallization to better reproduce white dwarf evolution. An overview of the main results are listed in the following:

- From our simulations we obtained white dwarf sequences characterized with C/O, O/Ne and Ne/O/Mg cores being: C/O cores for $M_{WD} \leq 1.088$ $M_\odot$, O/Ne cores for $1.088 < M_{WD} \leq 1.147$ $M_\odot$, Ne/O/Mg cores for $M_{WD} > 1.147$ $M_\odot$. Note that these values correspond to sequences with initial metallicity $Z = 0.02$. We expect them to vary for different initial metallicities (Doherty et al., 2015). We compute a sequence with $M_{WD} = 1.13$ $M_\odot$ and $Z = 0.015$ and found that the chemical structure does not change considerably from the sequence with $Z = 0.02$ and a similar stellar mass in the cooling curve.
- All sequences with $M_{WD} \geq 1.024$ $M_\odot$ experienced inward propagating carbon flames with subsequent helium burning of the outer shells, in the post-AGB stage. The carbon flame for sequences with masses $1.024 \leq M_{WD} \leq 1.147$ $M_\odot$ does not reach the central regions, forming a hybrid C/O-O/Ne white dwarf. For sequences with $M_{WD} > 1.147$ $M_\odot$ the carbon flame reaches the center of the model producing a Ne/O/Mg core. Our hybrid models present an O/Ne core surrounded by a triple-layer of oxygen-carbon-helium, differing from the work of Denissenkov et al. (2013) where

they reported a C/O core surrounded by an O/Ne zone for hybrid C/O/Ne Super AGB stars.

- Our choice of the Coulomb Coupling parameter for crystallization $\Gamma_{full} = 220$, based on the latest asteroseismology results, instead of the default $\Gamma = 175$, can increase the cooling times by ≈ 0.26 Gyr and decrease the effective temperature at the onset of crystallization by $\approx 2000K$.

- The amount of hydrogen left at the envelope of a white dwarf has an important impact in determining the stellar mass and the cooling times. Even low quantities of hydrogen, as the ones expected for massive white dwarfs, can impact the radii and cooling times. In particular, our H-atmosphere sequences show cooling times $\sim 0.23 - 0.66$ Gyr larger at $T_{eff} \approx 10\,000$ K, depending on stellar mass, when compared to He atmosphere sequence with the same mass.

- The derived masses for a selection of 252 massive stars from the SDSS DR12 catalog (Kepler et al., 2016) using our simulations are in fine agreement with masses computed using the evolutionary tracks of LPCODE Althaus et al. (2005), Romero et al. (2012), Romero et al. (2013).

In the future, we will employ the model grid computed in this dissertation to compute theoretical period spectrum and thus compare the theoretical periods with observed variable stars, a technique known as asteroseismology. Also, we will use the MESA code to produce massive white dwarf models considering binary evolution, studying the effects of accretion, core collapse and nova events and mergers.

Bibliography

Ahn, C. P. et al. The Tenth Data Release of the Sloan Digital Sky Survey: First Spectroscopic Data from the SDSS-III Apache Point Observatory Galactic Evolution Experiment. *The Astrophysical Journal, Supplement*, v. 211, p. 17, abr. 2014. Citado na página 26.

Alastuey, A.; Jancovici, B. Nuclear reaction rate enhancement in dense stellar matter. *The Astrophysical Journal*, v. 226, p. 1034, dec 1978. ISSN 0004-637X. Disponível em: <http://adsabs.harvard.edu/doi/10.1086/156681>. Citado na página 37.

Althaus, L. G. et al. New Chemical Profiles for the Asteroseismology of ZZ Ceti Stars. *The Astrophysical Journal*, v. 717, p. 897–907, jul. 2010. Citado na página 33.

Althaus, L. G. et al. Evolutionary and pulsational properties of white dwarf stars. *The Astronomy and Astrophysics Review*, v. 18, p. 471–566, out. 2010. Citado 2 vezes nas páginas 13 and 29.

Althaus, L. G. et al. On the Formation of Hot DQ White Dwarfs. *The Astrophysical Journal Letter*, v. 693, p. L23–L26, mar. 2009. Citado na página 28.

Althaus, L. G. et al. The age and colors of massive white dwarf stars. *Astronomy & Astrophysics*, v. 465, p. 249–255, abr. 2007. Citado na página 33.

Althaus, L. G.; Miller Bertolami, M. M.; Córsico, A. H. New evolutionary sequences for extremely low-mass white dwarfs. Homogeneous mass and age determinations and asteroseismic prospects. *Astronomy & Astrophysics*, v. 557, p. A19, set. 2013. Citado na página 33.

Althaus, L. G. et al. New Evolutionary Sequences for Hot H-Deficient White Dwarfs on the Basis of a Full Account of Progenitor Evolution. *The Astrophysical Journal*, v. 704, p. 1605–1615, out. 2009. Citado na página 33.

Althaus, L. G. et al. New evolutionary models for massive ZZ Ceti stars. I. First results for their pulsational properties. *Astronomy and Astrophysics*, v. 404, p. 593–609, jun. 2003. Citado na página 33.

Althaus, L. G. et al. The formation and evolution of hydrogen-deficient post-AGB white dwarfs: The emerging chemical profile and the expectations for the PG 1159-DB-DQ evolutionary connection. *Astronomy & Astrophysics*, v. 435, p. 631–648, maio 2005. Citado 4 vezes nas páginas 33, 54, 55, and 58.

Arny, T. The star makers: A history of the theories of stellar structure and evolution. *Vistas in Astronomy*, v. 33, p. 211, 1990. Citado na página 34.

Bedin, L. R. et al. The Bottom of the White Dwarf Cooling Sequence in the Old Open Cluster NGC 2158. *The Astrophysical Journall*, v. 708, p. L32–L35, jan. 2010. Citado na página 28.

Bethe, H. A. Energy production in stars. *Phys. Rev.*, American Physical Society, v. 55, p. 434–456, Mar 1939. Disponível em: <https://link.aps.org/doi/10.1103/PhysRev.55.434>. Citado na página 30.

Bischoff-Kim, A.; Montgomery, M. H. WDEC: A Code for Modeling White Dwarf Structure and Pulsations. *The Astronomical Journal*, v. 155, p. 187, maio 2018. Citado na página 32.

Bloecker, T. Stellar evolution of low and intermediate-mass stars. I. Mass loss on the AGB and its consequences for stellar evolution. *Astronomy and Astrophysics*, v. 297, p. 727–738, 1995. Disponível em: <http://adsabs.harvard.edu/abs/1995A{&}A...297..7>. Citado 2 vezes nas páginas 38 and 41.

Brooks, J. et al. Carbon Shell or Core Ignitions in White Dwarfs Accreting from Helium Stars. *The Astrophysical Journal*, v. 821, p. 28, abr. 2016. Citado 2 vezes nas páginas 33 and 35.

Brooks, J. et al. Accretion-induced Collapse from Helium Star + White Dwarf Binaries. *The Astrophysical Journal*, v. 843, p. 151, jul. 2017. Citado 2 vezes nas páginas 33 and 35.

Brooks, J. et al. Convection Destroys the Core/Mantle Structure in Hybrid C/O/Ne White Dwarfs. *The Astrophysical Journall*, v. 834, p. L9, jan. 2017. Citado 2 vezes nas páginas 33 and 35.

Burbidge, E. M. et al. Synthesis of the Elements in Stars. *Reviews of Modern Physics*, v. 29, p. 547–650, 1957. Citado na página 31.

Burgers, J. M. *Flow Equations for Composite Gases*. [S.l.: s.n.], 1969. Citado 2 vezes nas páginas 37 and 39.

Campos, F. et al. A comparative analysis of the observed white dwarf cooling sequence from globular clusters. *Monthly Notices of the Royal Astronomical Society*, v. 456, p. 3729–3742, mar. 2016. Citado na página 28.

Castanheira, B. G. et al. Discovery of five new massive pulsating white dwarf stars. *Monthly Notices of the Royal Astronomical Society*, v. 430, p. 50–59, mar. 2013. Citado na página 34.

Catalán, S. et al. The initial-final mass relationship of white dwarfs revisited: effect on the luminosity function and mass distribution. *Monthly Notices of the Royal Astronomical Society*, v. 387, p. 1693–1706, jul. 2008. Citado na página 28.

Chaboyer, B. et al. Heavy-Element Diffusion in Metal-poor Stars. *The Astrophysical Journal*, v. 562, p. 521–527, nov. 2001. Citado na página 32.

Chandrasekhar, S. The Maximum Mass of Ideal White Dwarfs. *The Astrophysical Journal*, v. 74, p. 81, jul. 1931. Citado na página 26.

Charbonnel, C. et al. Grids of stellar models. VI. Horizontal branch and early asymptotic giant branch for low mass stars (Z=0.020, 0.001). *Astronomy and Astrophysics Supplement Series*, v. 115, p. 339, fev. 1996. Citado na página 32.

Chen, M. C. et al. The dependence of the evolution of Type Ia SN progenitors on the C-burning rate uncertainty and parameters of convective boundary mixing. *Monthly Notices of the Royal Astronomical Society*, v. 440, p. 1274–1280, maio 2014. Citado 2 vezes nas páginas 33 and 35.

Choi, J. et al. Mesa Isochrones and Stellar Tracks (MIST). I. Solar-scaled Models. *The Astrophysical Journal*, v. 823, p. 102, jun. 2016. Citado 4 vezes nas páginas 32, 33, 34, and 35.

Córsico, A. H.; Althaus, L. G. Asteroseismic inferences on GW Virginis variable stars in the frame of new PG 1159 evolutionary models. *Astronomy and Astrophysics*, v. 454, p. 863–881, ago. 2006. Citado na página 33.

Cox, J. P.; Giuli, R. T. *Principles of stellar structure* . [S.l.: s.n.], 1968. Citado na página 37.

Curd, B. et al. Four new massive pulsating white dwarfs including an ultramassive DAV. *Monthly Notices of the Royal Astronomical Society*, v. 468, p. 239–249, jun. 2017. Citado na página 34.

Cyburt, R. H. et al. The JINA REACLIB Database: Its Recent Uptades and Impact on Type-I X-Ray Burst. *The Astrophysical Journal Supplement Series*, IOP Publishing, v. 189, n. 1, p. 240–252, jul 2010. ISSN 0067-0049. Disponível em: <http://stacks.iop.org/0067-0049/189/i=1/a=240?key=crossref.e7cdc09d4c969f0d1a5715de7519d4cc>. Citado na página 37.

Denissenkov, P. A. et al. The C-flame Quenching by Convective Boundary Mixing in Super-AGB Stars and the Formation of Hybrid C/O/Ne White Dwarfs and SN Progenitors. *The Astrophysical Journal*, v. 772, p. 37, jul. 2013. Citado 7 vezes nas páginas 27, 33, 35, 46, 50, 55, and 57.

DeWitt, H. E.; Graboske, H. C.; Cooper, M. S. Screening Factors for Nuclear Reactions 1. General Theory. *The Astrophysical Journal*, v. 181, n. April 15, p. 439–456, apr 1973. ISSN 0004-637X. Disponível em: <http://adsabs.harvard.edu/doi/10.1086/152061>. Citado na página 37.

Doherty, C. L. et al. Super- and massive AGB stars - IV. Final fates - initial-to-final mass relation. *Monthly Notices of the Royal Astronomical Society*, v. 446, p. 2599–2612, jan. 2015. Citado 8 vezes nas páginas 14, 25, 33, 46, 47, 49, 50, and 57.

Dotter, A. MESA Isochrones and Stellar Tracks (MIST) 0: Methods for the Construction of Stellar Isochrones. *The Astrophysical Journal, Supplement*, v. 222, p. 8, jan. 2016. Citado 4 vezes nas páginas 32, 33, 34, and 35.

Dotter, A. et al. The Dartmouth Stellar Evolution Database. *The Astrophysical Journal Supplement*, v. 178, p. 89–101, set. 2008. Citado na página 32.

Dufour, P. et al. Hot DQ White Dwarfs: Something Different. *The Astrophysical Journal*, v. 683, p. 978–989, ago. 2008. Citado na página 28.

Dufour, P. et al. White dwarf stars with carbon atmospheres. *Nature*, v. 450, p. 522–524, nov. 2007. Citado na página 28.

Eddington, A. S. On the radiative equilibrium of the stars. *Monthly Notices of the Royal Astronomical Society*, v. 77, p. 16–35, nov. 1916. Citado na página 30.

Eddington, A. S. On the relation between the masses and luminosities of the stars. *Monthly Notices of the Royal Astronomical Society*, v. 84, p. 308–332, mar. 1924. Citado na página 30.

Eggleton, P. P. The evolution of low mass stars. *Monthly Notices of the Royal Astronomical Society*, v. 151, p. 351, 1971. Citado na página 32.

Emden, R. Gaskugeln, Leipzig, B.G Teubner. 1907. Citado na página 30.

Falcon, R. E. et al. A Gravitational Redshift Determination of the Mean Mass of White Dwarfs. DA Stars. *The Astrophysical Journal*, v. 712, p. 585–595, mar. 2010. Citado na página 26.

Farmer, R.; Fields, C. E.; Timmes, F. X. On Carbon Burning in Super Asymptotic Giant Branch Stars. *The Astrophysical Journal*, v. 807, p. 184, jul. 2015. Citado 6 vezes nas páginas 27, 33, 35, 46, 50, and 55.

Faulkner, J.; Iben JR., I. The Evolution of Population II Stars. *The Astrophysical Journal*, v. 144, p. 995, jun. 1966. Citado na página 32.

Gamow, G. Nuclear energy sources and stellar evolution. *Phys. Rev.*, American Physical Society, v. 53, p. 595–604, Apr 1938. Disponível em: <https://link.aps.org/doi/10.1103/PhysRev.53.595>. Citado na página 30.

Gamow, G. Tracks of stellar evolution. *Phys. Rev.*, American Physical Society, v. 53, p. 907–908, Jun 1938. Disponível em: <https://link.aps.org/doi/10.1103/PhysRev.53.907>. Citado na página 30.

Garcia-Berro, E.; Iben, I. On the formation and evolution of super-asymptotic giant branch stars with cores processed by carbon burning. 1: Spica to Antares. *The Astrophysical Journal*, v. 434, p. 306–318, out. 1994. Citado na página 33.

García-Berro, E.; Isern, J.; Hernanz, M. The cooling of oxygen-neon white dwarfs. *Monthly Notices of the Royal Astronomical Society*, v. 289, p. 973–978, ago. 1997. Citado 7 vezes nas páginas 25, 27, 28, 33, 41, 42, and 55.

García-Berro, E.; Ritossa, C.; Iben JR., I. On the Evolution of Stars that Form Electron-Degenerate Cores Processed by Carbon Burning. III. The Inward Propagation of a Carbon-Burning Flame and Other Properties of a 9 $M_\odot$ Model Star. *The Astrophysical Journal*, v. 485, p. 765–784, ago. 1997. Citado 2 vezes nas páginas 33 and 46.

García-Berro, E. et al. The white dwarf cooling sequence of 47 Tucanae. *Astronomy & Astrophysics*, v. 571, p. A56, nov. 2014. Citado na página 28.

Graboske, H. et al. Screening Factors for Nuclear Reactions. II. Intermediate Screen-Ing and Astrophysical Applications. *The Astrophysical Journal*, v. 181, p. 457–474, apr 1973. ISSN 0004-637X. Disponível em: <http://adsabs.harvard.edu/doi/10.1086/152062>. Citado na página 37.

Guenther, D. B. et al. Standard solar model. *The Astrophysical Journal*, v. 387, p. 372–393, mar. 1992. Citado na página 32.

Guerrero, J.; García-Berro, E.; Isern, J. Smoothed Particle Hydrodynamics simulations of merging white dwarfs. *Astronomy & Astrophysics*, v. 413, p. 257–272, jan. 2004. Citado na página 28.

Hansen, B. M. S. et al. The White Dwarf Cooling Sequence of NGC 6397. *The Astrophysical Journal*, v. 671, p. 380–401, dez. 2007. Citado na página 28.

Härm, R.; Schwarzschild, M. The Helium Flash in Population II Giants. *Astronomical Journal*, v. 66, p. 45, mar. 1961. Citado na página 31.

Hayashi, C.; Hōshi, R.; Sugimoto, D. Evolution of the Stars. *Progress of Theoretical Physics Supplement*, v. 22, p. 1–183, 1962. Citado na página 32.

Henrich, L. R.; Chandrasekhar, S. Stellar Models with Isothermal Cores. *The Astrophysical Journal*, v. 94, p. 525, nov. 1941. Citado na página 30.

Henyey, L. G.; Lelevier, R.; Levée, R. D. The Early Phases of Stellar Evolution. *Publications of the Astronomical Society of the Pacific*, v. 67, p. 154, jun. 1955. Citado na página 31.

Henyey, L. G. et al. A Method for Automatic Computation of Stellar Evolution. *The Astrophysical Journal*, v. 129, p. 628, maio 1959. Citado 2 vezes nas páginas 31 and 35.

Hermes, J. J. et al. Discovery of an Ultramassive Pulsating White Dwarf. *The Astrophysical Journal Letters*, v. 771, p. L2, jul. 2013. Citado na página 34.

Herwig, F. The evolution of AGB stars with convective overshoot. *Astronomy & Astrophysics*, v. 360, p. 952–968, ago. 2000. Citado na página 38.

Hidalgo, S. L. et al. The Updated BaSTI Stellar Evolution Models and Isochrones. I. Solar-scaled Calculations. *The Astrophysical Journal*, v. 856, p. 125, abr. 2018. Citado na página 32.

Horowitz, C. J.; Schneider, A. S.; Berry, D. K. Crystallization of Carbon-Oxygen Mixtures in White Dwarf Stars. *Physical Review Letters*, v. 104, n. 23, p. 231101, jun. 2010. Citado 2 vezes nas páginas 38 and 45.

Hoyle, F.; Schwarzschild, M. On the Evolution of Type II Stars. *The Astrophysical Journal*, v. 121, p. 776–778, maio 1955. Citado na página 31.

Hughto, J. et al. Direct molecular dynamics simulation of liquid-solid phase equilibria for a three-component plasma. *Physical Review E*, v. 86, n. 6, p. 066413, dez. 2012. Citado na página 38.

Iben, J. I. Stellar Evolution. VII. The Evolution of a 2.25 $M_\odot$ Star from the Main Sequence to the Helium-Burning Phase. *The Astrophysical Journal*, v. 147, p. 650, fev. 1967. Citado na página 32.

Iben JR., I. Stellar Evolution. I. The Approach to the Main Sequence. *The Astrophysical Journal*, v. 141, p. 993, abr. 1965. Citado na página 32.

Iben JR., I. Stellar Evolution. II. The Evolution of a 3 $M_\odot$ Star from the Main Sequence Through Core Helium Burning. *The Astrophysical Journal*, v. 142, p. 1447, nov. 1965. Citado na página 32.

Iben JR., I. Stellar Evolution. III. The Evolution of a 5 $M_\odot$ Star from the Main Sequence Through Core Helium Burning. *The Astrophysical Journal*, v. 143, p. 483, fev. 1966. Citado na página 32.

Iben JR., I. Stellar Evolution. V. The Evolution of a 15 $M_\odot$ Star from the Main Sequence Through Core Helium. *The Astrophysical Journal*, v. 143, p. 516, fev. 1966. Citado na página 32.

Iben JR., I. Stellar Evolution.IV. The Evolution of a 9 $M_\odot$ Star from the Main Sequence Through Core Helium Burning. *The Astrophysical Journal*, v. 143, p. 505, fev. 1966. Citado na página 32.

Iben JR., I. Stellar Evolution.VI. Evolution from the Main Sequence to the Red-Giant Branch for Stars of Mass 1 $M_\odot$, 1.25 $M_\odot$, and 1.5 $M_\odot$. *The Astrophysical Journal*, v. 147, p. 624, fev. 1967. Citado na página 32.

Iben JR., I. et al. On the evolution of those nuclei of planetary nebulae that experience a final helium shell flash. *The Astrophysical Journal*, v. 264, p. 605–612, jan. 1983. Citado na página 27.

Iben JR., I.; Ritossa, C.; García-Berro, E. On the Evolution of Stars that Form Electron-degenerate Cores Processed by Carbon Burning. IV. Outward Mixing During the Second Dredge-up Phase and Other Properties of a 10.5 $M_\odot$ Model Star. *The Astrophysical Journal*, v. 489, p. 772–790, nov. 1997. Citado na página 33.

Iglesias, C. A.; Rogers, F. J. Updated Opal Opacities. *The Astrophysical Journal*, v. 464, p. 943, jun. 1996. Citado na página 38.

Isern, J. et al. Axions and White Dwarfs. *ArXiv e-prints*, out. 2010. Citado na página 29.

Istrate, A. G.; Fontaine, G.; Heuser, C. A Model of the Pulsating Extremely Low-mass White Dwarf Precursor WASP 0247-25B. *The Astrophysical Journal*, v. 847, p. 130, out. 2017. Citado 2 vezes nas páginas 33 and 35.

Istrate, A. G. et al. Models of low-mass helium white dwarfs including gravitational settling, thermal and chemical diffusion, and rotational mixing. *Astronomy & Astrophysics*, v. 595, p. A35, out. 2016. Citado 2 vezes nas páginas 33 and 35.

Itoh, N. et al. Neutrino Energy Loss in Stellar Interiors. VII. Pair, Photo-, Plasma, Bremsstrahlung, and Recombination Neutrino Processes. *The Astrophysical Journal, Supplement*, v. 102, p. 411, fev. 1996. Citado na página 37.

Itoh, N. et al. Enhancement of thermonuclear reaction rate due to strong screening. II - Ionic mixtures. *The Astrophysical Journal*, v. 234, p. 1079–1084, dec 1979. ISSN 0004-637X. Disponível em: <http://adsabs.harvard.edu/doi/10.1086/157590>. Citado na página 37.

Jones, S. et al. Advanced Burning Stages and Fate of 8-10 $M_\odot$ Stars. *The Astrophysical Journal*, v. 772, p. 150, ago. 2013. Citado 2 vezes nas páginas 33 and 35.

Kepler, S. O. et al. White dwarf mass distribution in the SDSS. *Monthly Notices of the Royal Astronomical Society*, v. 375, p. 1315–1324, mar. 2007. Citado 2 vezes nas páginas 26 and 27.

Kepler, S. O. et al. New white dwarf stars in the Sloan Digital Sky Survey Data Release 10. *Monthly Notices of the Royal Astronomical Society*, v. 446, p. 4078–4087, fev. 2015. Citado na página 26.

Kepler, S. O. et al. New white dwarf and subdwarf stars in the Sloan Digital Sky Survey Data Release 12. *Monthly Notices of the Royal Astronomical Society*, v. 455, p. 3413–3423, fev. 2016. Citado 7 vezes nas páginas 13, 26, 27, 53, 54, 55, and 58.

Kippenhahn, R.; Ruschenplatt, G.; Thomas, H.-C. The time scale of thermohaline mixing in stars. *Astronomy & Astrophysics*, v. 91, p. 175–180, nov. 1980. Citado na página 38.

Kleinman, S. J. et al. SDSS DR7 White Dwarf Catalog. *The Astrophysical Journal, Supplement*, v. 204, p. 5, jan. 2013. Citado 2 vezes nas páginas 26 and 28.

Lamb, D. Q.; van Horn, H. M. Evolution of crystallizing pure C-12 white dwarfs. *The Astrophysical Journal*, v. 200, p. 306–323, set. 1975. Citado na página 32.

Lane, J. H. On The Theoretical Temperature of the Sun. *American Journal of Science*, v. 2, p. 57–74, 1870. Citado na página 30.

Langer, N. Presupernova Evolution of Massive Single and Binary Stars. *Annual Review of Astronomu & Astrophysics*, v. 50, p. 107–164, set. 2012. Citado na página 25.

Langer, N.; Fricke, K. J.; Sugimoto, D. Semiconvective diffusion and energy transport. *Astronomy & Astrophysics*, v. 126, p. 207, set. 1983. Citado na página 38.

Lauffer, G. R.; Romero, A. D.; Kepler, S. O. New full evolutionary sequences of H and He atmosphere massive white dwarfs stars using MESA. *Monthly Notices of the Royal Astronomical Society*, 2018. Citado na página 41.

Liebert, J.; Bergeron, P.; Holberg, J. B. The Formation Rate and Mass and Luminosity Functions of DA White Dwarfs from the Palomar Green Survey. *The Astrophysical Journal, Supplement*, v. 156, p. 47–68, jan. 2005. Citado na página 26.

Liebert, J.; Fontaine, G.; Wesemael, F. The luminosity function and the evolution of surface abundances of white dwarfs. *The Astrophysical Journal*, v. 58, p. 17–31, 1987. Citado na página 28.

Liebert, J. et al. Temperatures for hot and pulsating DB white dwarfs obtained with the IUE Observatory. *The Astrophysical Journal*, v. 309, p. 241–252, out. 1986. Citado na página 28.

Lorén-Aguilar, P.; Isern, J.; García-Berro, E. High-resolution Smoothed Particle Hydrodynamics simulations of the colaescence of double white dwarfs. In: Kunze, K. E.; Mars, M.; Vázquez-Mozo, M. A. (Ed.). *American Institute of Physics Conference Series*. [S.l.: s.n.], 2009. (American Institute of Physics Conference Series, v. 1122), p. 320–323. Citado na página 28.

McGraw, J. T. et al. PG1159-035: A new, hot, non-DA pulsating degenerate. In: van Horn, H. M.; Weidemann, V.; Savedoff, M. P. (Ed.). *IAU Colloq. 53: White Dwarfs and Variable Degenerate Stars*. [S.l.: s.n.], 1979. p. 377–381. Citado na página 27.

Mestel, L. On the theory of white dwarf stars: I. the energy sources of white dwarfs. *Monthly Notices of the Royal Astronomical Society*, v. 112, n. 6, p. 583–597, 1952. Disponível em: <http://dx.doi.org/10.1093/mnras/112.6.583>. Citado na página 31.

Meynet, G. et al. Grids of massive stars with high mass loss rates. V. From 12 to 120 $M_\odot$ at Z=0.001, 0.004, 0.008, 0.020 and 0.040. *Astronomy and Astrophysics Supplement Series*, v. 103, p. 97–105, jan. 1994. Citado na página 32.

Mowlavi, N. et al. Grids of stellar models. VII. From 0.8 to 60 $M_\odot$ at $Z = 0.10$. *Astronomy and Astrophysics Supplement Series*, v. 128, p. 471–474, mar. 1998. Citado na página 32.

Obi, S. The Structure of Stellar Model with Double Energy Source and its Application to the Study on Stellar Evolution. *Publications of the Astronomical Society of Japan*, v. 9, p. 26, 1957. Citado na página 31.

Oke, J. B.; Schwarzschild, M. Inhomogeneous Stellar Models. I. Models with a Convective Core and a Discontinuity in the Chemical Composition. *The Astrophysical Journal*, v. 116, p. 317, set. 1952. Citado na página 31.

Öpik, E. Tracks of stellar evolution. *Pub. Obs. Astron. Tartu.*, v. 3, 1938. Citado na página 30.

Paxton, B. et al. Modules for Experiments in Stellar Astrophysics (MESA). *The Astrophysical Journal, Supplement*, v. 192, p. 3, jan. 2011. Citado 4 vezes nas páginas 13, 33, 35, and 37.

Paxton, B. et al. Modules for Experiments in Stellar Astrophysics (MESA): Planets, Oscillations, Rotation, and Massive Stars. *The Astrophysical Journal, Supplement*, v. 208, p. 4, set. 2013. Citado 3 vezes nas páginas 33, 35, and 38.

Paxton, B. et al. Modules for Experiments in Stellar Astrophysics (MESA): Binaries, Pulsations, and Explosions. *The Astrophysical Journal, Supplement*, v. 220, p. 15, set. 2015. Citado 2 vezes nas páginas 33 and 35.

Paxton, B. et al. Modules for Experiments in Stellar Astrophysics (MESA): Convective Boundaries, Element Diffusion, and Massive Star Explosions. *The Astrophysical Journal, Supplement*, v. 234, p. 34, fev. 2018. Citado 3 vezes nas páginas 33, 35, and 36.

Pietrinferni, A. et al. A Large Stellar Evolution Database for Population Synthesis Studies. I. Scaled Solar Models and Isochrones. *The Astrophysical Journal*, v. 612, p. 168–190, set. 2004. Citado na página 32.

Pignatari, M. et al. NuGrid Stellar Data Set. I.Stellar Yields from H to Bi for Stars with Metallicities $Z = 0.02$ and $Z = 0.01$. *The Astrophysical Journal, Supplement*, v. 225, p. 24, ago. 2016. Citado 4 vezes nas páginas 32, 33, 34, and 35.

Poelarends, A. J. T. et al. The Supernova Channel of Super-AGB Stars. *The Astrophysical Journal*, v. 675, p. 614–625, mar. 2008. Citado na página 25.

Potekhin, A. Y.; Chabrier, G. Thermodynamic Functions of Dense Plasmas: Analytic Approximations for Astrophysical Applications. *Contributions to Plasma Physics*, v. 50, p. 82–87, jan. 2010. Citado 3 vezes nas páginas 17, 37, and 38.

Prada Moroni, P. G.; Straniero, O. Calibration of White Dwarf Cooling Sequences: Theoretical Uncertainty. *The Astrophysical Journal*, v. 581, p. 585–597, dez. 2002. Citado na página 29.

Rebassa-Mansergas, A. et al. The mass function of hydrogen-rich white dwarfs: robust observational evidence for a distinctive high-mass excess near 1 $M_{\odot}$. *Monthly Notices of the Royal Astronomical Society*, v. 452, p. 1637–1642, set. 2015. Citado 3 vezes nas páginas 13, 26, and 27.

Reimers, D. Circumstellar absorption lines and mass loss from red giants. *Mémoires of the Société Royale des Sciences de Liège*, v. 8, p. 369–382, 1975. Disponível em: <http://adsabs.harvard.edu/abs/1975MSRSL...8..369R>. Citado na página 38.

Ritossa, C.; Garcia-Berro, E.; Iben JR., I. On the Evolution of Stars That Form Electron-degenerate Cores Processed by Carbon Burning. II. Isotope Abundances and Thermal Pulses in a 10 $M_{\odot}$ Model with an ONe Core and Applications to Long-Period Variables, Classical Novae, and Accretion-induced Collapse. *The Astrophysical Journal*, v. 460, p. 489, mar. 1996. Citado na página 33.

Ritossa, C.; García-Berro, E.; Iben JR., I. On the Evolution of Stars that Form Electron-degenerate Cores Processed by Carbon Burning. V. Shell Convection Sustained by Helium Burning, Transient Neon Burning, Dredge-out, Urca Cooling, and Other Properties of an 11 M_{solar} Population I Model Star. *The Astrophysical Journal*, v. 515, p. 381–397, abr. 1999. Citado na página 28.

Ritter, A. On the Constitution of Gaseous Celestial Bodies. *The Astrophysical Journal*, v. 8, p. 293, dez. 1898. Citado na página 30.

Ritter, C. et al. NuGrid Stellar Data Set. II. Stellar Yields from H to Bi for Stellar Models with Mzams = 1 to 25$M_{\odot}$ and Z = 0.0001 to 0.02. *ArXiv e-prints*, set. 2017. Citado 4 vezes nas páginas 32, 33, 34, and 35.

Rogers, F. J.; Nayfonov, A. Updated and Expanded OPAL Equation-of-State Tables: Implications for Helioseismology. *The Astrophysical Journal*, v. 576, p. 1064–1074, set. 2002. Citado 2 vezes nas páginas 17 and 37.

Romero, A. D.; Campos, F.; Kepler, S. O. The age-metallicity dependence for white dwarfs stars arXiv : 1504 . 03945v1 [astro-ph . SR] 15 Apr 2015. v. 000, n. April, apr 2015. Disponível em: <http://arxiv.org/abs/1504.03945http://dx.doi.org/10.1093/mnras/stv848>. Citado na página 33.

Romero, A. D. et al. Toward ensemble asteroseismology of ZZ Ceti stars with fully evolutionary models. *Monthly Notices of the Royal Astronomical Society*, v. 420, p. 1462–1480, fev. 2012. Citado 7 vezes nas páginas 15, 33, 41, 42, 45, 55, and 58.

Romero, A. D. et al. Asteroseismological Study of Massive ZZ Ceti Stars with Fully Evolutionary Models. *The Astrophysical Journal*, v. 779, n. 1, p. 58, oct 2013. ISSN 0004-637X. Disponível em: <http://arxiv.org/abs/1310.4137>. Citado 9 vezes nas páginas 15, 33, 38, 41, 42, 45, 54, 55, and 58.

Salaris, M.; Althaus, L. G.; García-Berro, E. Comparison of theoretical white dwarf cooling timescales. *Astronomy & Astrophysics*, v. 555, p. A96, jul. 2013. Citado na página 33.

Salpeter, E. E. The Luminosity Function and Stellar Evolution. *Astrophysical Journal*, v. 121, p. 161, jan. 1955. Citado 2 vezes nas páginas 25 and 26.

Sampson, R. A. Sun, rotation and mechanical state of the. *Monthly Notices of the Royal Astronomical Society*, v. 55, p. 280, mar. 1895. Citado na página 30.

Saumon, D.; Chabrier, G.; van Horn, H. M. An Equation of State for Low-Mass Stars and Giant Planets. *The Astrophysical Journal, Supplement*, v. 99, p. 713, ago. 1995. Citado 2 vezes nas páginas 17 and 37.

Schaerer, D. et al. Grids of stellar models. II - From 0.8 to 120 solar masses at Z = 0.008. *Astronomy and Astrophysics Supplement Series*, v. 98, p. 523–527, maio 1993. Citado na página 32.

Schaller, G. et al. New grids of stellar models from 0.8 to 120 solar masses at Z = 0.020 and Z = 0.001. *Astronomy and Astrophysics Supplement Series*, v. 96, p. 269–331, dez. 1992. Citado na página 32.

Schneider, A. S. et al. Direct molecular dynamics simulation of liquid-solid phase equilibria for two-component plasmas. *Physical Review E*, v. 85, n. 6, p. 066405, jun. 2012. Citado na página 38.

Schoenberner, D. Asymptotic giant branch evolution with steady mass loss. *Astronomy & Astrophysics*, v. 79, p. 108–114, out. 1979. Citado na página 27.

Schönberg, M.; Chandrasekhar, S. On the Evolution of the Main-Sequence Stars. *The Astrophysical Journal*, v. 96, p. 161, set. 1942. Citado na página 31.

Schwab, J.; Bildsten, L.; Quataert, E. The importance of Urca-process cooling in accreting ONe white dwarfs. *Monthly Notices of the Royal Astronomical Society*, v. 472, p. 3390–3406, dez. 2017. Citado 2 vezes nas páginas 33 and 35.

Schwarzschild, K. On the equilibrium of the Sun's atmosphere. *Nachrichten von der Königlichen Gesellschaft der Wissenschaften zu Göttingen. Math.-phys. Klasse, 195, p. 41-53*, v. 195, p. 41–53, 1906. Citado na página 30.

Siess, L. Evolution of massive AGB stars. I. Carbon burning phase. *Astronomy & Astrophysics*, v. 448, p. 717–729, mar. 2006. Citado 2 vezes nas páginas 33 and 46.

Siess, L. Evolution of massive AGB stars. II. model properties at non-solar metallicity and the fate of Super-AGB stars. *Astronomy & Astrophysics*, v. 476, p. 893–909, dez. 2007. Citado 4 vezes nas páginas 27, 28, 41, and 46.

Siess, L. Evolution of massive AGB stars. III. the thermally pulsing super-AGB phase. *Astronomy & Astrophysics*, v. 512, p. A10, mar. 2010. Citado 5 vezes nas páginas 14, 25, 33, 47, and 49.

Sun, M.; Arras, P. Formation of Extremely Low-mass White Dwarfs Binaries. *ArXiv e-prints*, mar. 2017. Citado 3 vezes nas páginas 33, 35, and 39.

Thoul, A. A.; Bahcall, J. N.; Loeb, A. Element diffusion in the solar interior. *The Astrophysical Journal*, v. 421, p. 828–842, fev. 1994. Citado na página 38.

Timmes, F. X.; Swesty, F. D. The Accuracy, Consistency, and Speed of an Electron-Positron Equation of State Based on Table Interpolation of the Helmholtz Free Energy. *The Astrophysical Journal, Supplement*, v. 126, p. 501–516, fev. 2000. Citado 2 vezes nas páginas 17 and 37.

Tremblay, P.-E. et al. Spectroscopic analysis of DA white dwarfs with 3D model atmospheres. *Astronomy & Astrophysics*, v. 559, p. A104, nov. 2013. Citado 2 vezes nas páginas 26 and 54.

Ulrich, R. K. Thermohaline Convection in Stellar Interiors. *The Astrophysical Journal*, v. 172, p. 165, fev. 1972. Citado na página 38.

van Horn, H. M. Crystallization of White Dwarfs. *The Astrophysical Journal*, v. 151, p. 227, jan. 1968. Citado na página 38.

Van Horn, H. M. Crystallization of a classical, one-component coulomb plasma. *Physics Letters A*, v. 28, p. 706–707, fev. 1969. Citado na página 38.

von Weizsäcker, C. F. Über elementumwandlungen in innern der sterne ii. *Physikalische Zeitschrift.*, v. 39, p. 633–646, 1938. Citado na página 30.

Wang, B.; Podsiadlowski, P.; Han, Z. He-accreting carbon-oxygen white dwarfs and Type Ia supernovae. *Monthly Notices of the Royal Astronomical Society*, v. 472, p. 1593–1599, dez. 2017. Citado 3 vezes nas páginas 29, 33, and 35.

Weaver, T. A.; Zimmerman, G. B.; Woosley, S. E. Presupernova evolution of massive stars. *The Astrophysical Journal*, v. 225, p. 1021–1029, nov. 1978. Citado na página 32.

Winget, D. E. et al. An independent method for determining the age of the universe. *The Astrophysical Journall*, v. 315, p. L77–L81, abr. 1987. Citado na página 28.

Woosley, S. E.; Heger, A. The Remarkable Deaths of 9-11 Solar Mass Stars. *The Astrophysical Journal*, v. 810, p. 34, set. 2015. Citado 3 vezes nas páginas 25, 33, and 47.

APPENDIX A – Submitted Paper

MNRAS **000**, 1–14 (2018) Preprint 14 June 2018 Compiled using MNRAS LaTeX style file v3.0

New full evolutionary sequences of H and He atmosphere massive white dwarfs stars using MESA

G.R. Lauffer,[1]★ A. D. Romero,[1] S.O. Kepler[1]
[1] *Instituto de Física, Universidade Federal do Rio Grande do Sul, Av. Bento Goncalves 9500, Porto Alegre 91501-970, RS, Brazil*

Accepted XXX. Received YYY; in original form ZZZ

ABSTRACT

We explore the evolution of hydrogen-rich and hydrogen-deficient white dwarfs stars with masses between 1.012 and 1.307 $M_\odot$, and initial metallicity of $Z = 0.02$. These sequences are the result of main sequence stars with masses between 8.8 and 11.8 $M_\odot$. The simulations were performed with MESA, starting at the zero-age main sequence, through thermally pulsing and mass-loss phases, ending at the white dwarfs cooling sequence. We present reliable chemical profiles for the whole mass range considered, covering the different expected central compositions, i.e. C/O, O/Ne and Ne/O/Mg, and its dependence with the stellar mass. In addition, we present detailed chemical profiles of hybrid C/O-O/Ne core white dwarfs, found in the mass range between 1.024 and 1.15 $M_\odot$. We present the initial-to-final mass relation, mass-radius relation, and cooling times considering the effects of atmosphere and core composition.

Key words: stars: white dwarfs, evolution – methods: numerical

1 INTRODUCTION

White dwarf stars are the most common final stage of stellar evolution. They are the end product of main sequence stars with masses up to 5 – 12 $M_\odot$ (García-Berro et al. 1997a; Poelarends et al. 2008; Siess 2010; Langer 2012; Woosley & Heger 2015; Doherty et al. 2015), depending on metallicity, which correspond to 95–97% of all stars in the Galaxy. White dwarf stars are excellent galactic chronometers as they are slowly cooling, releasing the heat stored in the core. The age of stellar populations can be obtained by comparisons of theoretical computations with the distribution in the color-magnitude Diagram (Hansen et al. 2007; Campos et al. 2016) or from the white dwarf luminosity function (Winget et al. 1987; Bedin et al. 2010; García-Berro et al. 2014). The connection between the properties of progenitor stars and white dwarfs is printed in the initial-to-final mass relation (IFMR) which leads to constraints on the upper mass limit that separates white dwarfs progenitors of Type II supernovae (Siess 2007; Catalán et al. 2008). Also binary systems with white dwarfs are believed to produce Type Ia supernovae as result of accretion that exceeds the upper mass limit (e.g. Wang et al. 2017). Finally, a comparison between models and observations of white dwarfs can enhance the comprehension of the physical properties of high density matter (e.g. Prada Moroni & Straniero 2002; Isern et al. 2010).

The white dwarf stars can be divided into two main classes: DA and non-DA types, based on the main component of their atmosphere. The DA spectral class shows an hydrogen rich atmosphere and represent ≃ 84% of all white dwarfs (e.g. Kepler et al. 2007) while non-DA's have hydrogen deficient atmospheres. The non-DA white dwarfs can be classified by the dominant element in the atmosphere and effective temperature: DO class with strong lines of HeII and effective temperatures of $T_{\rm eff} \approx 45,000 - 200,000$ K, DB class with strong HeI lines and $T_{\rm eff} \approx 11,000 - 30,000$ K, and for effective temperatures bellow $T_{\rm eff} \approx 11,000$ K there are DC, DQ and DZ types with traces of carbon and metals in their spectra. The helium-rich white dwarfs are believed to be progeny of PG 1159 stars (McGraw et al. 1979) formed by a Born-Again episode (Schoenberner 1979; Iben et al. 1983) in which a helium flash occurs during the cooling sequence (i.e. very late thermal pulse) forcing the star to evolve back to the asymptotic giant branch (AGB). As a result, this very late thermal pulse burns out all hydrogen left in the atmosphere of the star.

White dwarfs with stellar masses in the range 0.4 – 1.05 $M_\odot$ are believed to harbor a carbon-oxygen (C/O) core after central hydrogen and helium burning on earlier stages of evolution. On the other hand, the progenitors of white dwarfs with masses larger than ≈ 1.05 $M_\odot$ (García-Berro et al. 1997a; Siess 2007) should reach temperature high enough to achieve stable carbon burning forming a oxygen-neon (O/Ne) or neon-oxygen-magnesium (Ne/O/Mg) core, depending if carbon burning ignites off-center or at the center of the star. When carbon burning starts off-center, ignition is followed by a inward propagation of the burning front (hereafter carbon flame). This carbon flame may or may not

---

★ E-mail: gabriel.lauffer@ufrgs.br

© 2018 The Authors

reach the center. If the flame does not reach the center a hybrid C/O+O/Ne white dwarf will form (Denissenkov et al. 2013; Farmer et al. 2015), whilst a flame which reaches the center will form a Ne/O/Mg white dwarf. These results are dependent on the evolutionary code and input physics considered. Siess (2007) calculated sequences for several metallicities, with and without overshooting, and found that for $Z = 0.02$ the minimum core mass for O/Ne/ cores is 1.04 $M_\odot$. Doherty et al. (2015), based on models at the thermally pulsing asymptotic giant branch phase (TP-AGB), found that for $Z = 0.02$ the minimum core mass for a O/Ne core white dwarf star is 1.154 $M_\odot$. The determination of the mass range for each type of core composition is fundamental to improve our understanding of the populations of massive white dwarf stars.

The number of spectroscopically confirmed white dwarf stars has increase to more than ≈ 30 000 with surveys like the Sloan Digital Sky survey (Ahn et al. 2014). The mass distribution for DA white dwarf stars presented by Kleinman et al. (2013) is centered at 0.649 $M_\odot$ but presents another peak at 0.811 $M_\odot$ (Kepler et al. 2015). In addition, an analysis of 112 isolated massive white dwarfs performed by Należyty & Madej (2004) showed that, for known white dwarfs with masses ≥ 0.8 $M_\odot$, the mass distribution has a primary peak at ≈ 0.8 $M_\odot$ and a secondary peak at 1.04 $M_\odot$. Around 20% of all DA white dwarfs are more massive than 0.8 $M_\odot$ (Liebert et al. 2005; Kepler et al. 2007) and about 9% have mass around 1.12 $M_\odot$ (Kepler et al. 2007). Recent works presents a high mass tail on the mass distribution with an excess for masses around $M_{\rm WD} \approx 1.0$ $M_\odot$ (Falcon et al. 2010; Tremblay et al. 2013; Rebassa-Mansergas et al. 2015; Kepler et al. 2016).

In the literature, several evolutionary models for low and intermediate mass white dwarf stars can be found. For instance Romero et al. (2012, 2013) and Althaus et al. (2009) for C/O core DA and non-DA white dwarfs, respectively, and Althaus et al. (2013); Istrate et al. (2014, 2016, 2017); Sun & Arras (2017) for low and extremely low mass white dwarfs, are just some recent works. On the other hand, there is a lack of full evolutionary models for massive white dwarfs. Some recent work computed the evolution of super asymptotic branch stars until the end of the thermally pulsing phase (Siess 2010; Gil-Pons et al. 2013; Jones et al. 2013; Doherty et al. 2015), but they do not compute the following post-AGB stage nor the white dwarf evolution. Other authors computed white dwarf models by generating static/politropic models at the top of the cooling sequence and/or by rescaling the mass and/or artificially inserting a previously calculated chemical profile with fixed O/Ne ratios and fixed hydrogen and helium layers on the atmosphere (Benvenuto & Althaus 1999; Salaris et al. 2000; Althaus et al. 2005b, 2007; Salaris et al. 2013).

The present work is intended to fill the gap due to the lack of full evolutionary sequences for massive white dwarfs, computed from the Zero Age Main Sequence (ZAMS) through red giant branch (RGB) and AGB to the white dwarf cooling sequence. To this end we used the MESA evolutionary code (Paxton et al. 2011, 2013, 2015, 2018). We computed full evolutionary sequences with initial masses in the range of $8.8 - 11.8$ $M_\odot$ resulting in white dwarfs models with masses in the range of $1.01 - 1.31$ $M_\odot$, adding both hydrogen and helium-rich envelopes. This paper is organized as follows. On section 2 we present the MESA evolutionary code and the input physics considered in our computations. The results from our full evolutionary computations are presented in section 3. Section 4 is intended to discuss the mass-radius relation of our sequences. Finally we present our final remarks on section 5.

2 NUMERICAL SIMULATIONS

The numerical simulations where performed using the MESA code (Paxton et al. 2011, 2013, 2015, 2018) version r8845. We started the computations on the ZAMS, considering an initial metallicity $Z = 0.02$. We computed the hydrogen burning and helium burning stages, and the RGB and AGB mass loss phases. The sequences ended as C/O or O/Ne/Mg white dwarfs cooling until $\log L/L_\odot \sim -4$, which represents $T_{\rm eff} \approx 7\,000 - 10\,000$ K depending on final mass.

The MESA evolutionary code has been extensively used to perform calculations of extremely low-mass white dwarfs (Istrate et al. 2016, 2017; Sun & Arras 2017), hybrid C/O/Ne white dwarfs and Type Ia SN progenitors (Jones et al. 2013; Denissenkov et al. 2013; Chen et al. 2014; Farmer et al. 2015; Brooks et al. 2017a), accreting white dwarf binaries with C/O core (Brooks et al. 2016; Wang et al. 2017) and O/Ne core (Schwab et al. 2017; Brooks et al. 2017b), white dwarf isochrones (Dotter 2016) and set of sequences covering the white dwarf mass range (Choi et al. 2016; Pignatari et al. 2016; Ritter et al. 2017).

We detail the input physics considered prior and during white dwarf evolution in the following subsections.

2.1 Pre-white dwarf evolution

On the evolutionary phases prior to the cooling sequence we considered the nuclear network `co_burn_plus.net` which has 16 elements from hydrogen to silicon, ^{1}H, ^{3,4}He, ^{12,13}C, $^{13-15}$N, $^{16-18}$O, ^{19}F, ^{20,22}Ne, ^{24}Mg, and ^{28}Si. This network has 67 nuclear reactions, including pp-chain, CNO cycle, triple-alpha and some auxiliary reactions. We used JINA reaclib (Cyburt et al. 2010) with electron screening factors for thermonuclear reactions from Graboske et al. (1973) and DeWitt et al. (1973) for weak and intermediate screening, and Alastuey & Jancovici (1978) for the strong screening regime. Plasma parameters are those from Itoh et al. (1979). The energy-loss rates including the derivatives from thermal neutrinos are from Itoh et al. (1996). The equation of state (EOS) is based on the OPAL EOS tables (Rogers & Nayfonov 2002) including the SCVH tables (Saumon et al. 1995) for lower temperatures and densities and the HELM (Timmes & Swesty 2000) and PC (Potekhin & Chabrier 2010) EOS for higher temperatures and densities.

Convection was consider using Ledoux criterion, which takes into account the composition gradient, along with the Cox implementation of MLT (Cox & Giuli 1968) with a mixing length free parameter $\alpha_{\rm MLT} = 2$. The diffusion and gravitational settling in MESA are calculated by solving the equations from Burgers (1969) with coefficients of Thoul et al. (1994). In the overshoot region MESA treats convective mixing as a time-dependent diffusion process, with a diffusion coefficient given by,

$$D_{\rm OV} = D_{\rm conv,0} \exp - \frac{2z}{f \lambda_{\rm P,0}} \tag{1}$$

where $D_{\rm conv,0}$ is the MLT derived diffusion coefficient at the convective boundary, z is the distance from the convective boundary, $\lambda_{\rm P,0}$ is the local pressure scale height and f is the adjustable parameter (Herwig 2000), which can have different values at the upper and lower convective boundaries for H-burning, He-burning, metal-burning (i.e all burning regions that are not H or He-burning) and non-burning convection zones. Due to convergence issues, overshooting was only considered for the lower boundary of metal-burning convective region with parameters set to `overshoot_f_below_burn_z_shell` = 0.1 and `overshoot_f0_below_burn_z_shell` = 0.01. The mixing in regions unstable to Schwarzschild but stable to Ledoux is treated by semiconvection (Langer et al. 1983) using the dimensionless efficiency parameter $\alpha_{\rm sc} = 0.01$. Thermohaline mixing (Ulrich 1972; Kippenhahn et al. 1980) is also considered with efficiency parameter set to $\alpha_{\rm th} = 2$. For details in the implementation of semiconvection and thermohaline mixing the reader is referred to section 4 of Paxton et al. (2013).

Mass loss was considered during the giant phases, i.e. RGB and AGB phases. We used the mass loss formula from Reimers (1975) with $\eta = 0.1$ during RGB, followed by the Bloecker (1995) scheme with $\eta = 10$ on the AGB. The opacity tables are those from OPAL type 2 (Iglesias & Rogers 1996) for enhanced C/O variations in composition. We used a gray atmosphere for the entire evolution. Finally, we do not consider rotation in our computations.

2.2 White dwarf evolution

Chemical diffusion and gravitational settling was modeled following the formulation from Burgers (1969). Sun & Arras (2017) suggested that the routine `diffusion_use_cgs_solver` is better suited for electron degeneracy, however they considered only very low mass white dwarf models with stellar mass below $M_{\rm WD} < 0.17$ M$_\odot$. Employing this formulation for diffusion in massive models leads to numerical instabilities and to non-physical chemical profiles. Convection was shut down due to numerical instabilities during the cooling sequence. We found no differences in the final ages of simulations with and without convection and the Sun & Arras (2017) formulation on the cooling sequence. Thus, our treatment of diffusion and convection do not affect the cooling times in the mass range considered in this work. The energy-loss rates from thermal neutrinos and its derivatives are from Itoh et al. (1996).

White dwarf stars are expected to undergo crystallization as a result of strong Coulomb interactions in their dense interiors (van Horn 1968). The transition occurs when the energy of the Coulomb interaction between neighboring ions is much larger than their thermal energy. The ratio between these two contributions can be expressed as a coupling parameter $\Gamma = \bar{Z}^2 e^2 / a_i k_B T$ where $\bar{Z}$ is the average ion charge, a_i is the mean ion spacing and the other symbols have their usual meaning. Crystallization for pure oxygen plasma begins when $\Gamma \approx 175$ (Van Horn 1969). The onset of crystallization also depends on the adopted phase diagram. Near the crystallization limit ($\Gamma \sim 175$) MESA uses the Potekhin & Chabrier (2010) equation of state (PC EOS) which accounts for the thermodynamics of crystals. By default, MESA changes from HELM EOS to PC EOS when the Coulomb coupling parameter $\Gamma > 80$ and considers a mixture of solid and liquid for $\Gamma_{\rm i} = 150$ and a full crystal when $\Gamma_{\rm full} = 175$. Those values where obtained by Potekhin & Chabrier (2010). Results from the asteroseismological analysis performed by Romero et al. (2013) indicates that the azeotropic type phase diagram from Horowitz et al. (2010) (see also Schneider et al. 2012; Hughto et al. 2012) better represents the crystallization on white dwarfs cores. Hence, we modified the values for the coupling constant Γ to $\Gamma_{\rm i} = 215$ and $\Gamma_{\rm full} = 220$ in our computations. Thus, the release of latent heat occur for $\Gamma = 215 - 220$. This modification had to be done on the file `pc_eos.f` located inside MESA `eos` module. Until MESA version r8845 used in this work there was not an option to control those parameters.

The Debye cooling regime, which affects the cooling times of white dwarfs at lower luminosities, was not considered in our simulations. However, this effect will not be important since it occurs for temperatures below ~ 10 000 K and luminosities lower than $\log L/L_\odot < -4.06$ (Althaus et al. 2007) for the mass range considered in this work (see section 3.6).

3 EVOLUTION FROM THE ZAMS TO THE COOLING CURVE

We calculated 16 full evolutionary sequences with initial metallicity $Z = 0.02$ and initial mass at the ZAMS between 8.80 and 11.80 M$_\odot$. As a result we obtained white dwarf models with stellar masses ranging from 1.012 to 1.307 M$_\odot$. Further refinement on the initial masses can lead to the Chandrasekhar mass limit. Note that within this mass range there are two possible core compositions, i.e, C/O and O/Ne/Mg. These computations complement at high stellar masses the works of Romero et al. (2012, 2013) who computed C/O core white dwarf sequences with stellar masses below $M_{WD} = 1.050$ M$_\odot$. Our H and He atmosphere sequences have evolved equally on the stage prior to the cooling sequence, therefore there is no distinction on the evolution previous to the white dwarf stage.

During the AGB, the computations present numerical difficulties related to the mass loss episodes. In this stage we use the mass loss prescription of Bloecker (1995) with a factor η=10, that leads to the complete removal of the hydrogen envelope, preventing the occurrence of thermal pulses, in all sequences. A less efficient mass loss rate, achieve by decreasing the value of η, does not allow us to compute the stages following the AGB stage and also leads to the complete removal of hydrogen. The same occurs for other built in mass loss schemes. García-Berro et al. (1997a) discussed that models with rapid radiative wind during AGB phase are expected to loss all its hydrogen layer on atmosphere and most of its helium layer leading to a PG 1159 star, but real massive white dwarfs are known with H and He envelopes. In order to produce hydrogen atmosphere white dwarf sequences we artificially added hydrogen at the surface of the models. This procedure was performed at high effective temperature, near the beginning of the cooling sequences, so the transitory ef-

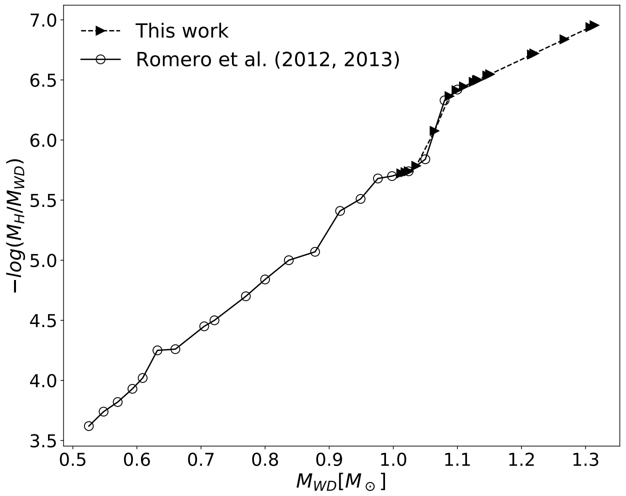

Figure 1. Range of star mass and hydrogen envelope mass. Circles are from Romero et al. (2012, 2013) and triangles are the extrapolated data.

fects caused by the artificial procedure are rapidly washed out. The amount of hydrogen added to each sequence was computed by a linear extrapolation to higher stellar mass the results of Romero et al. (2012, 2013). The amount of hydrogen as a function of the white dwarf stellar mass is shown in Figure 1. Circles correspond to the results from Romero et al. (2012, 2013), while the triangles correspond to the values extrapolated for higher stellar masses.

As an example, Figure 2 shows two chemical profile in terms of outer mass fraction at $T_{\rm eff} \approx 80\,000$ K on the cooling curve for a sequence with stellar mass $M_{\rm WD} = 1.019$ $M_\odot$ and a C/O core. The bottom panel shows the chemical profile for the helium atmosphere case and the top panel presents the chemical profile for the hydrogen atmosphere sequence, after $M_{\rm H} = 1 \times 10^{-5.7} M_{\rm WD}$ of hydrogen was artificially added to the model. Note that the only difference between the two chemical profiles shown in Figure 2 is the chemical abundance of the outer layers, while the core regions remain the same.

The sequences with final masses $M_{\rm WD} \geq 1.024$ $M_\odot$ experience loops at high luminosity and high effective temperature region in the post-AGB stage (see Figure 3). The loops are due to carbon shell-burning followed by helium shell-burning which, for sequences with $M_{\rm WD} \geq 1.132$ $M_\odot$, burns all the helium content in the outer layers. These helium shell-burning happens due to the huge temperature gradient on the shells surrounding the core. Thus, enough shells must be added in the numerical models in these regions to account for the large temperature gradients and composition gradients in the shell burning regions.

For sequences with $M_{\rm WD} \geq 1.132$ $M_\odot$ helium was added on top of the model at the beginning of the cooling sequence using the same procedure as to add hydrogen. The amount of helium to be added was extrapolated from our sequences which had not burnt all helium. The amount of hydrogen and helium for each sequence is presented in columns 3 and 4 of table 1, along with the initial mass at the ZAMS and the white dwarf mass in column 1 and 2, respectively. Helium atmosphere sequences were produced by not adding hydrogen on top of the models.

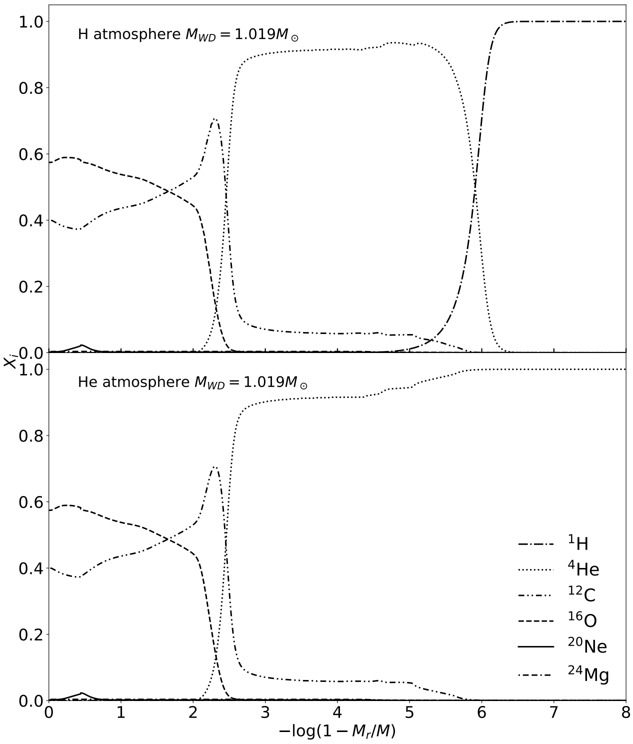

Figure 2. Example of chemical profile in terms of the outer mass fraction at $T_{\rm eff} \approx 80,000$ K on the cooling sequence for H atmosphere (top) and He atmosphere (bottom) white dwarf with 1.019 $M_\odot$. Hydrogen had to be added on all sequences due to losses on mass loss phase. The quantities added on each evolution are shown in table 1. This figure show that only the atmosphere of the star was changed. The nuclei composition are identical to both H and He atmosphere sequences.

The Hertzprung-Russell diagram from ZAMS to white dwarf cooling sequence is shown in Figure 3 for three sequences with initial masses 8.9, 10 and 11 $M_\odot$ and final masses of 1.019, 1.11 and 1.22 $M_\odot$ in the cooling curve, respectively. Each sequence in this figure have a different core composition as a white dwarf star. The solid, dashed, and dotted lines represent a C/O core white dwarf with $M_{\rm WD} = 1.019$ $M_\odot$, an O/Ne core white dwarf with $M_{\rm WD} = 1.11$ $M_\odot$ and a Ne/O/Mg white dwarf with $M_{\rm WD} = 1.22$ $M_\odot$, respectively.

The $M_{\rm WD} = 1.019$ $M_\odot$ sequence with C/O core experienced a core hydrogen burning stage lasting for 24.51 Myr, and then during the next 2.80 Myr helium has burn until depletion at the center. For more massive sequences the time spent on main sequence and central helium burning decreases. For the sequences with final mass $M_{\rm WD} = 1.11$ $M_\odot$, with a O/Ne core, the total main sequence time is 19.75 Myr plus 2.28 Myr to burn all helium. Last, the sequence with final mass $M_{\rm WD} = 1.22$ $M_\odot$ burnt hydrogen for 16.83 Myr until depletion at the center and burnt helium for 1.81 Myr until extinction at the center. The ages for hydrogen and helium depletion at center and progenitor age, i.e., age at the beginning of the cooling sequence, are listed in columns 3, 4 and 5 of Table 3, respectively (see section 3.6).

Table 1. Values of initial mass at ZAMS ($M_{\rm ZAMS}$), White dwarfs masses ($M_{\rm WD}$) and hydrogen content for H-rich sequences and helium contents for both H and He atmosphere sequences. Hydrogen abundances where extrapolated from Romero et al. (2012, 2013). The Helium abundances were extrapolated for sequences with $M_{\rm WD} \geq 1.132$.

$M_{\rm ZAMS}$ [$M_\odot$]	$M_{\rm WD}$ [$M_\odot$]	$-\log M_{\rm H}/M_{\rm WD}$	$-\log M_{\rm He}/M_{\rm WD}$
8.80	1.012	5.722	2.451
8.90	1.019	5.732	2.466
9.00	1.024	5.740	3.477
9.20	1.036	5.785	3.349
9.50	1.064	6.076	2.958
9.80	1.088	6.365	4.006
10.00	1.110	6.446	3.517
10.10	1.125	6.484	2.447
10.20	1.131	6.498	2.489
10.30	1.132	6.500	2.495
10.45	1.147	6.536	2.597
10.50	1.151	6.547	2.628
10.80	1.216	6.711	3.089
11.00	1.220	6.720	3.116
11.40	1.267	6.838	3.449
11.80	1.307	6.939	3.735

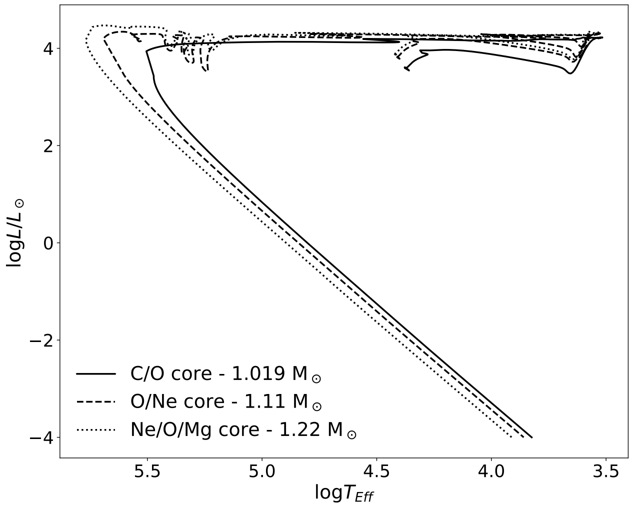

Figure 3. Evolutionary tracks for three sequences in the HR diagram, with initial masses 8.9 (solid line), 10 (dashed line) and 11 M$_\odot$ (dotted line) and final masses 1.019, 1.11 and 1.22 M$_\odot$, respectively. Each sequence has a different core composition in the cooling curve stage, being C/O, O/Ne and Ne/O/Mg for the sequences with white dwarf masses 1.019, 1.11 and 1.22 M$_\odot$, respectively.

3.1 Carbon flame

As can be seen from Figure 3, the sequences characterized with white dwarf masses of $1.11 M_\odot$ and $1.22 M_\odot$ presents loops on the upper left region of the HR diagram, prior to entering the white dwarf cooling sequence. Those loops are due to carbon burning which ignites off-center and moves inwards to the center of the star. In particular, towards the end of the loop, just before the extinction of the carbon burning, helium ignites on a shell near the surface. All sequences with $M_{\rm WD} \geq 1.024$ M$_\odot$ experiences an off-center carbon ignition prior to the white dwarf stage, and for sequences with $M_{\rm WD} \geq 1.132$ M$_\odot$ the subsequent helium burning consumes all the helium content in the outer layers. If the carbon flame do not reach the center of the star, a hybrid C/O-O/Ne white dwarf will form (Denissenkov et al. 2013), while if the flame propagates to the center a O/Ne/Mg white dwarf will be produced. The occurrence of the late carbon flashes can be an explanation for the Be star CD-59 6479 (Henize 1976; Reindl et al. 2014).

All sequences which experienced a carbon flame presented subsequent flames which started further away from the center and were quenched before the starting point of the previous flame. Figure 4 shows the location in mass where the first carbon ignition occurs (full line) and the location of the extinction of the carbon flame which got closest to center (dashed line), as a function of the white dwarf mass which experienced a carbon flame. Note that the sequences with stellar mass $M_{\rm WD} < 1.024$ M$_\odot$ do not experience carbon ignition. The dotted vertical lines separate the mass range for different core compositions (see subsection 3.3). As can be seen from this figure, the position of the first carbon ignition gets closer to the center of the model for increasing white dwarf mass. As the core mass increases the central degeneracy is lower allowing the inner maximum temperature to be near the center causing a carbon ignition closer to center on more massive sequences.

Specifically, the sequence with $M_{\rm ZAMS} = 10$ M$_\odot$ ($M_{\rm WD}$ = 1.11 M$_\odot$) experience an off-center carbon ignition starting at $M_{\rm r}/M_{\rm WD} \sim 0.3$ which moves inwards until $M_{\rm r}/M_{\rm WD} \sim 0.1$, while for the sequence with $M_{\rm ZAMS} = 11.0$ M$_\odot$ ($M_{\rm WD}$ = 1.220 M$_\odot$) carbon ignition starts at $M_{\rm r}/M_{\rm WD} \sim 0.094$ and, in this case, reaches the center of the star. Carbon ignition in all sequences started on regions with density $\rho \sim 1.5 \times 10^6$ gcm^{-3}, agreeing with the results for super-AGB sequences from Farmer et al. (2015). For a detailed discussion about carbon burning we refer to the works of Siess (2006, 2007) and of Farmer et al. (2015) and references therein.

From our computations, some sequences with C/O core in the white dwarf stages experienced a carbon ignition, but the carbon flame only reaches $M_{\rm r}/M_{\rm WD} \sim 0.2$ for those models. When the carbon flame reaches the regions closer than $M_{\rm r}/M_{\rm WD} < 0.2$, a hybrid C/O-O/Ne white dwarf with O/Ne core is formed. For sequences with $M_{\rm WD} > 1.15$ M$_\odot$ the carbon flame reaches the center of the star producing a Ne/O/Mg core white dwarf. The details of core composition and chemical profile will be analyzed on the following subsections.

3.2 The Initial to Final mass relation

Figure 5 presents the Initial to Final Mass Relation obtained from our computations compared to the results of Siess (2010) and Doherty et al. (2015), within the stellar mass range considered in this work. We consider models with metallicity $Z = 0.02$. The final mass obtained in this work is systematically lower than previous results, due to the different input physics considered in each case. Siess (2010) considers the Vassiliadis & Wood (1993) mass loss scheme, a mixing length parameter of $\alpha_{\rm MLT} = 1.75$ and no core overshooting. On the oder hand, Doherty et al. (2015) consider mass loss rate from Reimers (1975) on the RGB, followed

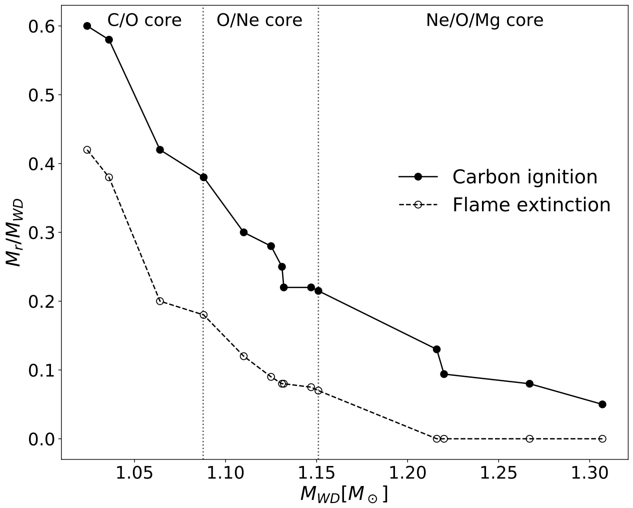

Figure 4. Mass location of the first ignition of carbon and mass location of closest to center flame extinction as function of white dwarf masses which experienced a carbon flame. Vertical dotted lines delimits the mass range for core composition. See text for details.

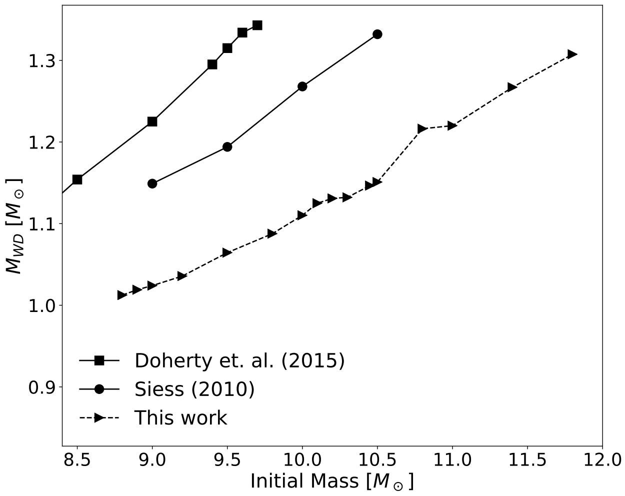

Figure 5. Initial to Final Mass Relation obtained from our computations (triangle) as compared to the results from Siess (2010) (circle) and Doherty et al. (2015) (square). In all cases the initial metallicity is $Z = 0.02$. The data form Doherty et al. (2015) was truncated to show only their massive models.

by Bloecker (1995) at high luminosities and change to Vassiliadis & Wood (1993) on thermally pulsing phase, with similar convection treatment than Siess (2010). Also, both authors evolved their sequences until TP-AGB phase, and then consider the mass of the He-free core as the final mass in the white dwarf stage. As discussed in Siess (2010) the final mass is dependent of core growth and mass loss scheme. In our computations, we calculated full evolutionary sequences by employing the mass loss formula from Reimers (1975) on RGB and Bloecker (1995) on the AGB with a larger efficiency parameter than the mass loss rates considered by previous authors, thus evolving the sequences to post-AGB phase and leading to a lower final mass in the cooling curve. Thus, from our computations, the upper limit of progenitor mass to produce a white dwarf star is $M_{ZAMS} = 11.8\ M_\odot$ for $Z = 0.02$, 21.6% greater than the value found by Doherty et al. (2015) and 12.4% greater compared to Siess (2010) for the same initial metallicity. Considering the dispersion in the Initial to Final Mass relation from the different authors in figure 5, we can estimate for a given initial mass in the ZAMS a range of final white dwarf masses. For instance, a sequence with initial mass of 9 $M_\odot$ can produce a white dwarf with masses ranging from 1.024 to 1.225 $M_\odot$, depending on the input physics applied, specially the mass loss formulation.

3.3 Central abundances in the cooling sequence

Within the stellar mass range studied in this work, we expect to have three main core compositions, i.e., C/O and O/Ne (García-Berro et al. 1997b; Doherty et al. 2015) or Ne/O/Mg, changing with increasing stellar mass. Figure 6 shows central abundances of carbon, oxygen, neon and magnesium in a logarithmic scale, as a function of the white dwarf mass. The values are taken at $T_{\rm eff} \approx 40\,000$ K, a effective temperature low enough to give time for diffusion act on the central composition and still high to prevent crystallization. As shown on Figure 6, the C/O core is dominant for $M_{\rm WD} \leq 1.088\ M_\odot$ due to carbon being more abundant than neon. Between $1.088 < M_{\rm WD} \leq 1.147\ M_\odot$ we have a O/Ne core as neon increases its composition but is still lower than oxygen, whilst for masses $M_{\rm WD} > 1.147\ M_\odot$ neon is the most abundant element on the central composition, followed by oxygen and then by magnesium, so we define the core composition as Ne/O/Mg core. Note that sequences with $M_{\rm WD} > 1.15\ M_\odot$ experienced a carbon flame which reaches to the center of the stars as shown on Figure 4 and discussed on subsection 3.1. Also, the sequence with $M_{\rm WD} = 1.024\ M_\odot$ is the sequences with the lowest stellar mass to experience carbon burning, but it does not reaches the center producing an hybrid C/O-O/Ne white dwarf. This explains the step in the central ^{20}Ne abundance observed in Figure 6 for that stellar mass. Doherty et al. (2015) computed sequences for super-AGB stars and found that, for $Z = 0.02$, sequences with core masses $M_{\rm c} < 1.075\ M_\odot$ become a C/O core white dwarf, sequences with core masses $1.075 \leq M_{\rm c} < 1.154\ M_\odot$ presented a C/O/Ne core and for core masses $M_{\rm c} \geq 1.154\ M_\odot$ the sequences are O/Ne white dwarfs. Woosley & Heger (2015) also calculated sequences on the limit of SN progenitors and obtained models with O/Ne core for a range of core mass $1.088 \leq M_{\rm c} \leq 1.345\ M_\odot$. Chemical profiles from Doherty et al. (2015) and Woosley & Heger (2015) are not publicly available so we can not compare the internal abundances of the last models computed. It is important to note that Doherty et al. (2015) and Woosley & Heger (2015) does not computed the cooling curve, leading to non-full evolutionary model, opposite to the present work. They also uses different evolutionary codes with different nuclear reaction and input physics.

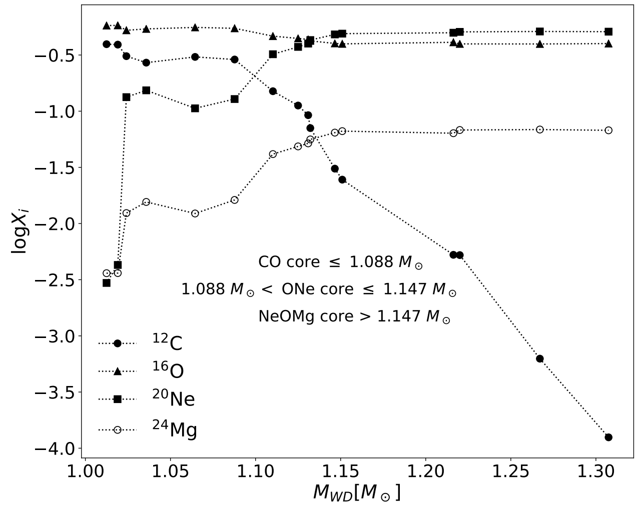

Figure 6. Central abundances versus final mass of the white dwarfs stars before crystallization starts ($T_{\rm eff} \approx 40\,000$ K). The black circles represent ^{12}C, triangles are ^{16}O, squares are ^{20}Ne and empty circles are ^{24}Mg. We can identify three regions, one for C/O core for masses below or equal to 1.088 M$_\odot$ where neon is lower than carbon, another region between 1.088 and 1.147 M$_\odot$ in which neon is greater than carbon and lower than oxygen but magnesium is lower than carbon defining a O/Ne core, and a third region for masses greater than 1.147 M$_\odot$ with a O/Ne/Mg core due to neon being greater than oxygen and magnesium greater than carbon.

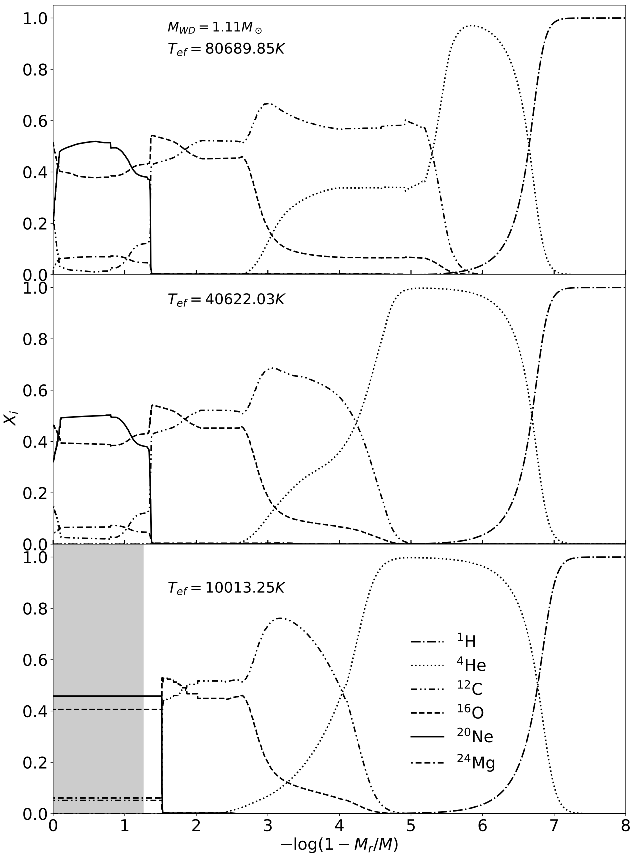

Figure 7. Chemical profile in terms of outer mass fraction for selected elements for three different stages of the cooling sequence: $T_{\rm eff} \approx 80\,000$ K on top, $T_{\rm eff} \approx 40\,000$ K on middle and $T_{\rm eff} \approx 10\,000$ K on bottom panels. The chemical profiles are for a H atmosphere white dwarf with $M_{\rm WD} = 1.11 M_\odot$. The shaded region represents the crystallized zone of the star.

3.4 Chemical profiles in the cooling sequence

In Figure 7 we show three chemical profiles for models along the cooling sequence for an O/Ne core H–atmosphere white dwarf with stellar mass $M_{\rm WD} = 1.11$ M$_\odot$. The abundance profiles are in terms of outer mass fraction and correspond to three effective temperatures, $T_{\rm eff} \approx 80\,000, 40\,000$ and $10\,000$ K, on top, middle and bottom panels, respectively. The effects of diffusion and gravitational settling on the entire chemical profile as the star cools are evident from this figure. Initially, the oxygen central abundance is $X_{\rm O} = 0.515$ while for neon it is $X_{\rm Ne} = 0.195$ (top panel). Rehomogenization processes change the central abundances to a flat profile with $X_{\rm O} = 0.406$ and $X_{\rm Ne} = 0.458$ when the star reaches effective temperatures $\sim 10,000$ K (bottom panel). Also there is a carbon-oxygen-helium triple-layer structure at $2.7 < -\log(1 - M_{\rm r}/M) < 5.5$ for high effective temperatures, which diminish due to diffusion processes. Note that, for the sequence with white dwarf mass 1.11 M$_\odot$ the carbon flame experienced in the pre-white dwarf stage, did not reach the center of the model, giving rise to a hybrid C/O-O/Ne core white dwarfs (Denissenkov et al. 2013; Doherty et al. 2015; Farmer et al. 2015). The hybrid models presented in Denissenkov et al. (2013) are characterized by a C/O core surrounded by an O/Ne region at the super AGB stage. This chemical structure differs from the one characterizing our models (see Figure 7) , since they are taken from the white dwarf cooling curve, where rehomogenization process are taken into account. To our knowledge this is the first time a chemical profile for the entire stars is presented for a hybrid C/O-O/Ne white dwarf. The shaded region on the bottom panel depicts the crystallized zone, which is defined as the regions where $\Gamma \geq 220$ (see section 3.5). For this sequence, crystallization starts at $T_{\rm eff} \approx 20\,000$ K. Finally, the chemical structure of the star can be separated into the outer layers, composed by hydrogen followed by an extended helium buffer, and the inner regions showing an triple-layer of carbon-oxygen-helium from $2 < -\log(1 - M_{\rm r}/M) < 4$ with a carbon peak ($-\log M_{\rm r}/M \sim 3.1$) on top of the Ne/O core. This chemical structure of the core is the result of burning events occurring in previous stages to the cooling sequence.

The composition of the core and its size has a strong impact on the chemical profile of the entire star. Figure 8 shows the chemical profiles in terms of outer mass fraction for three hydrogen atmosphere white dwarfs models with $T_{\rm eff} \approx 10\,000$ K, with stellar mass $M_{\rm WD} = 1.019$ M$_\odot$ (top panel), $M_{\rm WD} = 1.11$ M$_\odot$ (middle panel) and $M_{\rm WD} = 1.22$ M$_\odot$ (bottom panel). The shaded region represents the crystallized region of the model. From this figure, we note that the crystallization front is closer to the surface of the model for higher stellar mass, located at $-\log(1 - M_{\rm r}/M) \approx 0.9, 1.2$ and 2 for $M_{\rm WD} = 1.019$, $M_{\rm WD} = 1.11$ and $M_{\rm WD} = 1.22$ M$_\odot$ models, respectively. The sequence characterized by a stellar mass $M_{\rm WD} = 1.019$ M$_\odot$ has a C/O core with a core mass of $M_{\rm c} = 1.016$ M$_\odot$ extending to $-\log(1 - M_{\rm r}/M_*) = 2.6$

and present a triple-layer of carbon-oxygen-helium at $1.8 < -\log(1 - M_r/M_*) < 2.6$. On top of the core, the model has a helium buffer of $M_{He} = 10^{-2.47}M_{WD}$ and a hydrogen envelope with $M_H = 10^{-5.73}M_{WD}$. Althaus et al. (2010) and Romero et al. (2012, 2013) also obtained a triple-layer structure in their C/O core white dwarf models.

The sequence with $M_{WD} = 1.11$ M$_\odot$ has a O/Ne core, extending to $-\log(1 - M_r/M) = 4$, which represents in mass $M_c = 1.1099$ M$_\odot$. As discussed before, this O/Ne core model shows a triple-layer oxygen-carbon-helium with a peak of carbon at the outer boundary of the core, a helium buffer of $M_{He} = 10^{-3.52}M_{WD}$ and a hydrogen envelope of $M_H = 10^{-6.45}M_{WD}$. The $M_{WD} = 1.22$ M$_\odot$ sequence has a Ne/O/Mg core with $M_c = 1.219$ M$_\odot$ which extends to $-\log(1 - M_r/M) = 3.5$. It also presents a triple-layer of oxygen-carbon-helium with a sharp oxygen peak, instead of a carbon peak in the O/Ne core case. The Ne/O/Mg core model has an helium buffer of $M_{He} = 10^{-3.12}M_{WD}$ and a hydrogen envelope of $M_H = 10^{-6.72}M_{WD}$. The difference in core composition are due to final mass as shown on Figure 6. Also, asteroseismology will be able to distinguish these structure.

In Appendix A we present all chemical profiles for both H and He atmosphere sequences at effective temperatures $T_{eff} \approx 10\,000$ K.

3.5 Crystallization and the Coulomb coupling parameter

As stated before, the MESA code considers, as a standard input value, that a mixture of solid and liquid phases occurs for a coupling parameter $\Gamma_i = 150$ while a full crystal structure occurs when $\Gamma_{full} = 175$. However, Romero et al. (2013) calculated white dwarfs sequences considering two types of phase diagram and concluded that the azeotropic type from Horowitz et al. (2010) better represents the crystallization on the nuclei of white dwarfs. Hence, we modify the values of the Γ parameter to $\Gamma_i = 215$ for a liquid/solid coexisting phases and $\Gamma_{full} = 220$ for a full crystal phase, more consistent with the results obtained using the Horowitz et al. (2010) phase diagram. Paxton et al. (2018) calculated cooling sequences for a 0.6 M$_\odot$ white dwarf star, using MESA, varying $\Gamma_i = 174$ to 220 and $\Gamma_{full} = 176$ to 240 and found a difference in the cooling times of the order of Gyr. For the stellar mass range considered in this work, to assume $\Gamma_i = 215$ and $\Gamma_{full} = 220$, makes the effective temperature at which crystallization starts ≈ 2000 K lower, and the age ≈ 0.23 Gyr larger than the ones using the standard input values. The effective temperature and age on the onset of crystallization for three sequences considering the two values of Γ_{full}, are listed in table 2.

We compare the values of the effective temperature at the onset of crystallization, as a function of the white dwarf mass, with the results obtained by Romero et al. (2013) in Figure 9. Note that the results obtained in this work (triangles) are in well agreement with those from Romero et al. (2013) (circles), in the stellar mass range where both works overlap.

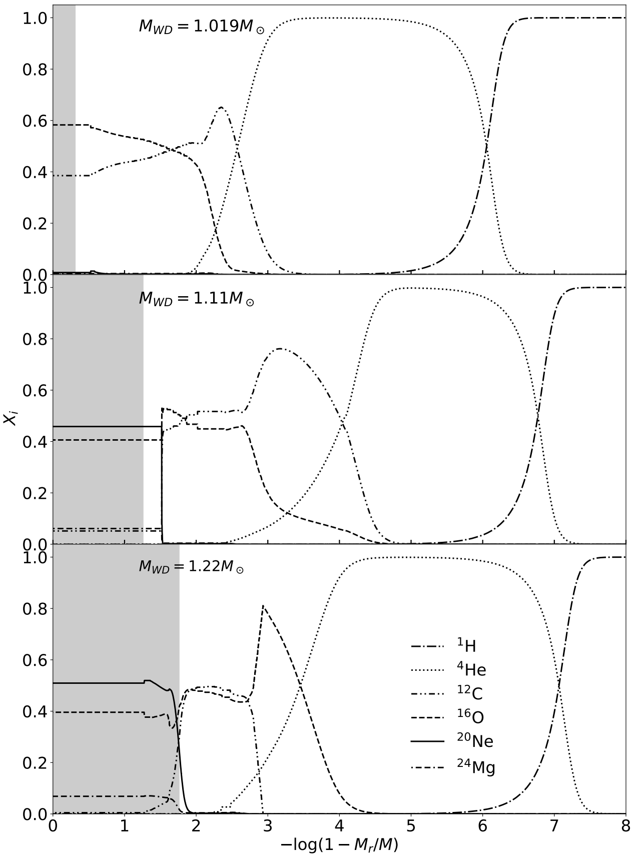

Figure 8. Chemical profile in terms of outer mass fraction for selected elements and for three different H atmosphere white dwarf with $T_{eff} \approx 10\,000$ K. From top to bottom we depict the chemical profile for a $M_{WD} = 1.019, 1.11, 1.22$ M$_\odot$. The shaded region represents the crystallized zone of the star

Table 2. Age and effective temperature on the onset of crystallization for different Coulomb coupling parameter. The age of crystallization is defined as time starting at the cooling sequence and ending at the onset of crystallization and is given in Gyr. Effective temperature in Kelvin. The effective temperature for $\Gamma_{full} = 220$ on the last row agrees with table 2 of Romero et al. (2013).

	$\Gamma_{full} = 175$		$\Gamma_{full} = 220$	
M_{WD} [M$_\odot$]	T_{eff} [K]	Age [Gyr]	T_{eff} [K]	Age [Gyr]
1.012	15095	0.6468	13152	0.8707
1.019	15376	0.6282	13396	0.8476
1.024	15552	0.6780	13584	0.9249

3.6 White dwarf cooling times

The cooling time is defined as the time spent by a star in the cooling sequence (t_{cool}). We define the beginning of the cooling sequences as the point of maximum effective temperature in the post-AGB stage, before the star enters the cooling sequence. The progenitor age (t_i) is defined as the time from the ZAMS to the beginning of the cooling sequence. Then the total age of a white dwarf star can be computed as $t_{total} = t_i + t_{cool}$. Table 3 summarizes the char-

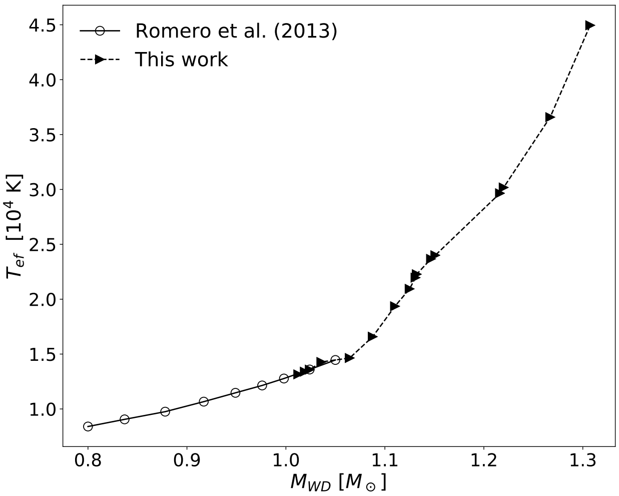

Figure 9. Comparison of effective temperature on onset of crystallization for a range of white dwarfs mass. Effective temperature on units of 10^4 K. Circles are the data extracted from Romero et al. (2013) and triangles are results from this work. There is a agreement between both works for values of mass $M_{\rm WD} \sim 1$ M$_\odot$ and the effective temperature raises as mass also increases.

acteristic time-scales for all the sequences computed in this work. Specifically, for each sequence we listed the initial mass in the ZAMS (column 1) and the final mass at the cooling curve (column 2), along with the age for hydrogen and helium exhaustion at the core in columns 3 and 4, respectively. The progenitor age t_i is listed in column 5. The age for hydrogen and helium depletion and the progenitor age are equal for both hydrogen and helium atmosphere white dwarfs sequences, since both have evolved equally on the stages prior to the cooling sequence. We also listed the effective temperature and the age in the cooling curve at the onset of crystallization for the hydrogen (columns 6 and 7) and helium atmosphere (columns 9 and 10) sequences. Finally, the cooling times corresponding to an effective temperature of 10 000 K are listed in columns 8 and 12 for sequences with hydrogen and helium atmospheres, respectively.

Figure 10 shows a comparison of cooling times, between H and He atmosphere sequences with the same stellar mass, 1.019 (solid line), 1.11 (dashed line) and 1.22 $M_\odot$ (dotted line), whose chemical profiles are presented in Figure 8. Gray lines represent hydrogen atmosphere and black lines correspond to helium atmosphere sequences. For luminosities $\log L/L_\odot \gtrsim -2.8$, He-atmosphere sequences cool somewhat slower then the H-atmosphere counterparts. On the other hand, for $\log L/L_\odot \lesssim -2.8$ He-atmosphere sequences cools considerably faster leading to differences in cooling age of ~ 1 Gyr for luminosities of $\log L/L_\odot \sim -4$. These behavior can be explain by means of the central temperature of the star. Figure 11 depicts the central temperature $T_{\rm c}$, in a logarithmic scale, in terms of the surface luminosity for the sequences presented in Figure 10.

On luminosities higher than $\log L/L_\odot \approx -3$ the central temperature for the He atmosphere sequences is slightly larger than in the case of a H-atmosphere sequence with the same mass. However, for lower luminosities there is a large difference in $T_{\rm c}$ between H and He atmosphere sequences.

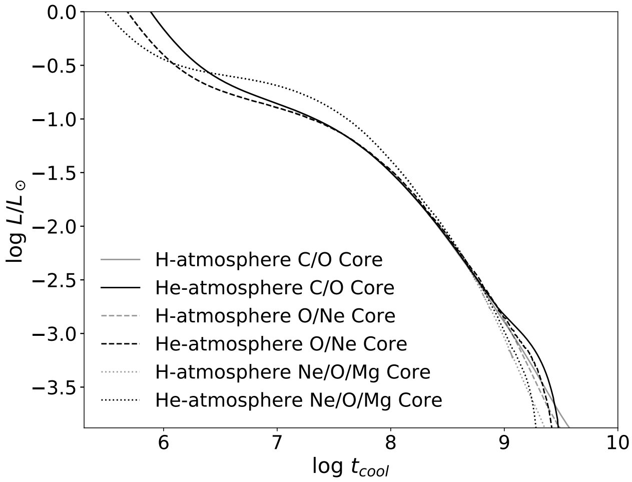

Figure 10. Comparison of cooling times for selected H and He atmosphere cooling sequences. We present 3 sets of H and He atmosphere sequences: A C/O core set with mass 1.019 M$_\odot$ as solid line. A O/Ne set with mass 1.11 as dashed line and a Ne/O/Mg set with mass 1.22 M$_\odot$ as dotted line. Gray lines represent H atmosphere and black lines are He atmosphere white dwarfs sequences. The final chemical profile for the H atmosphere are shown in Figure 8.

The release of internal energy due to crystallization occurs at higher luminosities for He atmosphere sequences, delaying the cooling for those luminosities. Since helium is more transparent than hydrogen, He-atmosphere sequences lose energy faster than H atmosphere sequences at lower luminosities. The results presented in figure 10 agrees with the results from Camisassa et al. (2017) (see their Figures 7 and 11), which calculated evolutionary sequences for lower mass white dwarfs ($M_{\rm WD} \leq 1$ M$_\odot$) with hydrogen-deficient atmosphere and compared against hydrogen rich white dwarfs from Camisassa et al. (2016).

The core composition also impacts the cooling times of white dwarfs stars. García-Berro et al. (1997a) compared cooling times for sequences with same mass and two core compositions, C/O and O/Ne , and obtained a difference in cooling time of the order of ~ 2 Gyr. This is due to the difference in the heat capacity of the core, which is lower for a O/Ne mixture than for an C/O mixture, reducing the cooling time for a core with a higher mean molecular weight.

The Debye regime of fast cooling for white dwarfs is important for low luminosities. In particular, Althaus et al. (2007) found that the Debye cooling regime for H-atmosphere white dwarfs starts to be important for luminosities below $\log L/L_\odot \sim -4$. Since our computations end at those luminosities, the cooling times presented in figure 10 are not affected by Debye cooling.

In the region of $0 > \log L/L_\odot > -1.5$ the effects of neutrino losses are present, as can be see from figure 10. The neutrino emission decreases at higher luminosities for the more massive sequences when compared to lower masses sequences, however, there are no difference between the H and He atmospheres sequences at those luminosities. The rate of neutrino emission become negligible at $\log L/L_\odot \sim -1$ for the sequences with masses 1.019 M$_\odot$ and 1.11 M$_\odot$, and at $\log L/L_\odot \sim -0.5$ for the sequence with 1.22 M$_\odot$, in agree-

Table 3. Mass at ZAMS, white dwarf mass, age when hydrogen is depleted at center ($t_{\rm H}$), age when helium is totally consumed at the center ($t_{\rm He}$), progenitor ages ($t_{\rm i}$), effective temperature on crystallization ($T_{\rm eff_c}$) and age at crystallization ($t_{\rm cryst}$, accounted from the beginning of the cooling sequence) and cooling time ($t_{\rm cool}$ = age at $T_{\rm eff} = 1 \times 10^4$ K minus t_i) for H and He atmosphere white dwarfs. Ages ($t_{\rm H}$, $t_{\rm He}$, $t_{\rm i}$) in units of Myr and crystallization and cooling times on units of Gyr.

					H-atmosphere			He-atmosphere		
$M_{\rm ZAMS}$ [M$_\odot$]	$M_{\rm WD}$ [M$_\odot$]	$t_{\rm H}$ [Myr]	$t_{\rm He}$ [Myr]	t_i [Myr]	$T_{\rm eff_c}$ [K]	$t_{\rm cryst}$ [Gyr]	$t_{\rm cool}$ [Gyr]	$T_{\rm eff_c}$ [K]	$t_{\rm cryst}$ [Gyr]	$t_{\rm cool}$ [Gyr]
8.80	1.012	24.99	27.87	28.53	13152	0.870	3.65	13738	0.839	2.99
8.90	1.019	24.50	27.30	27.94	13396	0.847	3.69	13837	0.839	2.99
9.00	1.024	23.88	26.61	27.26	13584	0.924	4.09	13634	0.933	3.48
9.20	1.036	22.99	25.73	26.24	14281	0.810	3.75	14714	0.756	3.36
9.50	1.064	21.63	24.17	24.63	14643	0.754	3.13	14098	0.924	2.85
9.80	1.088	20.49	22.82	23.24	16585	0.636	3.39	15858	0.742	2.90
10.00	1.11	19.75	22.03	22.45	19356	0.415	3.04	17945	0.538	2.62
10.10	1.125	19.42	21.64	22.03	20941	0.338	2.65	19552	0.405	2.34
10.20	1.131	19.06	21.23	21.62	21963	0.310	2.72	19815	0.387	2.48
10.30	1.132	18.75	20.87	21.26	22276	0.296	2.71	20383	0.376	2.57
10.45	1.147	18.35	20.37	20.74	23673	0.253	2.52	23006	0.285	2.21
10.50	1.151	18.19	20.17	20.54	24001	0.250	2.51	23339	0.278	2.21
10.80	1.216	17.38	19.31	19.55	29651	0.183	2.28	29982	0.181	1.91
11.00	1.22	16.83	18.63	18.88	30177	0.177	2.25	30244	0.179	1.90
11.40	1.267	15.86	17.51	17.73	36584	0.133	1.93	36808	0.132	1.71
11.80	1.307	15.02	16.55	16.75	44953	0.098	1.54	45137	0.099	1.31

ment with the results from Althaus et al. (2007). However, the evolution for luminosities lower than $\log L/L_\odot \sim -2$ in our computations differs from the ones computed by Althaus et al. (2007). In our computations we consider a crystallization treatment that mimic the results from the phase diagram presented by Horowitz et al. (2010), while Althaus et al. (2007) considers the phase diagram from Segretain et al. (1994), which increases the crystallization temperature in ∼ 2 000 K (see Romero et al. (2013) for details). Also Althaus et al. (2007) considers a fixed O/Ne core chemical profile for all stellar masses while, in the cooling sequences calculated in this work, the chemical profiles come from evolutionary computations and is consistent with the stellar mass and covers C/O, O/Ne and Ne/O/Mg. The difference in the cooling times between our computations and those from Althaus et al. (2007), are ∼ 0.6 Gyr at $\log L/L_\odot \sim -4$ for a stellar mass of $\sim 1.21 M_\odot$.

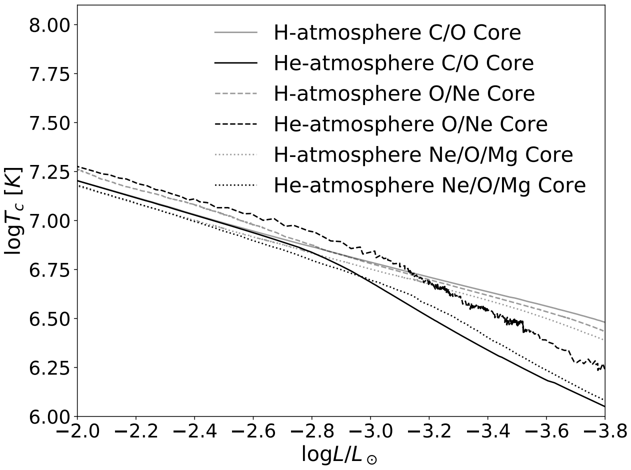

Figure 11. Logarithm of central temperature in terms of star luminosity. Three sets of H and He atmosphere are shown, the same as Figure 10. Faint lines represent H atmosphere and strong lines are He atmosphere white dwarfs.

4 MASS-RADIUS RELATION

Figure 12 show the mass-radius relation of our sequences with H and He atmosphere, as solid and dashed lines, respectively. We consider effective temperatures of 150 000 K, 100 000 K, 50 000 K, 25 000 K and 10 000 K, shown from top to bottom. The rate of contraction is higher for high effective temperatures compared to low effective temperatures. Due to their higher surface gravity, more massive sequence show a smaller range in the value of the radius for the different effective temperatures considered here. For a sequence with H atmosphere characterized by a stellar mass of $1.267 M_\odot$ the total radius changes from 4.83×10^{-3} R$_\odot$ to 4.34×10^{-3} R$_\odot$ when the star cools from $1.5{\times}10^5$ K to $1{\times}10^4$ K. On the other hand, for a sequence with a mass of $1.064 M_\odot$, the radius decreases from 8.31×10^{-3} R$_\odot$ to 6.95×10^{-3} R$_\odot$ for the same range of effective temperatures. This means a change in radius of ∼ 10% for the more massive and ∼ 16% for the latter. Those values change when sequences with He atmosphere are considered. For a He atmosphere sequence with $1.267 M_\odot$ the radius change from 4.74×10^{-3} R$_\odot$ to 4.32×10^{-3} R$_\odot$ (∼ 9%) and for the $1.064 M_\odot$ sequence there is a change from 8.02×10^{-3} R$_\odot$ to 6.09×10^{-3} (∼ 14%) when considering the same effective temperature range. Note that, although the contraction of H atmosphere sequences are slightly higher their final radii are higher compared to the He atmosphere counterparts, showing that a small amount of hydrogen of the order of $M_{\rm H} \approx 1 \times 10^{-6} M_{\rm WD}$ can change the radius by 8.6×10^{-4} R$_\odot$ for the $M_{\rm WD} = 1.064$ M$_\odot$ sequence.

The surface gravity $\log g$ as a function of effective temperature $T_{\rm eff}$ for H and He atmosphere sequences are pre-

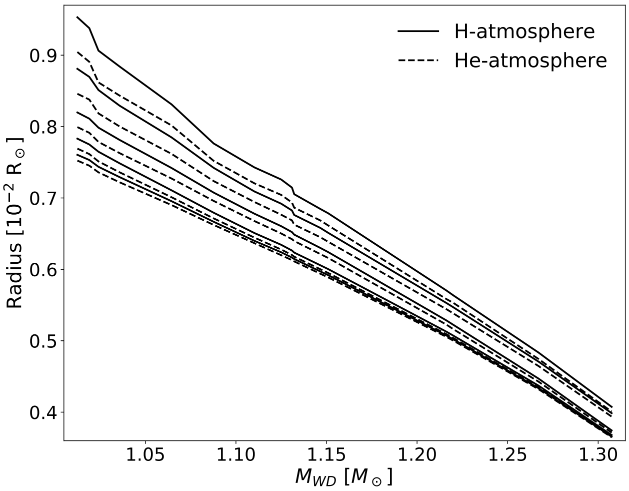

Figure 12. Mass-Radius relation for H and He atmosphere white dwarfs models, represented as solid and dashed lines, respectively. From top to bottom, the lines represent effective temperatures of 150 000 K, 100 000 K, 50 000 K, 25 000 K and 10 000 K. See text for details.

sented in Figures 13 and 14, respectively. The solid lines correspond to C/O cores sequences while dashed and dotted lines correspond to O/Ne and Ne/O/Mg core sequences, respectively. Stellar mass decreases from top to bottom. Also plotted, as empty circles, are a selection of white dwarfs with spectroscopic masses $M_{\rm WD} > 1$ M$_\odot$ from the SDSS DR12 catalog presented by (Kepler et al. 2016). Surface gravities and effective temperatures fro H-atmosphere white dwarfs are corrected to 3D convection (Tremblay et al. 2013) and have mean values of $\langle \log g \rangle = 8.987 \pm 0.21$ and $\langle T_{\rm eff} \rangle = 11\,591 \pm 501$. From Figure 13 we find a good agreement between observations and our theoretical cooling sequences with masses $M_{\rm WD} \leq 1.151$ M$_\odot$. Comparing Figures 13 and 14 we can see that the sequences are slightly shifted to smaller gravities, on average $\Delta \log g = 0.0135$, for lower effective temperatures due to contraction, which reduced the radius in $\Delta R = 3.246 \times 10^{-5}$ $R_\odot$ on average. The increase in $\log g$ at $\log T_{\rm eff} \sim 4.8 - 4.9$ presented in figures 13 and 14 for the Ne/O/Mg sequences with $M_{\rm WD} > 1.2$ M$_\odot$ is due the decrease in the luminosity due to neutrino emission, which causes a reduction in the radius of the model. This behavior agrees with the results from Althaus et al. (2005b) who were the first to report this phenomenon.

For comparison proposes, we compute the stellar mass of a sample of 252 stars from the SDSS DR12 catalog of Kepler et al. (2016) using the cooling sequence computed in this work and those obtained using the LPCODE evolutionary code (Althaus et al. 2005a; Romero et al. 2013). The results are shown in Figure 15 where we depict the stellar mass obtained from the MESA tracks against the mass computed using the LPCODE tracks. As can be seen, there is practically no difference between the two determinations. The deviations from the 1:1 correspondence for stellar masses around $1.05 M_\odot$ is due to the transition from a C/O to a O/Ne core composition, which occurs at $1.05 M_\odot$ for the LPCODE, while in our simulations occurs at $1.088 M_\odot$.

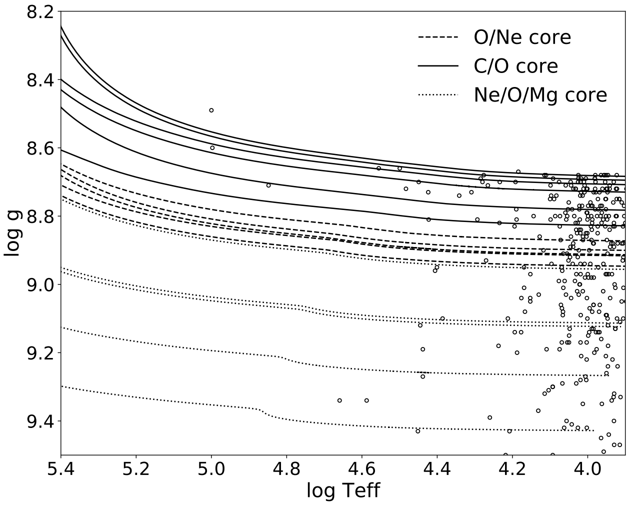

Figure 13. $\log g$ - $T_{\rm eff}$ relation for H atmosphere white dwarfs. $T_{\rm eff}$ from ≈ 250 000 K to ≈ 10 000 K. Empty circles correspond to 400 white dwarfs stars from the SDSS catalog presented in (Kepler et al. 2016). See text for details.

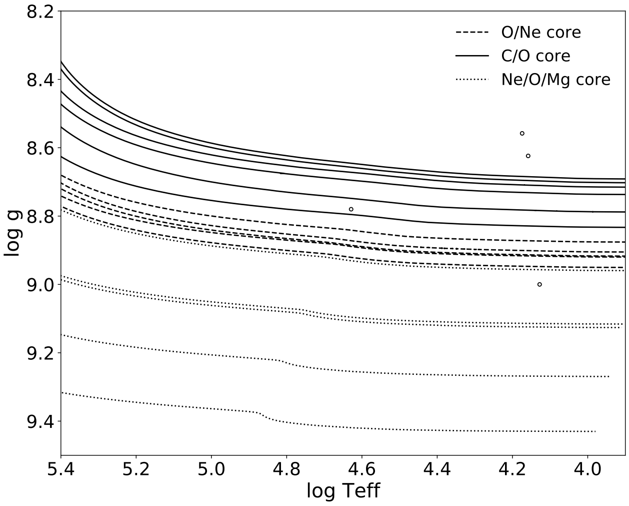

Figure 14. $\log g$ - $T_{\rm eff}$ relation for He atmosphere white dwarfs. $T_{\rm eff}$ from ≈ 250 000 K to ≈ 10 000 K. Empty circles correspond to 400 white dwarfs stars from the SDSS catalog presented in (Kepler et al. 2016). See text for details.

5 CONCLUSION

In the present work we have calculated full evolutionary sequences with $Z = 0.02$ for massive H and He atmosphere white dwarf stars using the evolutionary code MESA version r8845. Our sequences started from the zero-age main sequence with masses from 8.8 to 11.8 M$_\odot$, evolving through central hydrogen and helium burning, thermally pulsing and mass-loss phases ending as white dwarfs on the cooling sequence. The resulting white dwarfs sequences show stellar masses in a range of $M_{\rm WD} = 1.012 - 1.307$ M$_\odot$. We presented full chemical profiles, core mass range, cooling times with crystallization effects, mass-radius relation and initial-to-

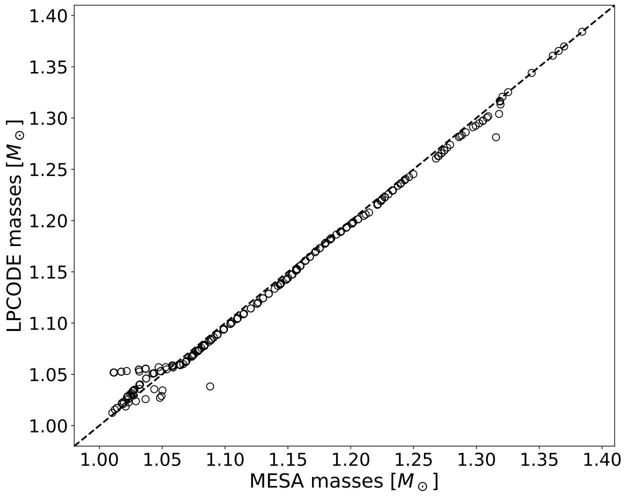

Figure 15. Comparison between the stellar mass for a sample of 252 spectroscopically identified DA white dwarf stars from the SDSS DR12 catalog, computed using the MESA sequences (x-axis) and LPCODE sequences (y-axis). The dashed line indicates the 1:1 correspondence.

final mass relation. We also calculated masses from our evolutionary tracks for a selection of 252 massive stars from the SDSS DR12 catalog (Kepler et al. 2016) and compared with derived masses from other evolutionary tracks presented on the literature.

Unlike models that only evolve to the AGB, our white dwarf sequences considers the entire evolutionary history of the corresponding progenitors, leading to realistic chemical profiles which are also consistent with stellar mass. Note that the amount of hydrogen and helium affects both the age and mass determinations of DA and non-DA white dwarfs. The final mass range of our sequences cover the entire range of C/O, O/Ne and Ne/O/Mg core composition and also accounts for hybrids C/O-O/Ne white dwarfs. Reliable chemical composition of core and the chemical transition regions presented on Figure 8 are of relevance for asteroseimological studies of pulsating white dwarf. The set of tracks presented here is the first in the literature to cover those core composition for massive white dwarfs, considering the evolutionary history of the progenitors, and presenting the entire chemical profiles for the sequences.

Our main results are the following:

(i) From our simulations we obtained white dwarf sequences characterized with C/O, O/Ne and Ne/O/Mg cores being: C/O cores for $M_{\rm WD} \leq 1.088$ M$_\odot$, O/Ne cores for $1.088 < M_{\rm WD} \leq 1.147$ M$_\odot$, Ne/O/Mg cores for $M_{\rm WD} > 1.147$ M$_\odot$. Note that these values correspond to sequences with initial metallicity $Z = 0.02$. We expect them to vary for different initial metallicities (Doherty et al. 2015) . We compute a sequence with $M_{WD} = 1.13$ M$_\odot$ and $Z = 0.015$ and found that the chemical structure does not change considerably from the sequence with $Z = 0.02$ and a similar stellar mass in the cooling curve.

(ii) All sequences with $M_{\rm WD} \geq 1.024$ M$_\odot$ experienced inward propagating carbon flames with subsequent helium burning of the outer shells, in the post-AGB stage. The carbon flame for sequences with masses $1.024 \leq M_{\rm WD} \leq 1.147$ M$_\odot$ does not reach the central regions, forming a hybrid C/O-O/Ne white dwarf. For sequences with $M_{\rm WD} > 1.147$ M$_\odot$ the carbon flame reaches the center of the model producing a Ne/O/Mg core. Our Hybrid models presents a O/Ne core surrounded by a triple-layer of oxygen-carbon-helium, differing from the work of Denissenkov et al. (2013) where they reported a C/O core surrounded by a O/Ne zone for hybrid C/O/Ne Super AGB stars.

(iii) Our choice of the Coulomb Coupling parameter for crystallization $\Gamma_{\rm full} = 220$, based on the latest asteroseismology results, instead of the default $\Gamma = 175$, can increase the cooling times by ≈ 0.26 Gyr and decrease the effective temperature at the onset of crystallization by $\approx 2000K$.

(iv) The amount of hydrogen left at the envelope of a white dwarf has an important impact in determining the stellar mass and the cooling times. Even low quantities of hydrogen, as the ones expected for massive white dwarfs, can impact the radii and cooling times. In particular, our H-atmosphere sequences shows cooling times $\sim 0.23 - 0.66$ Gyr larger at $T_{\rm eff} \approx 10\,000$ K, depending on stellar mass, when compared to He atmosphere sequence with the same mass.

(v) The derived masses for a selection of 252 massive stars from the SDSS DR12 catalog (Kepler et al. 2016) using our simulations are in fine agreement with masses computed using the evolutionary tracks of LPCODE Althaus et al. (2005a); Romero et al. (2012, 2013).

ACKNOWLEDGEMENTS

We acknowledge the valuable report of the anonymous referee. GRL acknowledges the support by CAPES-Brazil. ADR and SOK thank support from CNPq and PRONEX-FAPERGS/CNPq (Brazil). This research has made use of NASA's Astrophysics Data System.

REFERENCES

Ahn C. P., et al., 2014, ApJS, 211, 17
Alastuey A., Jancovici B., 1978, ApJ, 226, 1034
Althaus L. G., Serenelli A. M., Panei J. A., Córsico A. H., García-Berro E., Scóccola C. G., 2005a, A&A, 435, 631
Althaus L. G., García-Berro E., Isern J., Córsico A. H., 2005b, A&A, 441, 689
Althaus L. G., García-Berro E., Isern J., Córsico A. H., Rohrmann R. D., 2007, A&A, 465, 249
Althaus L. G., Panei J. A., Miller Bertolami M. M., García-Berro E., Córsico A. H., Romero A. D., Kepler S. O., Rohrmann R. D., 2009, ApJ, 704, 1605
Althaus L. G., Córsico A. H., Bischoff-Kim A., Romero A. D., Renedo I., García-Berro E., Miller Bertolami M. M., 2010, ApJ, 717, 897
Althaus L. G., Miller Bertolami M. M., Córsico A. H., 2013, A&A, 557, A19
Bedin L. R., Salaris M., King I. R., Piotto G., Anderson J., Cassisi S., 2010, ApJ, 708, L32
Benvenuto O. G., Althaus L. G., 1999, MNRAS, 303, 30
Bloecker T., 1995, Astronomy and Astrophysics, 297, 727
Brooks J., Bildsten L., Schwab J., Paxton B., 2016, ApJ, 821, 28
Brooks J., Schwab J., Bildsten L., Quataert E., Paxton B., 2017a, ApJ, 834, L9
Brooks J., Schwab J., Bildsten L., Quataert E., Paxton B., 2017b, ApJ, 843, 151

Burgers J. M., 1969, Flow Equations for Composite Gases

Camisassa M. E., Althaus L. G., Córsico A. H., Vinyoles N., Serenelli A. M., Isern J., Miller Bertolami M. M., García-Berro E., 2016, ApJ, 823, 158

Camisassa M. E., Althaus L. G., Rohrmann R. D., García-Berro E., Torres S., Córsico A. H., Wachlin F. C., 2017, ApJ, 839, 11

Campos F., et al., 2016, MNRAS, 456, 3729

Catalán S., Isern J., García-Berro E., Ribas I., 2008, MNRAS, 387, 1693

Chen M. C., Herwig F., Denissenkov P. A., Paxton B., 2014, MNRAS, 440, 1274

Choi J., Dotter A., Conroy C., Cantiello M., Paxton B., Johnson B. D., 2016, ApJ, 823, 102

Cox J. P., Giuli R. T., 1968, Principles of stellar structure

Cyburt R. H., et al., 2010, The Astrophysical Journal Supplement Series, 189, 240

DeWitt H. E., Graboske H. C., Cooper M. S., 1973, ApJ, 181, 439

Denissenkov P. A., Herwig F., Truran J. W., Paxton B., 2013, ApJ, 772, 37

Doherty C. L., Gil-Pons P., Siess L., Lattanzio J. C., Lau H. H. B., 2015, MNRAS, 446, 2599

Dotter A., 2016, ApJS, 222, 8

Falcon R. E., Winget D. E., Montgomery M. H., Williams K. A., 2010, ApJ, 712, 585

Farmer R., Fields C. E., Timmes F. X., 2015, ApJ, 807, 184

García-Berro E., Isern J., Hernanz M., 1997a, MNRAS, 289, 973

García-Berro E., Ritossa C., Iben Jr. I., 1997b, ApJ, 485, 765

García-Berro E., Torres S., Althaus L. G., Miller Bertolami M. M., 2014, A&A, 571, A56

Gil-Pons P., Doherty C. L., Lau H., Campbell S. W., Suda T., Guilani S., Gutiérrez J., Lattanzio J. C., 2013, A&A, 557, A106

Graboske H., Dewitt H., Grossman A., Cooper M., 1973, ApJ, 181, 457

Hansen B. M. S., et al., 2007, ApJ, 671, 380

Henize K. G., 1976, ApJS, 30, 491

Herwig F., 2000, A&A, 360, 952

Horowitz C. J., Schneider A. S., Berry D. K., 2010, Physical Review Letters, 104, 231101

Hughto J., Horowitz C. J., Schneider A. S., Medin Z., Cumming A., Berry D. K., 2012, Phys. Rev. E, 86, 066413

Iben Jr. I., Kaler J. B., Truran J. W., Renzini A., 1983, ApJ, 264, 605

Iglesias C. A., Rogers F. J., 1996, ApJ, 464, 943

Isern J., Catalan S., Garcia-Berro E., Salaris M., Torres S., 2010, preprint, (`arXiv:1010.5351`)

Istrate A. G., Tauris T. M., Langer N., Antoniadis J., 2014, A&A, 571, L3

Istrate A. G., Marchant P., Tauris T. M., Langer N., Stancliffe R. J., Grassitelli L., 2016, A&A, 595, A35

Istrate A. G., Fontaine G., Heuser C., 2017, ApJ, 847, 130

Itoh N., Totsuji H., Ichimaru S., Dewitt H., 1979, ApJ, 234, 1079

Itoh N., Hayashi H., Nishikawa A., Kohyama Y., 1996, ApJS, 102, 411

Jones S., et al., 2013, ApJ, 772, 150

Kepler S. O., Kleinman S. J., Nitta A., Koester D., Castanheira B. G., Giovannini O., Costa A. F. M., Althaus L., 2007, MNRAS, 375, 1315

Kepler S. O., et al., 2015, MNRAS, 446, 4078

Kepler S. O., et al., 2016, MNRAS, 455, 3413

Kippenhahn R., Ruschenplatt G., Thomas H.-C., 1980, A&A, 91, 175

Kleinman S. J., et al., 2013, ApJS, 204, 5

Langer N., 2012, ARA&A, 50, 107

Langer N., Fricke K. J., Sugimoto D., 1983, A&A, 126, 207

Liebert J., Bergeron P., Holberg J. B., 2005, ApJS, 156, 47

McGraw J. T., Starrfield S. G., Liebert J., Green R., 1979, in van Horn H. M., Weidemann V., Savedoff M. P., eds, IAU Colloq. 53: White Dwarfs and Variable Degenerate Stars. pp 377–381

Należyty M., Madej J., 2004, A&A, 420, 507

Paxton B., Bildsten L., Dotter A., Herwig F., Lesaffre P., Timmes F., 2011, ApJS, 192, 3

Paxton B., et al., 2013, ApJS, 208, 4

Paxton B., et al., 2015, ApJS, 220, 15

Paxton B., et al., 2018, ApJS, 234, 34

Pignatari M., et al., 2016, ApJS, 225, 24

Poelarends A. J. T., Herwig F., Langer N., Heger A., 2008, ApJ, 675, 614

Potekhin A. Y., Chabrier G., 2010, Contributions to Plasma Physics, 50, 82

Prada Moroni P. G., Straniero O., 2002, ApJ, 581, 585

Rebassa-Mansergas A., Rybicka M., Liu X.-W., Han Z., García-Berro E., 2015, MNRAS, 452, 1637

Reimers D., 1975, Mémoires of the Société Royale des Sciences de Liège, 8, 369

Reindl N., Rauch T., Parthasarathy M., Werner K., Kruk J. W., Hamann W.-R., Sander A., Todt H., 2014, A&A, 565, A40

Ritter C., Herwig F., Jones S., Pignatari M., Fryer C., Hirschi R., 2017, preprint, (`arXiv:1709.08677`)

Rogers F. J., Nayfonov A., 2002, ApJ, 576, 1064

Romero A. D., Córsico A. H., Althaus L. G., Kepler S. O., Castanheira B. G., Miller Bertolami M. M., 2012, MNRAS, 420, 1462

Romero A. D., Kepler S. O., Córsico A. H., Althaus L. G., Fraga L., 2013, ApJ, 779, 58

Salaris M., García-Berro E., Hernanz M., Isern J., Saumon D., 2000, ApJ, 544, 1036

Salaris M., Althaus L. G., García-Berro E., 2013, A&A, 555, A96

Saumon D., Chabrier G., van Horn H. M., 1995, ApJS, 99, 713

Schneider A. S., Hughto J., Horowitz C. J., Berry D. K., 2012, Phys. Rev. E, 85, 066405

Schoenberner D., 1979, A&A, 79, 108

Schwab J., Bildsten L., Quataert E., 2017, MNRAS, 472, 3390

Segretain L., Chabrier G., Hernanz M., Garcia-Berro E., Isern J., Mochkovitch R., 1994, ApJ, 434, 641

Siess L., 2006, A&A, 448, 717

Siess L., 2007, A&A, 476, 893

Siess L., 2010, A&A, 512, A10

Sun M., Arras P., 2017, preprint, (`arXiv:1703.01648`)

Thoul A. A., Bahcall J. N., Loeb A., 1994, ApJ, 421, 828

Timmes F. X., Swesty F. D., 2000, ApJS, 126, 501

Tremblay P.-E., Ludwig H.-G., Steffen M., Freytag B., 2013, A&A, 559, A104

Ulrich R. K., 1972, ApJ, 172, 165

Van Horn H. M., 1969, Physics Letters A, 28, 706

Vassiliadis E., Wood P. R., 1993, ApJ, 413, 641

Wang B., Podsiadlowski P., Han Z., 2017, MNRAS, 472, 1593

Winget D. E., Hansen C. J., Liebert J., van Horn H. M., Fontaine G., Nather R. E., Kepler S. O., Lamb D. Q., 1987, ApJ, 315, L77

Woosley S. E., Heger A., 2015, ApJ, 810, 34

van Horn H. M., 1968, ApJ, 151, 227

APPENDIX A: CHEMICAL PROFILES AT THE END OF COOLING SEQUENCE

In this section is presented the chemical profiles of all our models for H and He atmosphere white dwarfs. Figure A1 shows the chemical profiles for H atmosphere on the column on the left and He atmosphere profiles on column on the right. Each row presents a H atmosphere and a He atmosphere models for a same mass. All chemical profiles presented in this section are for $T_{\mathrm{eff}} \approx 10,000$ K.

This paper has been typeset from a TEX/LATEX file prepared by the author.

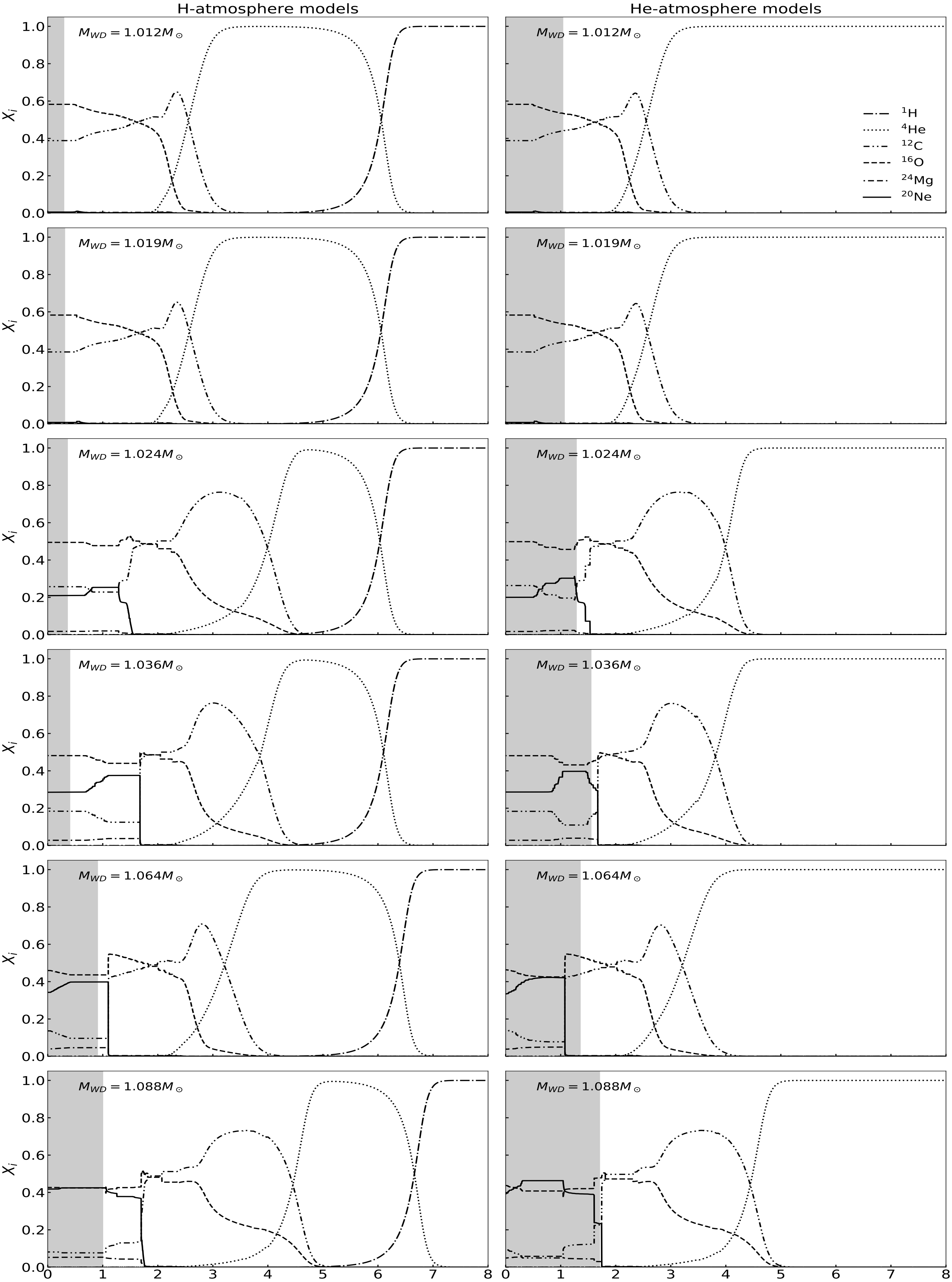

Figure A1. Chemical profiles in terms of outer mass fractions for H atmosphere (left) and He atmosphere (right) models at $T_{\rm eff} \approx 10\,000$ K in the cooling sequence. The shaded regions means crystallized portion of core. Each row presents a H atmosphere (left) and a He atmosphere (right) for a same mass

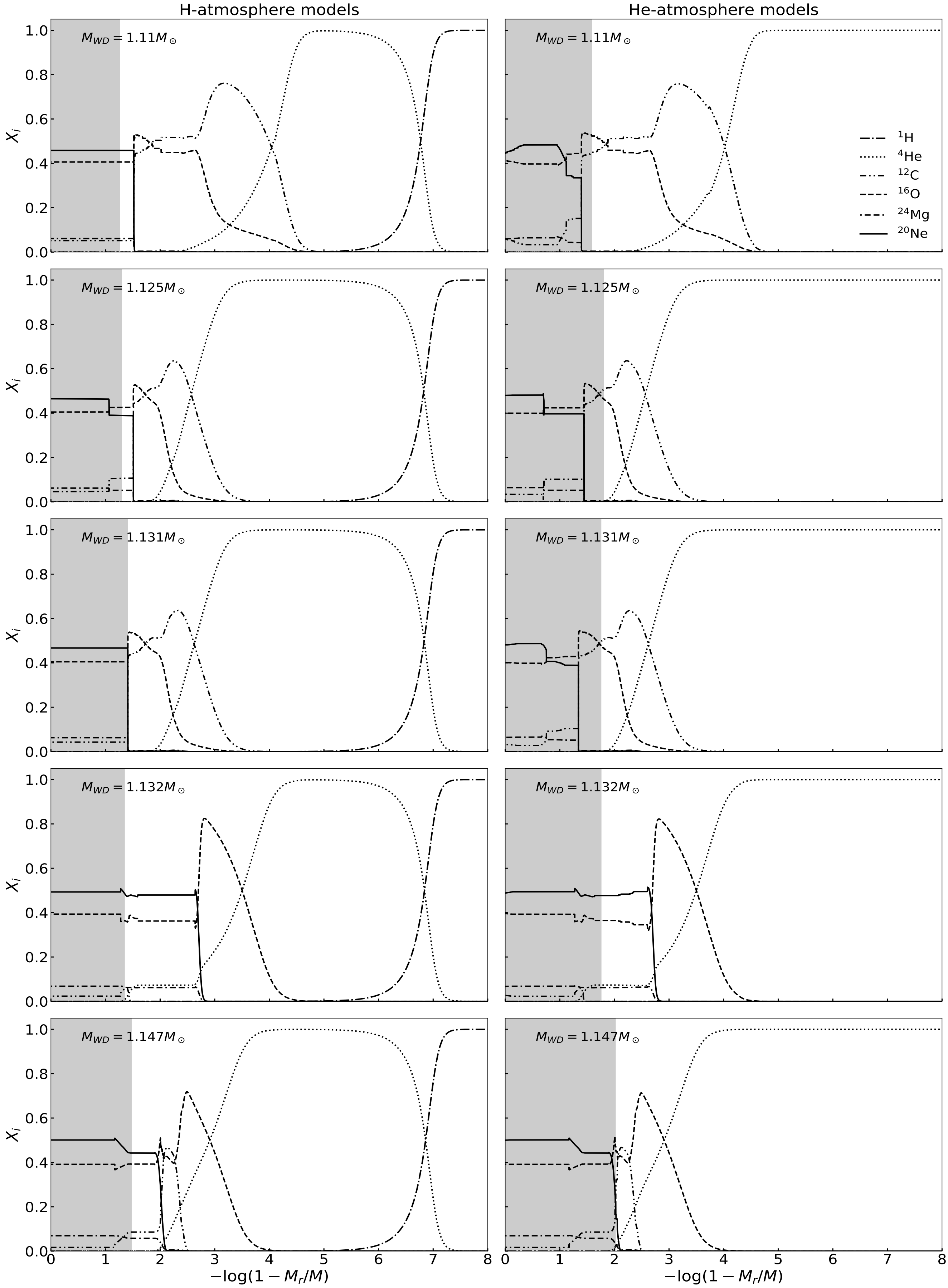

Figure A1 – *continued*

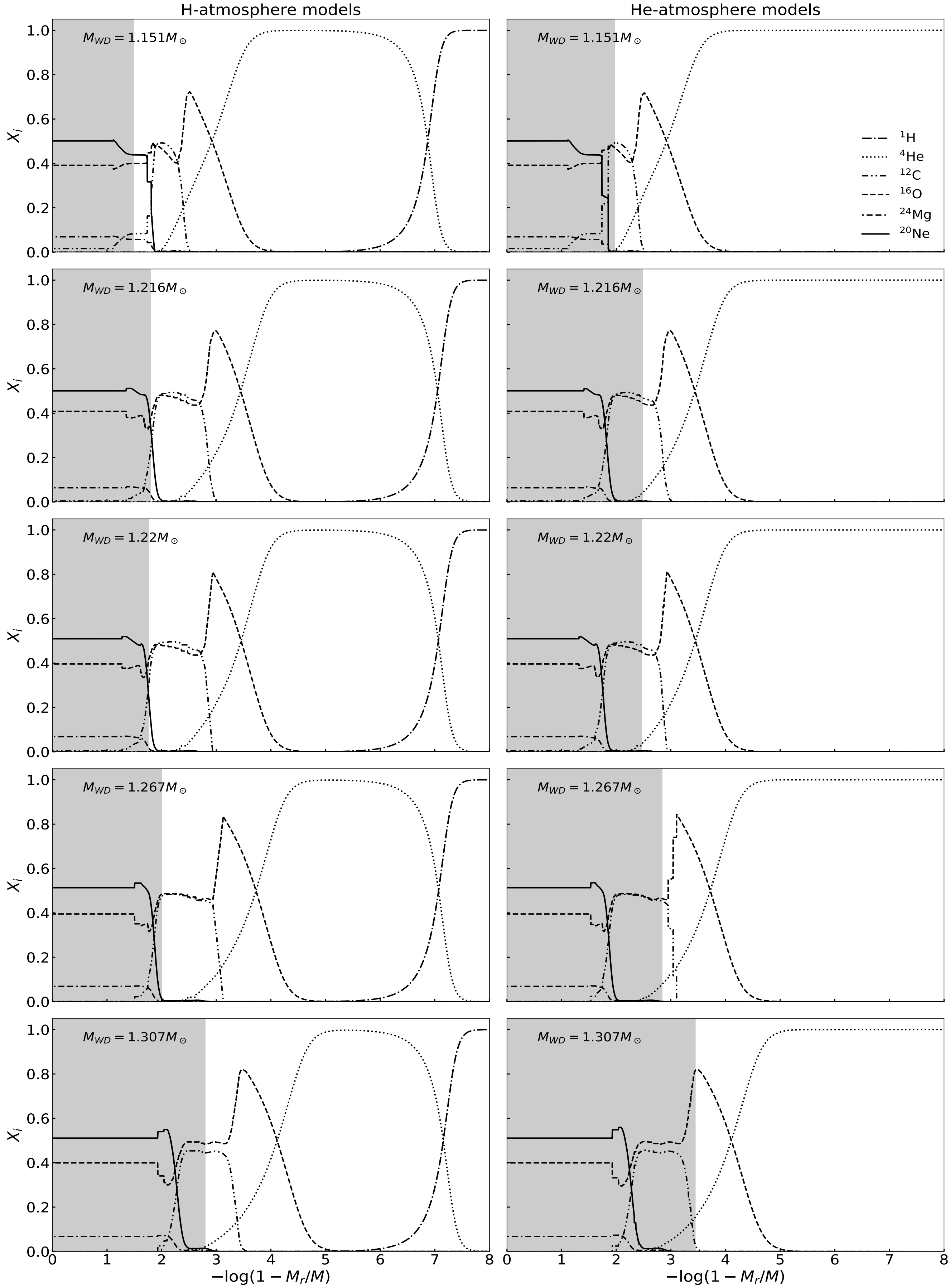

Figure A1 – *continued*